1

Explicitly Correlated Local Electron Correlation Methods

Hans-Joachim Werner, Christoph Köppl, Qianli Ma, and Max Schwilk

Institute for Theoretical Chemistry, University of Stuttgart, Germany

COPYRIGHTED MATERIAL

1.1 Introduction

Accurate wave function methods for treating the electron correlation problem are indispensable in quantum chemistry. A well-defined hierarchy of such methods exists, and in principle, these methods allow to approach the exact solution of the non-relativistic electronic Schrödinger equation to any desired accuracy. A much simpler alternative is density functional theory (DFT), which is probably most often used in computational chemistry. However, its failures and uncertainties are well known, and there is no way for systematically improving or checking the results other than comparing with experiment or with the results of accurate wave function methods.

Due to the steep scaling of the computational resources (CPU-time, memory, disk space) with the molecular size, conventional wave function methods such as CCSD(T) (coupled-cluster with single and double excitations and a perturbative treatment of triple excitations) can only be applied to rather small molecular systems. For example, the CPU-time of CCSD(T) scales as $\mathcal{O}(\mathcal{N}^7)$, where $\mathcal{N}$ is a measure of the molecular size (e.g., the number of correlated electrons) and even the simplest electron correlation method, MP2 (second-order Møller-Plesset perturbation theory) scales as $\mathcal{O}(\mathcal{N}^5)$. This causes a "scaling wall" that cannot be overcome. Even with massive parallelization and using the largest supercomputers, this wall can only be slightly shifted to larger systems. However, it is well known that electron correlation in insulators is a short-range effect. The pair correlation energies decay at long-range with R^{-6}, where R is the distance between two localized spin orbitals. Therefore, the steep scaling is unphysical. It results mainly from the use of canonical molecular orbitals, which are usually delocalized over larger parts of the molecule.

The scaling problem can be much alleviated by exploiting the short-range character of electron correlation using local orbitals and by introducing local approximations. This was first proposed in the pioneering work of Pulay *et al.* [1–6], and in the last 20 years enormous progress has been made in developing accurate local correlation methods. There are two different approaches, both of which are based on the use of local orbitals. The traditional one is to treat the whole molecule in one calculation and to apply various approximations that are based on the fast decay of the correlation energy. We will denote

Fragmentation: Toward Accurate Calculations on Complex Molecular Systems, First Edition.
Edited by Mark S. Gordon.
© 2017 John Wiley & Sons Ltd. Published 2017 by John Wiley & Sons Ltd.

such methods "local correlation methods." A large variety of such approaches has been published in the past [7–59].

The second approach is the so-called "fragmentation methods" [60–87], in which the system is split into smaller pieces. These pieces are treated independently, mostly using conventional methods (although the use of local correlation methods is also possible). The total correlation energy of the system is then assembled from the results of the fragment calculations. Various methods differ in the way in which the fragments are chosen and the energy is assembled. A special way of assembling the energy using a many-body expansion is used in the so-called incremental methods [88–96], but these also belong to the group of fragmentation methods. Fragmentation methods will be described in other chapters of this volume and are therefore not the subject of this chapter. However, in Section 1.13, we will comment on the relation of local correlation and fragmentation methods.

Another problem of the CCSD(T) method is the slow convergence of the correlation energy with the basis set size. Very large basis sets are needed to obtain converged results, and this makes conventional high-accuracy electron correlation calculations extremely expensive. This problem is due to the fact that the wave function has a cusp for $r_{12} \rightarrow 0$, where r_{12} is the distance between two electrons. The cusp is due to the singularity of the Coulomb operator $\frac{1}{r_{12}}$, and cannot be represented by expanding the wave function in antisymmetrized products of molecular orbitals (Slater determinants). This leads to the very slow convergence of the correlation energy with the size of the basis set, and in particular with the highest angular momentum of the basis functions. This problem can be solved by including terms into the wave function that depend explicitly on the distance r_{12}, and these methods are known as "explicit correlation methods" [97–155].

The combination of explicit correlation methods with local approximations has been particularly successful [140–153]. As will be explained and demonstrated later in this chapter, this does not only drastically reduce the basis set incompleteness errors, but also strongly reduces the errors caused by local approximations. Local correlation methods employ two basic approximations. The first is based on writing the total correlation energy as a sum of pair energies. Each pair describes the correlation of an electron pair (in a spin-orbital formulation), or, more generally, the correlation of the electrons in a pair of occupied local molecular orbitals (LMOs). Depending on the magnitude of the pair energies, it is possible to introduce a hierarchy of "strong," "close," "weak," or "distant" pairs [7, 18, 31, 32]. Different approximations can be introduced for each class, ranging from a full local coupled-cluster (LCCSD) treatment for strong pairs to a non-iterative perturbation correction for distant pairs, which can be evaluated very efficiently using multipole approximations [12, 13]. We will denote such approximations as "pair approximations." The second type of local approximations is the "domain approximation," which is applied to each individual pair. A domain is a subset of local virtual orbitals which is spatially close to the LMO pair under consideration. Asymptotically, the number of orbitals in each pair domain (the "domain sizes") become independent of the molecular size. Also the number of pairs in each class (except for the distant pairs) becomes independent of the molecular size. This leads to linear scaling of the computational effort as a function of molecular size, as has already been demonstrated for LMP2 and up to the LCCSD(T) level of theory more than 25 years ago [12–18].

The critical question is, of course, how quickly the correlation energy as well as relative energies (e.g., reaction energies, activation energies, intermolecular interaction energies, and electronic excitation energies) converge with the domain sizes and how they depend on the pair approximations. The domain sizes which are necessary to reach a certain accuracy (e.g., 99.9% of the canonical correlation energy) depends sensitively on the choice of the virtual orbitals. As is known since the 1960s, fastest convergence is obtained with pair natural orbitals (PNOs) [156], and this has first been fully exploited in the seminal PNO-CI and PNO-CEPA methods of Meyer [157, 158], and somewhat later also by others [159–163]. The problem with this approach is that the PNOs are different for each pair and non-orthogonal between different pairs. This leads to complicated integral transformations and prevented the application of PNO methods to large molecules for a long time. The method was revived by Neese and coworkers in 2009 and taken up also by others (including us) later on [32, 33, 48–57, 146–150]. The problem of evaluating the integrals was overcome by using local density-fitting approximations [22]. Furthermore, the integrals are first computed in a basis of projected atomic orbitals (PAOs), which are common to all pairs, and subsequently transformed to the pair-specific PNO domains [54, 146, 147, 150]. Also, hybrid methods, in which so-called orbital-specific virtuals (OSVs) [164–167] are used at an intermediate stage, have been proposed [53, 146, 147]. Later sections of this chapter will explain these approaches in some detail.

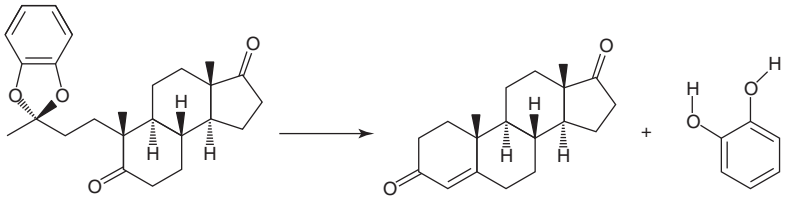
Local approximations have also been developed for multi-reference wave functions [168–176]. The description of these methods is beyond the scope of the current article, but we mention that recently very efficient and accurate PNO-NEVPT2 [175] (*N*-electron valence state perturbation-theory) and PNO-CASPT2 [176] (complete active space second-order perturbation theory) methods have been described.

In the current article, we will focus on new developments of well-parallelized PNO-LMP2-F12 and PNO-LCCSD-F12 methods recently developed in our laboratory. These methods also have a close relation to the methods of Neese *et al.* [54–57, 153]. After introducing some benchmark systems, which will be used later on, we will first outline the principles of local correlation and describe the choice of the local occupied and virtual orbitals as well as of the domains. The convergence of the correlation energy as a function of the domain sizes will be demonstrated for various types of virtual orbitals for LMP2. Subsequently, based on these foundations, we will discuss more advanced approximations for distant pairs and close/weak pair approximations used in local coupled cluster methods. Next, we will present an introduction to local explicit correlation methods, and demonstrate the improvements achieved by the F12 approach both for LMP2-F12 and LCCSD-F12. Finally, we will describe some important technical details, such as local density fitting and parallelization. A summary concludes the chapter.

1.2 Benchmark Systems

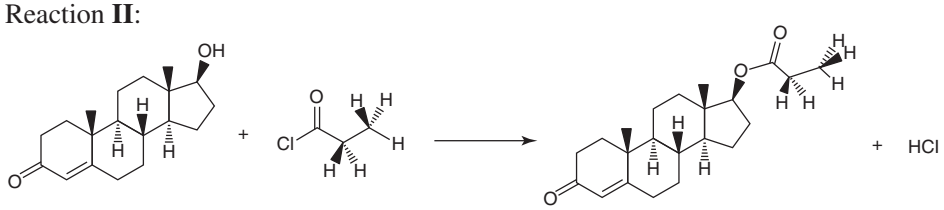
Some large molecules and reactions, which we have used extensively to benchmark our methods [32, 145, 147, 148], are shown in Figures 1.1 and 1.2. For easy reference, we have given short names to some of the molecules, which are shown in the figure and will be used throughout this article. Reaction **I** is the last step in the synthesis of androstendione. In reaction **II**, testosterone is esterified to make it more lipophilic for a longer

Reaction **I**:



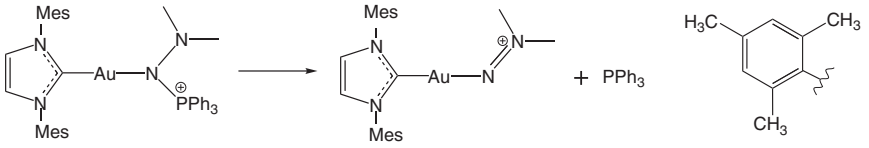
"Precursor" Androstendione

Reaction **II**:

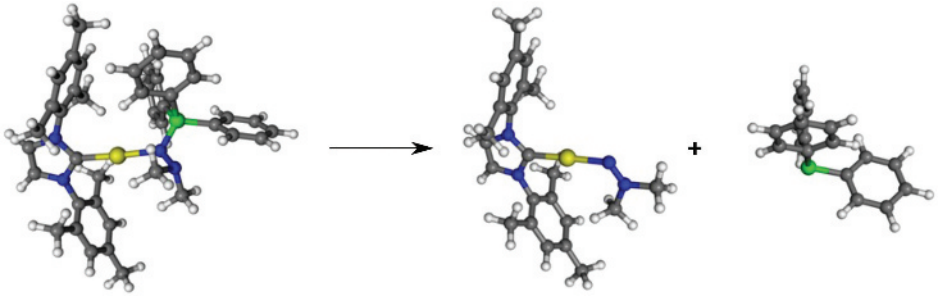


Testosterone "Ester"

Reaction **III**:

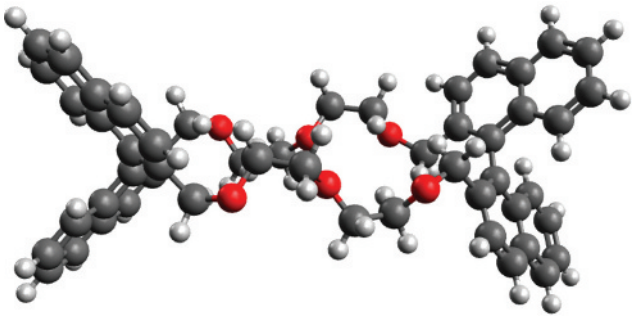


"Auamin" "Auamin2s" Mes=Mesityl-

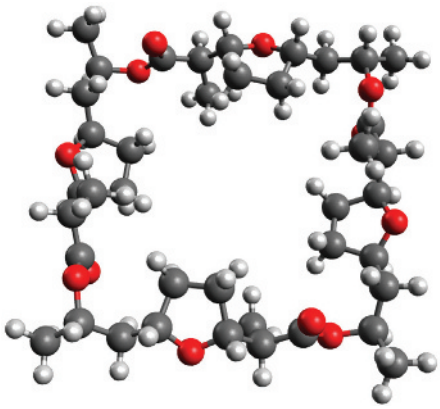


"Auamin" "Auamin2s" $P(Ph)_3$

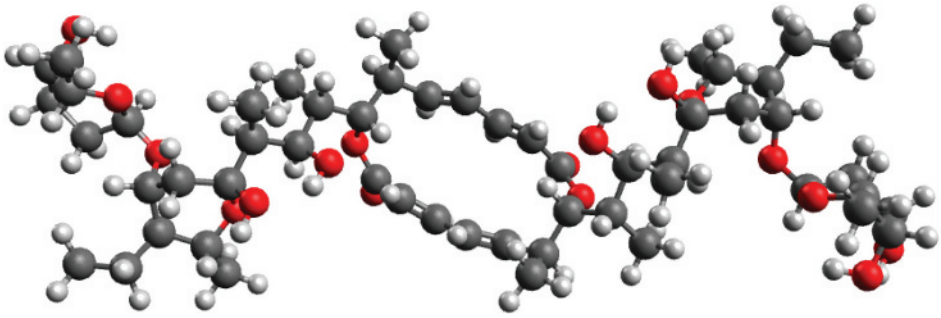
Figure 1.1 Benchmark molecules and reactions.



$C_{52}O_6H_{48}$ (106 atoms)



Nonactin (116 atoms)



Elaiophylin (160 atoms)

Figure 1.2 Visualization of a selection of large molecules mentioned in Tables 1.3 and 1.4.

retention time in body tissues. Reaction **III** is the dissociation of a gold(I)-aminonitrene complex ($AuC_{41}H_{45}N_4P$, for simplicity denoted Auamin, see Figure 1.1). This reaction is taken from Ref. [177] and plays an important role in catalytic aziridination and insertion reactions. The Auamin molecule has three phenyl and three mesityl groups and therefore strong long-range dispersion interactions are expected.

In Figure 1.2, some representative medium-sized organic molecules with about 100–150 atoms are shown. The selection of molecules contains a modified crown-ether ($C_{52}O_6H_{48}$) as well as the biologically active molecules nonactin and elaiophylin. We use these and some other molecules to demonstrate the convergence of our local correlation methods toward the canonical results and to perform benchmark calculations.

Most calculations have been carried out using the cc-pVDZ-F12 (VDZ-F12) and cc-pVTZ-F12 (VTZ-F12) basis sets [154]. For the gold atom, the ECP60MDF effective core potential [178] for the inner 60 electrons along with the aug-cc-pVDZ-PP and aug-cc-pVTZ-PP basis sets [179] were used. Density-fitting (DF) approximations were employed throughout this work for the evaluation of 2-electron integrals, and the aug-cc-pVTZ/MP2FIT basis set [180] was used as the DF auxiliary basis. We also used the aug-cc-pVTZ/JKFIT basis, which was derived from the cc-pVTZ/JKFIT basis set [181] by adding for each angular momentum another shell of diffuse functions, as the auxiliary basis for the resolution of the identity (RI) in F12 calculations. Unless otherwise stated, the parameters for local approximations are our program defaults, as described in the following sections.

For reaction **III**, the computed dissociation energy can be directly compared to an experimental gas-phase value [177] of 196.5 ±11.2 kJ mol^{-1}, which has been obtained by subtracting the PW91/cc-pVTZ-pp zero-point correction [177] of −8.2 kJ mol^{-1} from the measured value. The Hartree–Fock value is computed to be 92 kJ mol^{-1}. Thus, the correlation contribution to the dissociation energy is very large, and, as will be demonstrated later, very sensitive to local approximations. The reaction therefore provides an excellent "difficult" benchmark system.

All methods described and used in this article are implemented in the development version of the MOLPRO quantum chemistry package [182, 183], and will be made available for general use in the next release.

1.3 Orbital-Invariant MP2 Theory

The basic approximations in local correlation methods can be well understood by considering the closed-shell MP2 method. We will therefore discuss local MP2 (LMP2) methods first; more advanced coupled cluster methods will be presented in Section 1.9.

Since we intend to use localized orbitals, the theory must be formulated in a way that is invariant with respect to unitary transformations within the occupied valence and virtual orbital spaces. This means that the Fock matrix is non-diagonal in each of these subspaces. The choice of local occupied and virtual orbitals will be discussed in the subsequent sections.

We will introduce quite a number of different orbital spaces and, for the sake of clarity, the index notation is summarized in Table 1.1.

The first-order MP2 wave function is written as

$$\Psi^{(1)} = \frac{1}{2}\sum_{i,j}^{\mathrm{val}}\sum_{a,b}^{\mathrm{virt}} |\Phi_{ij}^{ab}\rangle T_{ab}^{ij}, \quad T_{ab}^{ij} = T_{ba}^{ji}, \tag{1.1}$$

where i, j are occupied and a, b are virtual orbitals. The summation limit "val" over the first summation indicates that the sum runs only over the correlated valence orbitals

Table 1.1 Index notation for various orbital spaces.

Indices	Orbital space
μ, ν, ρ, σ	Orbital basis functions (AOs)
α, β	Complete space or non-orthogonal resolution of the identity (RI) basis functions
$\bar{\alpha}, \bar{\beta}$	Orthonormal RI functions
A, B	Density-fitting (DF) basis functions
General MOs and PAOs	
i, j, k, l	Localized occupied molecular orbitals (LMOs)
a, b, c, d	Canonical virtual molecular orbitals (VMOs)
$\tilde{r}, \tilde{s}, \tilde{t}, \tilde{u}$	Non-orthogonal projected atomic orbitals (PAOs)
Pair-specific virtuals for domain $[ij]$	
$\tilde{r}^{ij}, \tilde{s}^{ij}, \tilde{t}^{ij}, \tilde{u}^{ij}$	Non-orthogonal pair-specific virtuals (PSVs)
$r^{ij}, s^{ij}, t^{ij}, u^{ij}$	Pseudo-canonical pair-specific virtuals (PC-PSVs)
$\tilde{a}^{ij}, \tilde{b}^{ij}, \tilde{c}^{ij}, \tilde{d}^{ij}$	Pair natural orbitals (PNOs)
$a^{ij}, b^{ij}, c^{ij}, d^{ij}$	Pseudo-canonical pair natural orbitals (PC-PNOs)

(excluding uncorrelated core orbitals). $|\Phi_{ij}^{ab}\rangle$ are doubly excited configurations, which are obtained by applying spin-summed excitation operators $\hat{E}_i^a$ to the Hartree–Fock reference wave function $|0\rangle \equiv |\Phi_{\mathrm{HF}}\rangle$:

$$\left|\Phi_{ij}^{ab}\right\rangle = \hat{E}_i^a \hat{E}_j^b |0\rangle. \tag{1.2}$$

The MP2 amplitudes T_{ab}^{ij} can be determined by minimizing the Hylleraas functional

$$E_2 = 2\langle \Psi^{(1)}|\hat{H}|0\rangle + \langle \Psi^{(1)}|\hat{H}^{(0)} - E^{(0)}|\Psi^{(1)}\rangle, \tag{1.3}$$

which leads to the first-order amplitude equations

$$R_{ab}^{ij} = \left\langle \tilde{\Phi}_{ij}^{ab}|\hat{H}|0\right\rangle + \left\langle \tilde{\Phi}_{ij}^{ab}|\hat{H}^{(0)} - E^{(0)}|\Psi^{(1)}\right\rangle \stackrel{!}{=} 0. \tag{1.4}$$

The quantities R_{ab}^{ij} are *residuals*, which must vanish for the optimized amplitudes. Since the configurations $|\Phi_{ij}^{ab}\rangle$ are pairwise non-orthogonal for ij and ji, it is convenient to use in equation (1.4) contravariant configurations

$$\left|\tilde{\Phi}_{ij}^{ab}\right\rangle = \frac{1}{6}\left(2\left|\Phi_{ij}^{ab}\right\rangle + \left|\Phi_{ij}^{ba}\right\rangle\right), \tag{1.5}$$

which have the properties

$$\left\langle \tilde{\Phi}_{ij}^{ab}\middle|\Phi_{kl}^{cd}\right\rangle = \delta_{ac}\delta_{bd}\delta_{ik}\delta_{jl} + \delta_{ad}\delta_{bc}\delta_{il}\delta_{jk}, \tag{1.6}$$

$$\left\langle \tilde{\Phi}_{ij}^{ab}\middle|\Psi^{(1)}\right\rangle = T_{ab}^{ij}. \tag{1.7}$$

Expanding the first-order wave function as

$$|\Psi^{(1)}\rangle = \sum_{ij} \sum_{ab} |\tilde{\Phi}_{ij}^{ab}\rangle \tilde{T}_{ab}^{ij} \tag{1.8}$$

and equating this to equation (1.1) yields the corresponding contravariant amplitudes

$$\tilde{T}_{ab}^{ij} = 2T_{ab}^{ij} - T_{ba}^{ij}. \tag{1.9}$$

It is then straightforward to derive that

$$\langle \tilde{\Phi}_{ij}^{ab} | \hat{H} | 0 \rangle = (ai|bj), \tag{1.10}$$

where

$$(ai|bj) = \int_{\mathbb{R}^3} \mathrm{d}\mathbf{r}_1 \int_{\mathbb{R}^3} \mathrm{d}\mathbf{r}_2 \;\; \rho_{ai}(\mathbf{r}_1) \frac{1}{r_{12}} \rho_{bj}(\mathbf{r}_2) \tag{1.11}$$

are the electron repulsion integrals (ERIs) in Mulliken notation and $\rho_{ai}(\mathbf{r}) = \phi_a(\mathbf{r})\phi_i(\mathbf{r})$ are 1-electron charge distributions. In the following, we will often consider the integrals for a fixed pair ij as a matrix

$$[\mathbf{K}^{ij}]_{ab} = (ai|bj). \tag{1.12}$$

Similarly, the amplitudes $T_{ab}^{ij} = [\mathbf{T}^{ij}]_{ab}$ and residuals $R_{ab}^{ij} = [\mathbf{R}^{ij}]_{ab}$ are matrices, where superscripts denote different matrices, and subscripts their indices. Note that the matrices are all defined in the virtual orbital space, that is, their indices always refer to virtual orbitals. The Hylleraas functional (equation 1.3) can then be written as

$$E_2 = \sum_{i,j}^{\mathrm{val}} \sum_{a,b}^{\mathrm{virt}} \left(K_{ab}^{ij} + R_{ab}^{ij} \right) \tilde{T}_{ab}^{ij} = \sum_{i,j}^{\mathrm{val}} \mathrm{tr}[(\mathbf{K}^{ij} + \mathbf{R}^{ij})\tilde{\mathbf{T}}^{ji}]. \tag{1.13}$$

For optimized amplitudes the residuals R_{ab}^{ij} vanish, and the Hylleraas energy E_2 becomes equal to the standard second-order energy expression

$$E^{(2)} = \langle \Psi^{(1)} | \hat{H} | 0 \rangle = \sum_{i,j}^{\mathrm{val}} \mathrm{tr}[\mathbf{K}^{ij}\tilde{\mathbf{T}}^{ji}]. \tag{1.14}$$

The orbital-invariant form of the MP2 residuals is

$$[\mathbf{R}^{ij}]_{ab} = \left[\mathbf{K}^{ij} + \mathbf{F}\mathbf{T}^{ij} + \mathbf{T}^{ij}\mathbf{F} - \sum_{k}^{\mathrm{val}} \left(f_{ik}\mathbf{T}^{kj} + \mathbf{T}^{ik}f_{kj} \right) \right]_{ab}, \tag{1.15}$$

where $[\mathbf{F}]_{ab}$ and f_{kl} are the external (virtual) and internal (occupied) blocks of the closed-shell Fock matrix. In general, the linear equation system $R_{ab}^{ij} = 0$ (cf. equation 1.4) must be solved iteratively. In the special case where canonical HF orbitals are used (i.e., $f_{ij} = \delta_{ij}\epsilon_i$, $F_{ab} = \epsilon_a\delta_{ab}$), the solution reduces to

$$T_{ab}^{ij} = -\frac{K_{ab}^{ij}}{\epsilon_a + \epsilon_b - \epsilon_i - \epsilon_j}. \tag{1.16}$$

If the occupied orbitals are local but the virtual orbitals are still canonical, one can write

$$R_{ab}^{ij} = K_{ab}^{ij} + (\epsilon_a + \epsilon_b - f_{ii} - f_{jj})T_{ab}^{ij} + G_{ab}^{ij} + G_{ba}^{ji},$$
$$G_{ab}^{ij} = -\sum_{k\neq i} f_{ik} T_{ab}^{kj}. \tag{1.17}$$

Approximate amplitudes can then be obtained by neglecting the coupling terms G_{ab}^{ij}

$$T_{ab}^{ij} \approx -\frac{K_{ab}^{ij}}{\epsilon_a + \epsilon_b - f_{ii} - f_{jj}}. \tag{1.18}$$

This is denoted a *semi-canonical* amplitude approximation. The energies obtained with semi-canonical amplitudes are usually too inaccurate for practical applications, but these amplitudes will be useful for generating PNOs, cf. Section 1.6.3, or for distant pair approximations, cf. Section 1.8.

Similarly, the linear amplitude equations can be solved iteratively by computing in each iteration the residuals and from these, by applying first-order perturbation theory, the amplitude updates

$$\Delta T_{ab}^{ij} \approx -\frac{R_{ab}^{ij}}{\epsilon_a + \epsilon_b - f_{ii} - f_{jj}}. \tag{1.19}$$

The semi-canonical amplitudes are the first approximation in this iterative algorithm.

1.4 Principles of Local Correlation

Let us now assume that $|i\rangle$ is a local orbital with charge center at position $\mathbf{R}_i$. We also assume that $|i\rangle$ can be expanded in a local subset of atomic orbitals (AOs) which are spatially close to $\mathbf{R}_i$. Then the charge distributions $\rho_{ai}(\mathbf{r})$ will be local around $\mathbf{R}_i$. This is true even for canonical (delocalized) virtual orbitals $|a\rangle$, since only those parts of them will contribute to the charge distribution ρ_{ai} which overlap with $|i\rangle$. If the virtual orbitals are also local, the locality of the ρ_{ai} is further improved. If the occupied and virtual orbitals are both expanded in AOs that are close to $\mathbf{R}_i$ and $\mathbf{R}_a$, respectively, it follows from the exponential decay of the AOs that the integral $(ai|bj)$ is a sum of contributions that decay exponentially with the distances between the basis functions of $|i\rangle$ and $|a\rangle$.

Similar considerations hold for b and j, and so the integral $(ai|bj)$ will decay exponentially with the distances $R_{ai} = |\mathbf{R}_a - \mathbf{R}_i|$ and $R_{bj} = |\mathbf{R}_b - \mathbf{R}_j|$ (if these are sufficiently large). This forms the basis for *domain approximations*, which means that to each LMO $|i\rangle$, a subset of local virtual orbitals a can be assigned. We will denote such *orbital domains* as $a \in [i]$. Similarly, to each pair ij of LMOs, a pair domain $[ij] \equiv [i] \cup [j]$ can be assigned. In the LMP2 wave function, the excitations $|\Phi_{ab}^{ij}\rangle$ are restricted to the domain $a, b \in [ij]$. The sizes of these domains that are necessary to reach a certain accuracy depend crucially on the choice and construction of the virtual orbitals. This will be discussed in more detail in Section 1.6.

If LMO $|i\rangle$ is far from $|j\rangle$, the local charge distribution ρ_{ai} will also be far from ρ_{bj}. If the virtual orbitals $|a\rangle$, $|b\rangle$ are local with $|a\rangle$ being close to $|i\rangle$ and $|b\rangle$ close to $|j\rangle$, the exchange-type integrals $(bi|aj)$ will decay exponentially and can be neglected at large

distances of $|i\rangle$ and $|j\rangle$. Using the semi-canonical amplitude approximation (cf. equation 1.18) the distant pair energies E_{ij}^{dist} can then be approximated as

$$E_{ij}^{\text{dist}} \approx -4 \sum_{a\in[i]} \sum_{b\in[j]} T_{ab}^{ij}(ai|bj) = -4 \sum_{a\in[i]} \sum_{b\in[j]} \frac{(ai|bj)^2}{\epsilon_a + \epsilon_b - f_{ii} - f_{jj}}. \tag{1.20}$$

The integrals $(ai|bj)$ can be efficiently computed using local density-fitting techniques (cf. Section 1.12.1) or approximated by a *multipole expansion* [12, 13, 54] (cf. Section 1.8). Since the densities $\rho_{ai}(\mathbf{r})$ carry no charge ($\int \rho_{ai}(\mathbf{r})dr = 0$), the lowest-order contribution is the dipole–dipole interaction, which decays with R^{-3}, where R_{ij} is the distance between the charge centers of the LMOs i and j. Consequently, in a local orbital basis, the amplitudes and pair energies decay with R_{ij}^{-3} and R_{ij}^{-6}, respectively. This is the basis of *pair approximations*, which simplify the treatment of distant pairs ij, cf. Section 1.8.

1.5 Orbital Localization

Localized occupied molecular orbitals (LMOs) $|i\rangle \equiv |\phi_i^{\text{loc}}\rangle$ can be obtained from the canonical molecular orbitals (CMOs) $|\phi_k^{\text{can}}\rangle$ by a unitary transformation

$$|i\rangle \equiv |\phi_i^{\text{loc}}\rangle = \sum_k^{\text{val}} |\phi_k^{\text{can}}\rangle U_{ki}^{\text{loc}}. \tag{1.21}$$

Uncorrelated core orbitals are excluded from the localization, since mixing of core and valence orbitals would affect the correlation energy even without any local approximations. The localized valence orbitals $|i\rangle$ can be expressed in the atomic orbital (AO) basis $|\mu\rangle \equiv |\chi_\mu\rangle$ by a rectangular transformation matrix $\mathbf{L}$ ($N_{\text{AO}} \times N_{\text{val}}$), which is related to the corresponding canonical MO-coefficient matrix $\mathbf{C}$ by the unitary transformation $\mathbf{U}^{\text{loc}}$:

$$|i\rangle = \sum_{\mu=1}^{N_{\text{AO}}} |\mu\rangle L_{\mu i}, \qquad L_{\mu i} = \sum_k^{\text{val}} C_{\mu k} U_{ki}^{\text{loc}}. \tag{1.22}$$

In the following, the indices i, j, k, l will always refer to LMOs.

There are various criteria that can be used to determine the transformation matrix $\mathbf{U}^{\text{loc}}$. For a recent review, see Ref. [184]. Perhaps the most well-known ones are the methods of Foster and Boys (FB), Pipek-Mezey (PM) [185], and Edmiston and Ruedenberg (ER) [186, 187]. ER localization minimizes the overall inter-orbital electron repulsion. This requires the 2-electron integrals, and is therefore quite expensive and rarely used. In FB localization, the sum of the orbital variances

$$P^{\text{FB}} = \sum_p^{\{x,y,z\}} \sum_{i=1}^{\text{val}} \langle i|(\hat{p} - \langle i|\hat{p}|i\rangle)^2|i\rangle. \tag{1.23}$$

is minimized. PM localization maximizes the sum of the squared Mulliken partial charges q_{iA}:

$$P^{\mathrm{PM}} = \sum_{A}^{\mathrm{atoms}} \sum_{i}^{\mathrm{val}} q_{iA}^2, \tag{1.24}$$

$$q_{iA} = 2 \sum_{\mu \in A} L_{\mu i} \sum_{\nu} S_{\mu\nu} L_{\nu i}, \tag{1.25}$$

where the first sum in the latter equation runs over all basis functions μ centered at atom A. Effectively, this means that the number of centers at which the orbitals are localized is minimized. Pipek-Mezey (PM) localization often suffers from the problem that poor localization may result in calculations with large basis sets containing diffuse functions.

The latter problem can be avoided by using intrinsic bond orbitals (IBOs) [188]. In this case, a molecule-intrinsic minimal basis of polarized atomic orbitals (IAOs) $|\rho\rangle$ [188–191] is created, in which the occupied Hartree–Fock orbitals can be expanded exactly. The IAOs are generated from a suitable minimal basis of free-atom AOs $|\tilde{\rho}\rangle$ using projection operators [188] and are subsequently symmetrically orthogonalized. The free atom AOs $|\tilde{\rho}\rangle$ are stored in a basis set library (we use a subset of the generally contracted cc-pVTZ basis where available). The partial charges are then defined as

$$q_{iA} = 2 \sum_{\rho \in A} \langle i|\rho\rangle\langle\rho|i\rangle \tag{1.26}$$

and used in the PM localization. Alternatively, Knizia [188] has proposed to replace the exponent of two in equation (1.24) by four, which helps to converge the iterative localization procedure in highly symmetric cases where several equivalent solutions exist. We will denote the IBO localizations with exponents 2 and 4 as IBO2 and IBO4, respectively. The resulting IBOs closely resemble PM orbitals, but are very insensitive to basis set variations; in particular, the commonly encountered artifacts of PM orbitals with diffuse basis sets are absent. Additionally, the IBO construction yields stable partial orbital charges which can be used for defining domains (see Section 1.6.2). Closely related localization schemes were also put forward by Lehtola and Jónsson [192] and West *et al.* [191]. The relation between these schemes has been investigated by Janowski [189].

The construction of IBOs is simple and efficient, and since the iterative localization is carried out in the minimal IAO basis, it is much faster than the standard PM localization. Even though it scales cubically with molecular size, the time to generate IBOs is found to be short as compared to a PNO-LMP2 calculation, even for cases with about 10,000 basis functions.

A fourth localization scheme, which has been used in the past in local correlation methods [28], is based on the natural bond orbital (NBO) analysis of Weinhold and coworkers [193–196] and yields so-called natural localized molecular orbitals (NLMOs) [194]. Somewhat similar to IBOs, the NLMOs are obtained by a sequence of transformations which first yields natural atomic orbitals (NAOs), then NBOs, and finally the NLMOs. However, these transformations are much more complicated and less uniquely defined than in the IBO scheme. Based on these transformations partial charges can also be defined [28], which are quite stable with respect to basis set variations and are rather similar to IBO partial charges.

FB localization yields qualitatively different localized orbitals for double bonds than the other schemes. Usually, PM, IBO, and NLMO localization keeps σ- and π-orbitals separate (even in non-planar molecules). In contrary, Boys localization often generates two equivalent "banana-bond"-like orbitals. Some examples are shown in Figure 1.3 for naphtalene. The PM, IBO2, and NBO orbitals are qualitatively similar but not identical. The differences are rather small and therefore only the IBO2 orbitals are shown in Figure 1.3.

Table 1.2 shows a comparison of domain sizes and correlation energies using various localization schemes for a number of aromatic molecules. Despite the qualitative differences of the various localized orbitals, the localization method has only a minor effect on the domain sizes and correlation energies. Exceptions are special cases in which the LMOs are neither symmetry-adapted nor symmetry-equivalent. It may then happen that the domains are neither symmetry-adapted nor symmetry-equivalent, and this can cause spurious dipole moments perpendicular to a molecular plane and other artifacts. An example is the IBO4 localization of naphtalene, cf. Figure 1.3. In longer polycyclic aromatic hydrocarbons such as tetracene or pentacene, none of the localization methods creates symmetry-adapted or equivalent LMOs. In such cases, the non-equivalent orbital domains should be merged so that, overall, the symmetry properties are recovered.

1.6 Local Virtual Orbitals

In this section, we will discuss various types of virtual orbitals and the corresponding domain constructions. The choice of virtual orbitals is most essential for the accuracy and efficiency of local correlation methods. There are schemes which localize virtual orbitals in a similar way as the occupied orbitals, yielding orthonormal localized virtual orbitals (LVOs) [184]. Even though these orbitals have good locality properties and have been successfully used in fragmentation approaches, we have found that, in local correlation methods, much smaller domains are sufficient for a certain accuracy if projected atomic orbitals (PAOs), orbital-specific virtuals (OSVs), or pair natural orbitals (PNOs) are used. PAOs are obtained by projecting atomic orbitals or basis functions to the virtual space, yielding a single set of non-orthogonal functions. In contrast, in OSV and PNO methods, different orthonormal orbital sets are used for each orbital or orbital pair, respectively. These sets are mutually non-orthogonal. In contrast to LVOs, PAOs, OSVs, and PNOs are not obtained by applying a localization criterion, but they are inherently local by construction. The domain sizes that are necessary to obtain a certain fraction of the canonical correlation energy decrease in the order LVO > PAO > OSV > PNO. As will be shown later, the PNO domain sizes are typically one order of magnitude smaller than the PAO ones, which reduces the number of amplitudes to be optimized by two orders of magnitude. LVOs will not be further considered in this article. Before defining PAOs, OSVs, and PNOs in detail, some general considerations and definitions will be presented.

1.6.1 Pseudo-Canonical Pair-Specific Orbitals

In the most general case, one can use completely independent sets of virtual orbitals $\{\tilde{r}^{ij}\}$ for each pair ij. We will denote these as *pair-specific virtuals* (PSVs). PNOs are a special

JWST817-c01 JWST817-Gordon May 18, 2017 12:57 Printer Name: Trim: 244mm × 170mm

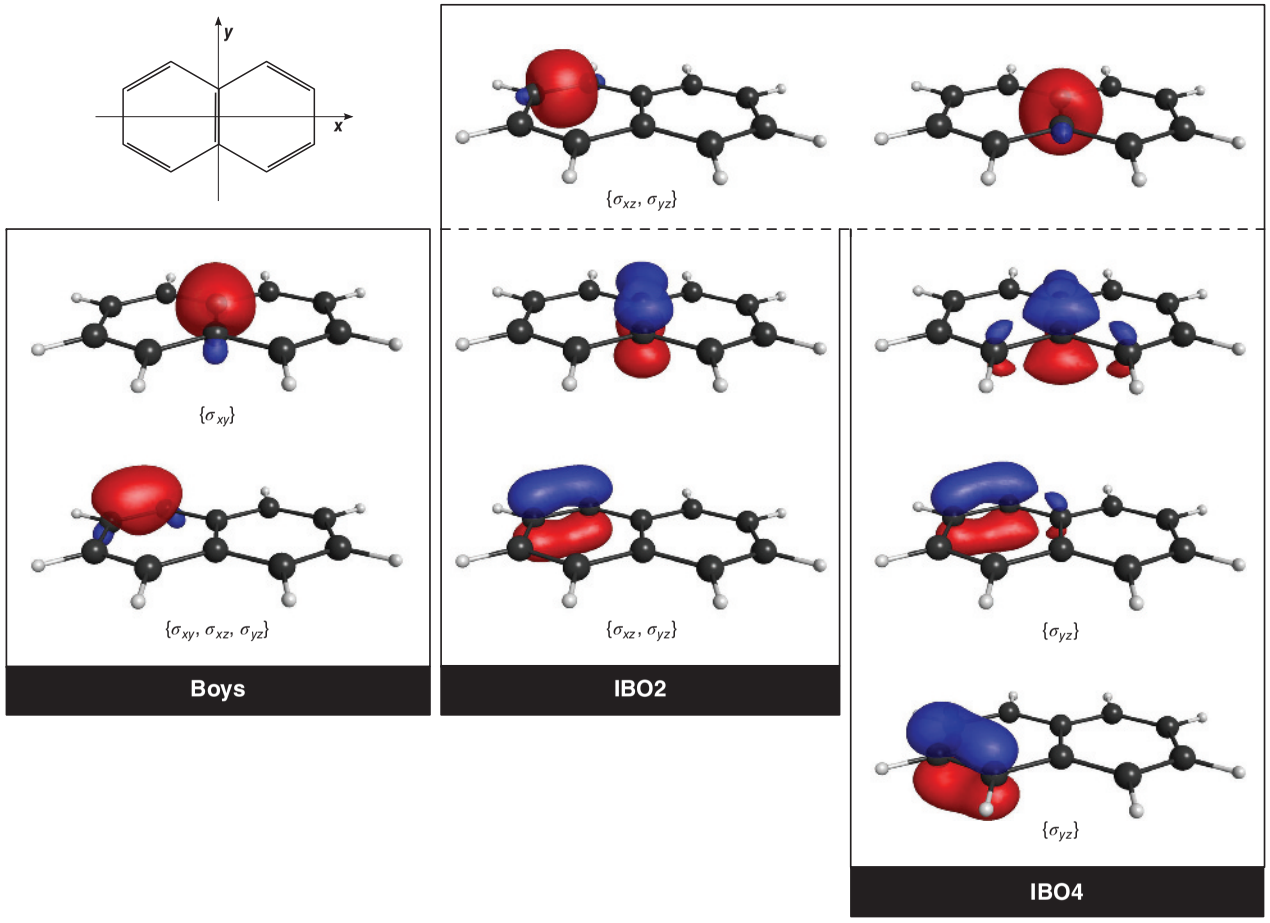


Figure 1.3 Localized C–C bonding orbitals of naphtalene. FB localization yields pairs of equivalent banana bonds, while the other localization schemes keep σ and π orbitals separate. Only the symmetry unique orbitals are shown. The specifications in curly brackets denote the symmetry operations (mirror planes) which generate equivalent orbitals. The IBO4 orbitals are not fully symmetry-adapted or equivalent. Basis set: VTZ.

Table 1.2 Domain sizes and PNO-LMP2 correlation energies (in E_h) using various localization schemes.

		IEXT=1			IEXT=2		
Molecule	**Method**	**PAO**	**PNO**	E_{corr}	**PAO**	**PNO**	E_{corr}
Benzene	FB	130	89.9	−0.947419	218	94.1	−0.949220
	PM	139	81.5	−0.947837	221	83.2	−0.949249
	NBO	130	83.6	−0.947445	218	86.5	−0.949243
	IBO4	139	81.9	−0.947804	221	83.8	−0.949237
	IBO2	139	82.1	−0.947820	221	83.8	−0.949245
Naphtalene	FB	139	85.3	−1.567535	254	91.1	−1.571672
	PM	139	77.1	−1.567584	254	81.3	−1.571771
	NBO	139	79.9	−1.567418	254	84.6	−1.571772
	IBO4	151	79.3	−1.568599	263	82.3	−1.571838
	IBO2	139	78.7	−1.567555	254	83.3	−1.571786
Adrenaline	FB	124	70.4	−2.390946	239	75.0	−2.397254
	PM	128	69.6	−2.391577	243	73.4	−2.397287
	NBO	124	68.4	−2.390728	240	73.1	−2.397304
	IBO4	128	67.5	−2.391431	243	71.5	−2.397313
	IBO2	128	67.9	−2.391531	243	71.8	−2.397338
Tryptophan	FB	130	69.3	−2.632653	247	73.7	−2.639520
	PM	130	72.1	−2.632561	247	76.7	−2.639579
	NBO	130	68.1	−2.632092	247	72.7	−2.639622
	IBO4	133	67.9	−2.633124	249	71.7	−2.639646
	IBO2	131	67.6	−2.632757	247	71.7	−2.639643
Androstenedione	FB	142	59.9	−3.618745	310	63.3	−3.630961
	PM	142	64.6	−3.618731	310	68.4	−3.631017
	NBO	142	63.8	−3.618596	310	67.9	−3.631058
	IBO4	142	61.9	−3.618602	310	65.7	−3.631016
	IBO2	142	61.8	−3.618642	310	65.7	−3.631036
Testosterone	FB	143	59.5	−3.655972	315	63.0	−3.668717
	PM	143	64.2	−3.655940	315	68.1	−3.668737
	NBO	143	63.8	−3.655829	315	69.0	−3.668776
	IBO4	143	61.7	−3.655852	315	65.6	−3.668740
	IBO2	143	61.7	−3.655877	315	65.6	−3.668752
Progesterone	FB	142	59.1	−3.973803	310	62.5	−3.987470
	PM	142	64.2	−3.973799	310	68.0	−3.987538
	NBO	142	63.1	−3.973658	310	67.1	−3.987574
	IBO4	142	61.1	−3.973689	310	64.9	−3.987538
	IBO2	142	61.0	−3.973726	310	64.7	−3.987552

Basis set: VTZ, $T_{LMO} = 0.2$, $T_{PNO}^{occ} = 10^{-8}$. The parameter `IEXT` and T_{PNO}^{occ} determine the PAO and PNO domain sizes, respectively (see Section 1.7).

choice of PSVs, but for the time being, we consider the problem in general. The tilde over the index indicates that the orbitals may be non-orthogonal (but they must always be orthogonal to the occupied orbital space). The PSVs are related to the orthonormal canonical virtuals (CMOs) $\{b\}$ by transformation matrices $\tilde{\mathbf{Q}}^{ij}$:

$$|\tilde{r}^{ij}\rangle = \sum_b |b\rangle \tilde{Q}^{ij}_{b\tilde{r}}. \tag{1.27}$$

These transformations are of course entirely useless unless they produce more local virtual orbitals so that one can restrict the PSV excitation subspaces to domains $[ij]_{\mathrm{PSV}}$. This means that we approximate the pair functions as

$$|\Psi_{ij}\rangle = \sum_{a,b} \left|\Phi^{ab}_{ij}\right\rangle T^{ij}_{ab} \approx \sum_{\tilde{r},\tilde{s}\in[ij]_{\mathrm{PSV}}} \left|\Phi^{\tilde{r}\tilde{s}}_{ij}\right\rangle T^{ij}_{\tilde{r}\tilde{s}}. \tag{1.28}$$

The transformation matrices $\tilde{\mathbf{Q}}^{ij}$ then become rectangular, with more rows than columns. To keep the formulation compact and to avoid superscripts on subscripts, we will always use the convention that the subscripts of matrices such as $\tilde{\mathbf{Q}}^{ij}$, $\mathbf{T}^{ij}$, or $\mathbf{K}^{ij}$ correspond to the pair ij given by the superscript of the matrix (here pair ij). The CMOs can be considered as a special case in which the domain $[ij]_{\mathrm{CMO}}$ is identical and complete for all pairs.

The PSVs may in general be non-orthogonal with overlap

$$S^{ij,kl}_{\tilde{r}\tilde{s}} = \langle \tilde{r}^{ij}|\tilde{s}^{kl}\rangle = \sum_b \tilde{Q}^{ij}_{b\tilde{r}} \tilde{Q}^{kl}_{b\tilde{s}} = [\tilde{\mathbf{Q}}^{ij\dagger}\tilde{\mathbf{Q}}^{kl}]_{\tilde{r}\tilde{s}}. \tag{1.29}$$

Note that here the indices $\tilde{r}$ and $\tilde{s}$ belong to different pairs, as indicated by the superscripts of the overlap matrix. Inserting equation (1.27) into equation (1.28) yields for the transformation of the amplitudes

$$T^{ij}_{ab} = \sum_{\tilde{r},\tilde{s}} \tilde{Q}^{ij}_{a\tilde{r}} T^{ij}_{\tilde{r}\tilde{s}} \tilde{Q}^{ij}_{b\tilde{s}}. \tag{1.30}$$

Integral and Fock matrices transform in the opposite way, for example,

$$(\tilde{r}^{ij} i|\tilde{s}^{ij} j) = \sum_{a,b} \tilde{Q}^{ij}_{a\tilde{r}} (ai|bj) \tilde{Q}^{ij}_{b\tilde{s}}. \tag{1.31}$$

In matrix form, these transformations can be written as

$$\mathbf{T}^{ij}_{\mathrm{CMO}} = \tilde{\mathbf{Q}}^{ij} \mathbf{T}^{ij}_{\mathrm{PSV}} \tilde{\mathbf{Q}}^{ij\dagger}, \tag{1.32}$$

$$\mathbf{K}^{ij}_{\mathrm{PSV}} = \tilde{\mathbf{Q}}^{ij\dagger} \mathbf{K}^{ij}_{\mathrm{CMO}} \tilde{\mathbf{Q}}^{ij}. \tag{1.33}$$

Since the number of PSVs per pair is in general smaller than the number of CMOs, the inverse transformations are not possible. Equation (1.32) shows that one can always transform the amplitudes from the PSV domain back to the CMO basis, but not vice versa. In contrary, integrals can only be transformed from the larger basis to the smaller one, cf. equation (1.33).

Within each domain $[ij]_{\mathrm{PSV}}$, the energy is still invariant with respect to transformations among the orbitals $|\tilde{r}^{ij}\rangle$. It is useful to apply another transformation within each domain which makes the orbitals *pseudo-canonical* (PC). This means that in the subspace of the domain $[ij]_{\mathrm{PSV}}$, the PSVs become orthonormal and diagonalize the Fock

matrix. The pseudo-canonical pair-specific orbitals (PC-PSVs) are denoted $|r^{ij}\rangle$ and are related to the original PSVs by the transformation

$$|r^{ij}\rangle = \sum_{\tilde{s}\in[ij]} |\tilde{s}^{ij}\rangle W^{ij}_{\tilde{s}r}, \quad r^{ij} \in [ij]. \tag{1.34}$$

so that

$$f^{ij}_{rs} = \langle r^{ij}|\hat{f}|s^{ij}\rangle = \epsilon^{ij}_r \delta_{rs}, \quad \langle r^{ij}|s^{ij}\rangle = \delta_{rs}. \tag{1.35}$$

In practice, this is achieved by first orthogonalizing the orbitals (by singular value decomposition if linear dependencies exist), and then diagonalizing the Fock matrix in the basis of the orthogonal PSVs. Note that the PC-PSVs of different pairs are still non-orthogonal. The total transformation from CMOs to PC-PSVs is then

$$|r^{ij}\rangle = \sum_a |a\rangle Q^{ij}_{ar}, \quad r^{ij} \in [ij], \tag{1.36}$$

$$\mathbf{Q}^{ij} = \tilde{\mathbf{Q}}^{ij}\mathbf{W}^{ij}. \tag{1.37}$$

If the domain spans the whole virtual space, the PC-PSVs become equal to the CMOs.

It is straightforward to transform the amplitude equations to the PC-PSV basis by forming $\mathbf{R}^{ij}_{\text{PC-PSV}} = \mathbf{Q}^{ij\dagger}\mathbf{R}^{ij}_{\text{CMO}}\mathbf{Q}^{ij}$ and inserting $\mathbf{T}^{ij}_{\text{CMO}} = \mathbf{Q}^{ij}\mathbf{T}^{ij}_{\text{PC-PSV}}\mathbf{Q}^{ij\dagger}$. Finally, the products $[\mathbf{Q}^{ij\dagger}\mathbf{Q}^{kl}]_{rs}$ are replaced by $[\mathbf{S}^{ij,kl}]_{rs}$ (cf. equation 1.29). This always occurs if an amplitude index is not connected to an integral index. For example, the LMP2 amplitude equations in equation (1.17) become

$$\begin{aligned} R^{ij}_{rs} &= K^{ij}_{rs} + \left(\epsilon^{ij}_r + \epsilon^{ij}_s - f_{ii} - f_{jj}\right) T^{ij}_{rs} + G^{ij}_{rs} + G^{ji}_{sr} = 0, \\ G^{ij}_{rs} &= -\sum_{k\neq i} f_{ik} \sum_{t,u\in[kj]_{\text{PC-PSV}}} S^{ij,kj}_{rt} T^{kj}_{tu} S^{kj,ij}_{us}. \end{aligned} \tag{1.38}$$

The optimized amplitudes are now defined by the conditions $R^{ij}_{rs} = 0$, $r, s \in [ij]_{\text{PC-PSV}}$. Due to the domain approximation, the number of amplitudes and corresponding equations is much smaller than in the canonical case. The Hylleraas functional in the PC-PSV basis is computed as

$$E_{\text{corr}} = \sum_{i\geq j}(2-\delta_{ij}) \sum_{r,s\,\in\,[ij]} \left(K^{ij}_{rs} + R^{ij}_{rs}\right)\left(2T^{ij}_{rs} - T^{ij}_{sr}\right). \tag{1.39}$$

In the following subsections, we will address the question how to define the PSVs and which are the most suitable ones.

1.6.2 Projected Atomic Orbitals

In a seminal series of papers on local correlation methods, Pulay has proposed to use projected atomic orbitals (PAOs) to span the virtual space [1], and this has been widely used later in local correlation methods. The PAOs are labeled by indices $\tilde{r}$ and are defined as:

$$|\tilde{r}\rangle \equiv \left|\phi^{\text{PAO}}_{\tilde{r}}\right\rangle = \hat{P}\left|\phi^{\text{AO}}_{\tilde{r}}\right\rangle, \tag{1.40}$$

where $|\phi_{\tilde{r}}^{\mathrm{AO}}\rangle$ are suitable atomic orbitals and $\hat{P}$ projects out the contributions of the occupied space,

$$\hat{P} = 1 - \sum_{i=1}^{N_{\mathrm{occ}}} |\phi_i\rangle\langle\phi_i|, \tag{1.41}$$

so that $\langle\phi_{\tilde{r}}^{\mathrm{PAO}}|\phi_i\rangle = 0$ for all $i, \tilde{r}$. In general, the atomic orbitals $|\phi_{\tilde{r}}^{\mathrm{AO}}\rangle$ can be represented in the AO basis by a block-diagonal matrix $\mathbf{C}^{\mathrm{AO}}$

$$|\phi_{\tilde{r}}^{\mathrm{AO}}\rangle = \sum_{\mu\in A} |\chi_\mu\rangle C_{\mu\tilde{r}}^{\mathrm{AO}}. \tag{1.42}$$

Each non-zero block of the coefficient matrix $\mathbf{C}^{\mathrm{AO}}$ corresponds to one center. In most cases, the coefficient matrix $C_{\mu\tilde{r}}^{\mathrm{AO}}$ is assumed to be diagonal, that is, the AO basis functions themselves are projected.

In the AO basis, the PAOs are represented by a coefficient matrix $\mathbf{P}$,

$$|\tilde{r}\rangle = \sum_{\mu=1}^{N_{\mathrm{AO}}} |\chi_\mu\rangle P_{\mu\tilde{r}}, \tag{1.43}$$

with

$$\mathbf{P} = (\mathbf{1} - \mathbf{L}\mathbf{L}^\dagger\mathbf{S})\mathbf{C}^{\mathrm{AO}} = \mathbf{C}_v\mathbf{C}_v^\dagger\mathbf{S}\mathbf{C}^{\mathrm{AO}}, \tag{1.44}$$

The rectangular $(N_{\mathrm{AO}} \times N_{\mathrm{virt}})$ coefficient matrix $\mathbf{C}_v$ represents the canonical virtual orbitals, and $[\mathbf{S}]_{\mu\nu} = \langle\mu|\nu\rangle$ is the overlap matrix of the basis functions. Thus, the PAOs can be obtained from the canonical virtual orbitals by a transformation

$$|\tilde{r}\rangle = \sum_a |\phi_a\rangle \tilde{Q}_{a\tilde{r}}, \tag{1.45}$$

$$\tilde{\mathbf{Q}} = \mathbf{C}_v^\dagger\mathbf{S}\mathbf{C}^{\mathrm{AO}}. \tag{1.46}$$

Note that the matrix $\tilde{\mathbf{Q}}$ is rectangular $(N_{\mathrm{virt}} \times N_{\mathrm{AO}})$, and the N_{AO} PAOs are non-orthogonal and linearly dependent. Their overlap matrix

$$\mathbf{S}^{\mathrm{PAO}} = \mathbf{P}^\dagger\mathbf{S}\mathbf{P} = \tilde{\mathbf{Q}}^\dagger\tilde{\mathbf{Q}} \tag{1.47}$$

has N_{occ} zero eigenvalues. The linear dependencies in the PAO set are removed by singular value decomposition for individual domains.

The PAOs are neither orbital- nor pair-specific, and each one can be related to an AO (or a basis function) at one atom. In most cases, PAO domains are therefore center-based, that is, all PAOs that originate from basis functions at a selection of centers comprise the orbital domains $[i]_{\mathrm{PAO}}$. The domains are then uniquely defined by a list of centers, independent of the basis set. For each LMO i, the centers can, for example, be selected based on their partial IBO charges Q_{iA} (cf. equation 1.26). PAO pair domains are then defined as the union of the two related orbital domains, $[ij]_{\mathrm{PAO}} = [i]_{\mathrm{PAO}} \cup [j]_{\mathrm{PAO}}$. These are orthonormalized and made pseudo-canonical, as explained in Section 1.6.1. More details about the choice of PAO domains will be given in Section 1.7.

An advantage of the non-orthogonal PAOs is that they are pair-independent, and the overlap or Fock matrices for a domain $[ij]_{\mathrm{PAO}}$ can always be extracted from the full $N_{\mathrm{AO}} \times N_{\mathrm{AO}}$ matrices $\mathbf{S}_{\mathrm{PAO}}$ or $\mathbf{F}_{\mathrm{PAO}}$, respectively. Also the integral transformation

is simpler than for truly pair-specific orbitals, in particular for local CCSD methods. In PAO-LMP2 or PAO-LCCSD methods, it is therefore advantageous to compute the residuals first in the non-orthogonal PAO basis, and transform them to the pair-specific PC-PAO basis just for the update of the amplitudes. Subsequently, the amplitude update is transformed back to the non-orthogonal PAO basis:

$$\mathbf{R}^{ij}_{\text{PC-PAO}} = \mathbf{W}^{ij\dagger}\mathbf{R}^{ij}_{\text{PAO}}\mathbf{W}^{ij}, \tag{1.48}$$

$$\Delta\mathbf{T}^{ij}_{\text{PAO}} = \mathbf{W}^{ij}\Delta\mathbf{T}^{ij}_{\text{PC-PAO}}\mathbf{W}^{ij\dagger}. \tag{1.49}$$

These transformations are similar to those in equations (1.32) and (1.33), but with $\mathbf{Q}^{ij}$ replaced by $\mathbf{W}^{ij}_{\text{PAO}}$.

Unfortunately, rather large PAO domains (400-600 PAOs per pair for triple-ζ basis sets) are necessary to recover about 99.9% of the canonical correlation energy in large molecules. Thus, the memory and CPU requirements of such calculations can be very large, despite the formally linear scaling (if distant pairs are approximated). The average domain sizes can be reduced by an order of magnitude if PNOs are used, which will be discussed next.

1.6.3 Pair Natural Orbitals

Pair natural orbitals (PNOs) are obtained by diagonalizing appropriate external pair density matrices. They were first discussed by Edmiston and Krauss [156] and used very successfully in the early 70s in the PNO-CI and PNO-CEPA methods by Meyer [157, 158] and somewhat later also by Ahlrichs, Kutzelnigg, Staemmler, and others [159–163]. In these methods, PNOs were defined separately for singlet ($p = 1$) and triplet pairs ($p = -1$). In terms of the configurations and amplitudes in equation (1.2) these can be defined as

$$\left|\Phi^{ab}_{ij,p}\right\rangle = \frac{1}{2}\left(\left|\Phi^{ab}_{ij}\right\rangle + p\left|\Phi^{ba}_{ij}\right\rangle\right), \tag{1.50}$$

and the corresponding amplitudes are

$$T^{ij,p}_{ab} = \frac{1}{2}\left(T^{ij}_{ab} + pT^{ij}_{ba}\right). \tag{1.51}$$

These configurations and amplitudes are symmetric or antisymmetric with respect to exchange of the indices i, j or a, b and the configurations are orthogonal for $i \geq j$ and $a \geq b$. Note that singlet and triplet refers to the coupling of the two electrons in the virtual orbitals a, b. The configurations $|\Phi^{ab}_{ij,p}\rangle$ have the same total spin eigenvalues as the reference function.

In terms of these configurations and amplitudes, the correlation energy is

$$E^{(2)} = \sum_{i\geq j}\sum_{p=\pm 1} N_{ij,p}\sum_{a,b} K^{ij,p}_{ab}T^{ij,p}_{ab}, \tag{1.52}$$

where $N_{ij,1} = (2 - \delta_{ij})$, $N_{ij,-1} = 6(1 - \delta_{ij})$, and $K^{ij,p}_{ab} = \frac{1}{2}(K^{ij}_{ab} + pK^{ij}_{ba})$. The external pair densities are defined as

$$[\mathbf{D}^{ij,p}]_{ab} = N_{ij,p}[\mathbf{T}^{ij,p\dagger}\mathbf{T}^{ij,p}]_{ab}. \tag{1.53}$$

For MP2, the external part of the total unrelaxed one-particle reduced density matrix (1-RDM) is the sum of the pair density matrices

$$\mathbf{D} = \sum_{i \geq j} \sum_{p=\pm 1} \mathbf{D}^{ij,p}. \tag{1.54}$$

The PNOs $|\tilde{a}^{ij,p}\rangle$ for a pair ij,p are obtained by diagonalizing the corresponding pair density $\mathbf{D}^{ij,p}$

$$|\tilde{a}^{ij,p}\rangle = \sum_{b} |b\rangle \tilde{Q}^{ij,p}_{b\tilde{a}}, \tag{1.55}$$

$$\left[\tilde{\mathbf{Q}}^{ij,p\dagger} \mathbf{D}^{ij,p} \tilde{\mathbf{Q}}^{ij,p}\right]_{\tilde{a}\tilde{b}} = \delta_{\tilde{a}\tilde{b}} n^{ij,p}_{\tilde{a}}. \tag{1.56}$$

The eigenvalues $n^{ij,p}_{\tilde{a}}$ are denoted *natural pair occupation numbers*. Since the transformation $\tilde{\mathbf{Q}}^{ij,p}$ is orthogonal and the singlet amplitude matrices are symmetric in the indices a,b, the matrices $\mathbf{Q}^{ij,p}$ also diagonalize the singlet amplitude matrices

$$\left[\tilde{\mathbf{Q}}^{ij,1\dagger} \mathbf{T}^{ij,1} \tilde{\mathbf{Q}}^{ij,1}\right]_{\tilde{a}\tilde{b}} = \delta_{\tilde{a}\tilde{b}} t^{ij,1}_{\tilde{a}}. \tag{1.57}$$

The non-zero elements $t^{ij,1}_{\tilde{a}}$ are related to the natural pair occupation numbers by the relation

$$n^{ij,1}_{\tilde{a}} = N_{ij,1} \left| t^{ij,1}_{\tilde{a}} \right|^2. \tag{1.58}$$

For the triplet pairs, all natural occupation numbers are doubly degenerate (if the matrix dimension is odd, the last one is zero), and the transformation of the amplitude matrix yields a block-diagonal matrix of the form

$$[\tilde{\mathbf{Q}}^{ij,-1\dagger} \mathbf{T}^{ij,-1} \tilde{\mathbf{Q}}^{ij,-1}] = \begin{pmatrix} 0 & -t^{ij,-1}_1 & 0 & 0 & \dots \\ t^{ij,-1}_1 & 0 & 0 & 0 & \dots \\ 0 & 0 & 0 & -t^{ij,-1}_2 & \dots \\ 0 & & t^{ij,-1}_2 & 0 & \dots \\ \dots & & & & \end{pmatrix}. \tag{1.59}$$

In this case, the natural occupation numbers are

$$n^{ij,-1}_{2\tilde{a}-1} = n^{ij,-1}_{2\tilde{a}} = N_{ij,-1} \left| t^{ij,p}_{\tilde{a}} \right|^2, \quad \tilde{a} = 1, 2, \dots, \mathrm{INT}(N_{\mathrm{virt}}/2), \tag{1.60}$$

where $\mathrm{INT}(N/2)$ equals $N/2$ if N is even and $(N-1)/2$ if N is odd. In the following, we will denote approximations which keep the diagonal or block-diagonal structure of the amplitude matrices as *diagonal PNO approximation*.

In total, the diagonal approximation reduces the number of non-zero amplitudes roughly by a factor $\frac{2}{3} N_{\mathrm{virt}}$, that is, depending on the number of virtual orbitals, by 2–3 orders of magnitude — an enormous reduction. An even further reduction is possible by neglecting amplitudes that correspond to small natural pair occupation numbers. This means that domains of PNOs are selected using an occupation number threshold $T^{\mathrm{occ}}_{\mathrm{PNO}}$, keeping only PNOs for which $n^{ij,p}_{\tilde{a}} \geq T^{\mathrm{occ}}_{\mathrm{PNO}}$. Unfortunately, the amplitudes must be known in advance to determine the PNOs, and so effectively nothing is gained except for a very compact representation of the wave function. The question is, however, how good an approximation can be obtained if the initial amplitudes are approximated at

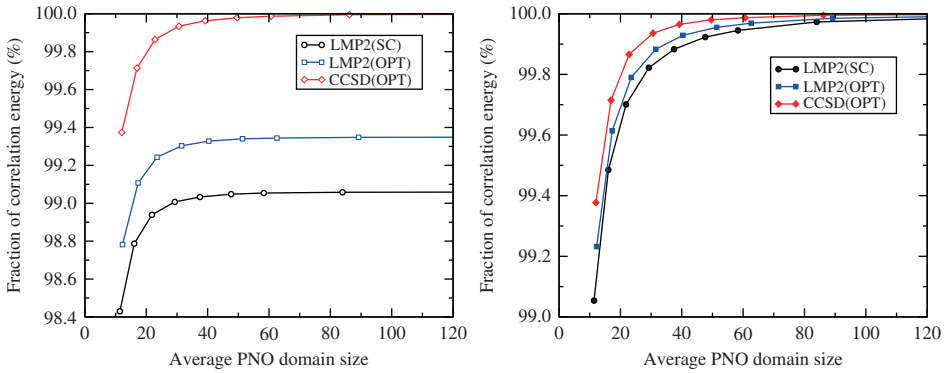


Figure 1.4 PNO-LCCSD correlation energies of propionyl chloride relative to the canonical values (in percent) as a function of the PNO domain sizes using separate PNOs for singlet and triplet pairs for three choices of amplitudes to generate the PNOs. *Left panel*: diagonal approximation (see text). *Right panel*: all amplitudes. Basis set: VDZ-F12.

a lower level. For example, one could either use semi-canonical or optimized LMP2 amplitudes to determine the PNOs, and then use these in a CCSD calculation, still keeping the (block) diagonal form of the amplitudes. The effect of these approximations is demonstrated in the left panel of Figure 1.4 for propionyl chloride (CH_3CH_2COCl) using the VDZ-F12 basis set. The figure shows the percentage of LCCSD correlation energy as a function of the average pair domain size relative to the full canonical calculation. The PNOs have been determined using either semi-canonical LMP2 amplitudes, fully optimized LMP2 amplitudes, or fully optimized LCCSD amplitudes, and the threshold $T_{\mathrm{PNO}}^{\mathrm{occ}}$ has been varied. If LCCSD amplitudes are used to define the PNOs, the correlation energy converges quickly to the canonical limit. With on average 30 PNOs per pair, more than 99.9% of the canonical correlation energy is already recovered. However, if approximate amplitudes are used, only a smaller fraction of the correlation energy is obtained, since the assumed diagonal form of the amplitudes becomes an approximation. With semi-canonical and optimized MP2 amplitudes, only 99.06% and 99.35%, respectively, of the canonical limit is recovered, even if all PNOs are used. Note that pseudo-canonical orbitals cannot be used in the diagonal approximation, which leads to slower convergence of the LCCSD iterations.

Essentially, the semi-canonical diagonal approximation corresponds to what was used by W. Meyer in his seminal PNO-CI calculations in the early 70s (in fact, he used a somewhat better amplitude approximation). Reaching $\geq$ 90% of the correlation energy for a given basis set was a big breakthrough at that time. However, even recovering 99% of the correlation energy is insufficient for computing relative energies (e.g., reaction energies) of large molecules, since 1% of the correlation energy can be a huge amount of absolute energy. Today, we therefore aim at approximations which recover about 99.9% of the canonical correlation energy for a given basis set.

The error of the LCCSD correlation energy obtained with full PNO domains (i.e., using all PNOs) is removed if the diagonal amplitude approximation is given up, and all amplitudes $T_{\tilde{a}\tilde{b}}^{ij,p}$ are used. Still, domain approximations can be applied by only including PNOs with natural occupation numbers greater than $T_{\mathrm{PNO}}^{\mathrm{occ}}$. The convergence of the correlation

energy with the domain sizes is shown in the right panel of Figure 1.4. Now the energy smoothly converges to the canonical limit for all 3 types of PNOs; as expected, convergence is fastest (and virtually identical to that of the diagonal amplitude approximation) if the PNOs are generated from LCCSD, but also the errors caused by using approximate amplitudes to generate the PNOs are small. In order to reach 99.92–99.93% of the canonical correlation energy one needs about 30, 40, and 50 PNOs per orbital pair with LCCSD, LMP2(opt), and LMP2(SC) initial amplitudes, respectively (the domain sizes depend on the basis set).

When full amplitude matrices are used, there is no particular advantage of using singlet and triplet configurations. In fact, using the original configurations $|\Phi_{ij}^{ab}\rangle$ and their contravariant counterparts leads to a simpler and more efficient formulation of the CCSD equations [197–199]. One can define symmetric spin-summed pair densities as

$$\mathbf{D}^{ij} = \sum_{p=\pm 1} N_{ij,p}\mathbf{D}^{ij,p} = \frac{1}{1+\delta_{ij}}\left(\tilde{\mathbf{T}}^{ij\dagger}\mathbf{T}^{ij} + \tilde{\mathbf{T}}^{ij}\mathbf{T}^{ij\dagger}\right). \tag{1.61}$$

and diagonalize these to obtain one set of PNOs for each pair $i \geq j$;

$$|\tilde{a}^{ij}\rangle = \sum_{b} |b\rangle \tilde{Q}_{b\tilde{a}}^{ij}, \tag{1.62}$$

$$\left[\mathbf{Q}^{ij\dagger}\mathbf{D}^{ij}\mathbf{Q}^{ij}\right]_{\tilde{a}\tilde{b}} = \delta_{\tilde{a}\tilde{b}} n_{\tilde{a}}^{ij}. \tag{1.63}$$

Again, PNO domains can be determined using the condition $n_a^{ij} > T_{\mathrm{PNO}}^{\mathrm{occ}}$. Subsequently, the PNOs in the domain are made pseudo-canonical, cf. equations (1.34)–(1.37).

The convergence of the correlation energy with respect to the average PNO domain size is shown in Figure 1.5 for spin-independent PNOs (left panel) and singlet and triplet PNOs (right panel). Somewhat unexpectedly it is found that the spin-independent PNOs generated from semi-canonical or optimized LMP2 amplitudes yield faster convergence to the canonical limit than the singlet and triplet ones. Overall, this requires a smaller

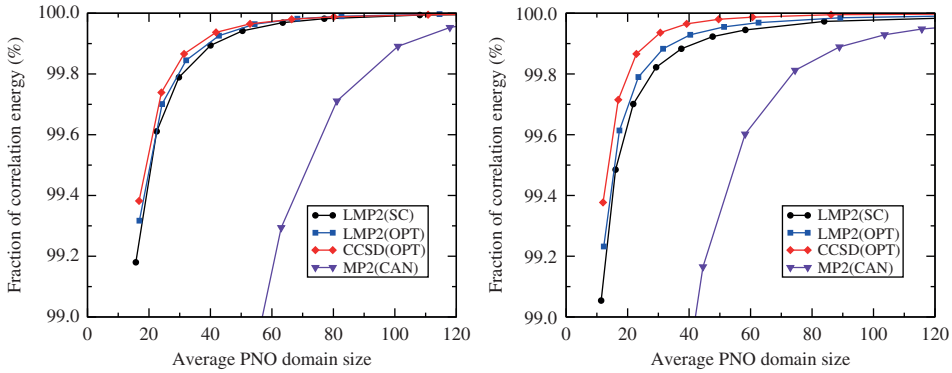


Figure 1.5 PNO-LCCSD correlation energies of propionyl chloride relative to the canonical values (in percent) as a function of the PNO domain sizes using various PNO types. *Left panel*: spin-averaged PNOs. *Right panel*: separate PNOs for singlet and triplet pairs. Basis set: VDZ-F12.

number of PNOs to reach a certain accuracy, in particular if a high percentage of correlation energy is desired. This behavior was also found for some other test molecules. Also shown in the figures is the case that canonical occupied orbitals are used, and the PNOs are generated from canonical MP2 amplitudes. This leads to much larger domains and clearly demonstrates the advantage of using LMOs, even for this relatively small molecule.

1.6.4 Linear Scaling PNO Generation

In the calculations presented in the previous section, the PNOs were generated from LMP2 amplitudes in the full virtual space. The computation of these amplitudes scales asymptotically as $\mathcal{O}(N^5)$, where N is a measure of the molecular size. Furthermore, the calculation of the pair density matrices and their diagonalization also scales as $\mathcal{O}(N^5)$. If distant pairs are neglected or treated by multipole approximations (cf. Section 1.8) this is reduced to $\mathcal{O}(N^4)$. Another problem is the calculation of the integrals $\mathbf{K}^{ij}_{\text{PNO}}$. Since the PNOs are different for each pair, their generation would be very expensive and require to keep all matrices $\mathbf{Q}^{ij}$ (or the AO $\rightarrow$ PNO transformation matrices $\mathbf{V}^{ij} = \mathbf{C}_{\text{v}}\mathbf{Q}^{ij}$) in memory.

These problems can be overcome by combining PAO and PNO approximations [54, 146, 150]. In this case, the initial LMP2(SC) amplitudes are computed in the PC-PAO basis, using large PAO domains (one can also fully optimize the PAO-LMP2 amplitudes, but this is much more expensive). The integrals $(\tilde{r}i|\tilde{s}j)$, $\tilde{r},\tilde{s} \in [ij]_{\text{PAO}}$ are then first computed in the non-orthogonal PAO basis. This can be done very efficiently using local density fitting, cf. Section 1.12.1. Next, the integrals are transformed to the pair-specific PC-PAO domains

$$\mathbf{K}^{ij}_{\text{PC-PAO}} = \mathbf{W}^{ij\dagger}\mathbf{K}^{ij}_{\text{PAO}}\mathbf{W}^{ij} \tag{1.64}$$

and used to determine the PC-PAO amplitudes T^{ij}_{rs}, $r,s \in [ij]_{\text{PC-PAO}}$. The PNO generation then proceeds exactly as explained in the previous section, except that the transformation matrices $\tilde{\mathbf{Q}}^{ij}$ are replaced by transformation matrices $\mathbf{V}^{ij}$, which transform from the PC-PAO basis to the PNO basis. A further transformation $\mathbf{U}^{ij}$ transforms from the initial PNO basis to the PC-PNO basis. Thus, the whole process proceeds in the following sequence

$$\text{AO} \xrightarrow{\mathbf{P}} [ij]_{\text{PAO}} \xrightarrow{\mathbf{W}^{ij}} [ij]_{\text{PC-PAO}} \xrightarrow{\mathbf{V}^{ij}} [ij]_{\text{PNO}} \xrightarrow{\mathbf{U}^{ij}} [ij]_{\text{PC-PNO}} \tag{1.65}$$

and the total transformation from the non-orthogonal PAO to the PC-PNO basis is

$$\mathbf{K}^{ij}_{\text{PC-PNO}} = \tilde{\mathbf{V}}^{ij\dagger}\mathbf{K}^{ij}_{\text{PAO}}\tilde{\mathbf{V}}^{ij}, \tag{1.66}$$

$$\tilde{\mathbf{V}}^{ij} = \mathbf{W}^{ij}\mathbf{V}^{ij}\mathbf{U}^{ij}. \tag{1.67}$$

The dimension of the transformation matrices $\tilde{\mathbf{V}}^{ij}_{\text{PNO}}$ for a given ij is asymptotically independent of the molecular size; the same is true for the number of operations needed to compute them. Thus, if the number of pairs ij scales linearly with the molecular size, the total memory and CPU time for the PNO generation also scales linearly with molecular size, provided we can compute the integrals $\mathbf{K}^{ij}_{\text{PAO}}$ in a linear scaling fashion. This problem will be addressed in Section 1.12.1.

1.6.5 Orbital-Specific Virtuals (OSVs)

Orbital-specific virtuals (OSVs) [164–167] are identical to the PNOs for diagonal pairs ii and can be obtained by diagonalizing either the amplitude matrices $\mathbf{T}^{ii}$ or the pair density matrices $\mathbf{D}^{ii}$. This yields one set of virtual orbitals for each valence orbital. Orbital domains $[i]_{\mathrm{OSV}}$ can be based on the natural pair occupation numbers using a threshold $T^{\mathrm{occ}}_{\mathrm{OSV}}$, exactly as for PNOs. Pair domains $[ij]_{\mathrm{OSV}}$ are then formed by taking the union of the related orbital domains, $[ij]_{\mathrm{OSV}} = [i]_{\mathrm{OSV}} \cup [j]_{\mathrm{OSV}}$. Since the OSVs in $[i]_{\mathrm{OSV}}$ and $[j]_{\mathrm{OSV}}$ are mutually non-orthogonal and may be linearly dependent, the orbitals in the domain $[ij]_{\mathrm{OSV}}$ must be orthogonalized and thus become pair-specific. Subsequently they are made pseudo-canonical, yielding a domain $[ij]_{\text{PC-OSV}}$.

Although a (near) linear scaling OSV-LCCSD(T) method has been implemented [166, 167], this has not been very successful for two reasons: First, the integral transformations are quite complicated and often more expensive than with PAOs. Second, even though the OSVs are near optimal for describing the electron correlation in a single orbital, they are much less well suited for describing inter-orbital correlations and long-range correlations. Therefore, the threshold $T^{\mathrm{occ}}_{\mathrm{OSV}}$ must be chosen rather small (10^{-9}) in order to obtain accurate results. This yields pair domains that are two to three times larger than the PNO domains, and consequently the computational effort for solving the LCCSD equations is at least one order of magnitude larger than with PNOs. Perhaps even more important, the number of 3-external and 4-external integrals is much larger than in the PNO case.

However, OSVs can be successfully used at an intermediate stage to generate the PNOs [146, 147]. In this approach semi-canonical amplitudes T^{ii}_{rs} are computed in the PC-PAO orbital domains $[i]_{\text{PC-PAO}}$ and used to generate the PC-OSVs. This leads to a significant reduction of the orbital domain sizes. For each LMO, a transformation matrix $\mathbf{Q}^{i}_{\tilde{r}a}$ (PAO → PC-OSV) is stored. Next, OSV pair domains are generated and transformed to pseudo-canonical domains $[ij]_{\text{PC-OSV}}$ (transformation matrices $\mathbf{W}^{ij}$). The integrals $\mathbf{K}^{ij}$ are first computed in the PAO basis and subsequently transformed to the PC-OSV basis. This can be done on the fly using the transformation matrices $\mathbf{Q}^{i}$, $\mathbf{Q}^{j}$, and $\mathbf{W}^{ij}$. Finally, semi-canonical amplitudes $\mathbf{T}^{ij}_{\text{PC-OSV}}$ are calculated and from these the PNOs, just as in the PAO-PNO method outlined in the previous section. The whole process can be summarized as follows:

$$\mathrm{AO} \xrightarrow{\mathbf{P}} [i]_{\mathrm{PAO}} \xrightarrow{\mathbf{Q}^{i}} [i]_{\text{PC-OSV}}, \tag{1.68}$$

$$[ij]_{\mathrm{OSV}} = [i]_{\text{PC-OSV}} \cup [j]_{\text{PC-OSV}}, \tag{1.69}$$

$$[ij]_{\mathrm{OSV}} \xrightarrow{\mathbf{W}^{ij}} [ij]_{\text{PC-OSV}} \xrightarrow{\mathbf{V}^{ij}} [ij]_{\mathrm{PNO}} \xrightarrow{\mathbf{U}^{ij}} [ij]_{\text{PC-PNO}}. \tag{1.70}$$

The last three steps are exactly as in equation (1.65), in which the OSV intermediates are skipped. The advantage of this stepwise approach is that the OSV pair domains are significantly smaller than the PAO pair domains, and therefore the computational effort for the transformations in equation (1.70) (which is dominated by the diagonalizations and depends cubically on the domain sizes) is significantly reduced as compared to equation (1.65). Furthermore, the memory requirements for the storage of the transformation matrices $\mathbf{V}^{ij}$ (which in this case transform from the OSV to the PC-PNO pair domains)

are much smaller. This is important for the parallel implementation, in which all data are kept in distributed high-speed memory (cf. Section 1.12.2).

1.7 Choice of Domains

For the accuracy of local correlation methods, the careful choice of domains is essential. In this section, we will summarize how in our current program the PAO, OSV, and PNO domains are chosen.

The PAO orbital domains are selected in a 2-step procedure: first, relatively small *primary domains* are chosen based on IBO partial charges with a threshold T_{LMO} (default 0.2). Typically, this includes only one center for a lone pair, two centers for σ and isolated π bonds, and two to three centers for conjugated or aromatic π bonds. However, these domains are too small for high-accuracy calculations. Therefore, in a second step, *extended domains* are generated which include all atoms that are bound to any atom in the primary domain. Centers are considered to be bound if the bond length is smaller than 1.2 × the sum of the atomic radii. This can be repeated by including all centers that are bound to any atom in the previous extension shell. The advantage of the connectivity criterion `IEXT` is its independence of the atomic types, since the atomic radii are directly related to the bond lengths. In addition, a distance criterion `REXT` is used and all centers that are within a radius `REXT` of any center in the primary domain are included. This ensures that atoms which happen to be close to an atom in the primary domain without being directly bound (e.g., at transition states or in molecular complexes) are also included in the extended domains. The default is to include two shells of neighbors (`IEXT=2`), and a radius of `REXT=5` (distances in a_0). In order to avoid distance criteria, Neese *et al.* [56] have recently proposed a criterion based on the differential overlap of LMOs and PAOs, but so far there is no evidence that this works better than our simple scheme. Alternatively, a completeness criterion has been described by Boughton and Pulay [200], but this also requires a ranking of the centers according to partial charges of the LMOs and is not well suited to define extended domains. Energy related criteria to define PAO pair domains have also been proposed [26, 201], but have rarely been used so far.

Extensive tests [147] have shown that an OSV threshold of 10^{-9} (or smaller) is necessary in order not to spoil the accuracy of the subsequent PNO calculation. But even with this small threshold, the OSV pair domains are typically three times smaller than the default PAO domains. This significantly speeds up the PNO generation and reduces the memory requirements.

The convergence of the correlation energy with the PNO threshold has already been demonstrated in Section 1.6.3. We have chosen a default threshold $T_{\mathrm{PNO}}^{\mathrm{occ}} = 10^{-8}$. It turned out, however, that this is insufficient for rather distant pairs. It may then happen that no PNOs are selected at all for such pairs, and this in turn affects the long-range dispersion energy. We have therefore introduced an additional energy criterion. After diagonalizing the pair density matrix, the orthogonal transformation matrix $\mathbf{V}^{ij}$ is used to transform the amplitudes $\mathbf{T}^{ij}$ and integrals $\mathbf{K}^{ij}$ into the PNO basis (without a further domain approximation, i.e., $\mathbf{V}^{ij}$ is a square matrix). Then, the PNO pair correlation energies $E_{\mathrm{corr}}^{\mathrm{PNO}}$ can be computed by adding one PNO after the other (in the order of decreasing pair natural occupation numbers), until a certain fraction of the PC-PAO (or PC-OSV if OSVs are used) pair energy is reached. The default energy threshold is

Table 1.3 Domain sizes and correlation energies relative to canonical MP2 (in %) for various LMP2 calculations.

	Average domain sizes				Relative LMP2 correlation energies			
Molecule	**PAO**	**OSV**	**PNO[a]**	**PNO[b]**	**PAO**	**OSV**	**PNO[a]**	**PNO[b]**
Testosterone	513.5	204.9	73.3	64.3	99.868	99.815	99.794	99.746
$C_{52}O_6H_{48}$	493.8	219.8	66.7	58.9	99.884	99.839	99.813	99.770
Nonactin	469.2	191.8	57.4	51.3	99.873	99.830	99.809	99.768
Elaiophylin	500.0	193.5	57.1	50.2	99.859	99.808	99.793	99.745

Basis set: cc-pVTZ, IEXT = 2, $T_{\mathrm{OSV}} = 10^{-9}$, $T_{\mathrm{PNO}}^{\mathrm{occ}} = 10^{-8}$, $T_{\mathrm{PNO}}^{\mathrm{en}} = 0.997$.
[a]Using PC-PAO amplitudes for PNO generation.
[b]Using PC-OSV amplitudes for PNO generation.

$T_{\mathrm{PNO}}^{\mathrm{en}} = 0.997$. This ensures that, for all pairs, at least 99.7% of the OSV pair correlation energies are obtained, even if the pair energies and natural occupation numbers are very small. One could of course set this threshold to 0.999 to reduce the error of the PNO domains, but this would increase the domains of distant pairs more than necessary.

Table 1.3 shows for some molecules the average PAO, OSV, and PNO pair domain sizes, the correlation energies (in percent relative to the canonical calculations) for PAO-LMP2, OSV-LMP2, and PNO-LMP2 calculations. In all cases, the same PAO orbital domains (`IEXT=2`) have been used. The PNOs are either generated from PC-PAO amplitudes or PC-OSV amplitudes. The corresponding timings are shown in Table 1.4. The average PAO pair domain sizes are for this basis (cc-pVTZ) around 500, and with these domains about 99.87% of the canonical correlation energy is recovered. The intermediate OSV step ($T_{\mathrm{OSV}} = 10^{-9}$) reduces the domain sizes to about 200, and this causes a 0.05% loss of correlation energy. The transformation from PAOs to PNOs ($T_{\mathrm{PNO}} = 10^{-8}$) reduces the correlation energy by about 0.07% and the domain sizes by one order of magnitude. Comparison of the last two columns of the table shows that the intermediate use of OSVs leads overall to a loss of 0.04–0.05% of the correlation energy, yielding in total

Table 1.4 Elapsed times for the various LMP2 calculations in Table 1.3 (excluding HF), using 10 cores of Xeon E5-2660 v3 @ 2.60GHz processors in one compute node.

			Elapsed times			
Molecule	**AOs**	**val**	**PAO**	**OSV**	**PNO[a]**	**PNO[b]**
Testosterone	1022	58	1711.2	164.9	122.7	63.7
$C_{52}O_6H_{48}$	2412	146	8557.5	1039.7	434.1	264.1
Nonactin	2456	148	6311.6	627.1	339.7	207.7
Elaiophylin	3392	206	13688.6	1279.7	668.5	392.2

[a]Using PC-PAO amplitudes for PNO generation.
[b]Using PC-OSV amplitudes for PNO generation.

about 99.75% of the canonical correlation energy. The elapsed time is reduced by roughly a factor of 2 and the memory usage by about 30%.

The 99.75% percent of correlation energy obtained with our default parameters is still below our goal to reproduce the canonical energy within 0.1%. Lowering the PNO threshold to 10^{-9} increases the PNO domains by about 20 orbitals, but improves the PNO-LMP2 correlation energy only by typically 0.05%. The remaining error is mainly due to the PAO domain approximation. Increasing the PAO domains further is possible but would significantly increase the computational effort for the integral transformation. However, as will be demonstrated in Section 1.11, a much better solution is to include explicitly correlated terms. This will reduce both the basis set incompleteness error as well as the domain error to negligible values and makes it possible to use even smaller PAO domains.

Finally, it is worthwhile to mention that for all three local MP2 methods, that is, PAO-LMP2, OSV-LMP2 and PNO-LMP2, Abelian point group symmetry can be used, provided the occupied orbitals localize in a symmetry-equivalent fashion [33]. This not only speeds up the calculation, but more importantly also reduces the memory requirements significantly.

1.8 Approximations for Distant Pairs

In this section, we will consider approximations for the integrals $(ai|bj)$ for distant pairs ij. We will assume that the four orbitals i, j, a, b are all local, and that $a \in [i]$, $b \in [j]$ are close to $|i\rangle$ and $|j\rangle$, respectively.

The integral $(ai|bj)$ describes the Coulomb interaction of the two local effective charge distributions $\rho_{ai}(\mathbf{r}_1) = \phi_a(\mathbf{r}_1)\phi_i(\mathbf{r}_1)$ and $\rho_{bj}(\mathbf{r}_2) = \phi_b(\mathbf{r}_2)\phi_j(\mathbf{r}_2)$, cf. equation (1.11). In general, Coulomb interactions of two non-overlapping and distant charge distributions can be described by a bipolar multipole expansion. Due to the orthogonality of the virtual and occupied orbitals, the charge distributions carry no charge, that is, $\int \rho_{ai}(\mathbf{r})d\mathbf{r} = 0$, $\int \rho_{bj}(\mathbf{r})d\mathbf{r} = 0$, and therefore the lowest-order contribution is the dipole–dipole interaction.

Charge-transfer type integrals $(ai|bj)$ with $a, b \in [i]$ or $a, b \in [j]$ as well as exchange type integrals with $a \in [j], b \in [i]$ decay exponentially with the distance of the local orbitals $|i\rangle$ and $|j\rangle$ and will be neglected. The effect of this approximation will be demonstrated later on.

1.8.1 Bipolar Multipole Approximations of Electron Repulsion Integrals

In the following, we will briefly summarize the theory for the bipolar multipole approximations as implemented in our program [12, 13]. We use cartesian multipole moment operators rather than traceless multipole operators as in other formulations [85, 202]. At least for low multipole orders this is simple and efficient.

Let $\mathbf{R}_i$ and $\mathbf{R}_j$ be the charge centers of two charge distributions, and $\mathbf{R} = \mathbf{R}_j - \mathbf{R}_i$ the vector between them. Since charge centers of the distributions $\rho_{ai}(\mathbf{r})$ and $\rho_{bj}(\mathbf{r})$ cannot be determined directly, we will use the charge centers of the two LMOs, $\mathbf{R}_i = \langle i|\mathbf{r}|i\rangle$ and $\mathbf{R}_j = \langle j|\mathbf{r}|j\rangle$. The distance between the charge centers is $R = |\mathbf{R}|$, and the unit vector in

direction of $\mathbf{R}$ is denoted $\hat{\mathbf{R}} = \mathbf{R}/R$. Let $\mathbf{r}_1$ and $\mathbf{r}_2$ be the coordinates of the two electrons in the global coordinate system, and $\bar{\mathbf{r}}_1$ and $\bar{\mathbf{r}}_2$ the coordinates of the two electrons relative to the corresponding charge centers, that is, $\bar{\mathbf{r}}_1 = \mathbf{r}_1 - \mathbf{R}_i$ and $\bar{\mathbf{r}}_2 = \mathbf{r}_2 - \mathbf{R}_j$. We have to keep in mind that $\bar{\mathbf{r}}_1$ depends on the charge center $\mathbf{R}_i$ and $\bar{\mathbf{r}}_2$ on the charge center $\mathbf{R}_j$. Let further $\hat{\mathbf{r}} = (\bar{\mathbf{r}}_2 - \bar{\mathbf{r}}_1)/R$ and $\hat{r} = |\hat{\mathbf{r}}|$.

The vector between the two electrons is

$$\mathbf{r}_{12} = \mathbf{r}_2 - \mathbf{r}_1 = R(\hat{\mathbf{R}} + \hat{\mathbf{r}}). \tag{1.71}$$

The Coulomb operator can then be expressed as

$$\frac{1}{r_{12}} = \left[(\mathbf{r}_{12})^2\right]^{-\frac{1}{2}} = \frac{1}{R}\left[1 + x\right]^{-\frac{1}{2}}, \tag{1.72}$$

where

$$x = 2\hat{\mathbf{R}}\hat{\mathbf{r}} + \hat{r}^2. \tag{1.73}$$

Expanding $(1 + x)^{-\frac{1}{2}}$ in a Taylor series at $x = 0$ yields

$$\frac{1}{r_{12}} = \frac{1}{R}\sum_{k}^{\infty} c_k x^k \tag{1.74}$$

with coefficients

$$c_k = \left[\frac{1}{k!}\frac{d^k}{dx^k}(1 + x)^{-\frac{1}{2}}\right]_{x=0} = (-1)^k \frac{1 \cdot 3 \cdots 2k - 1}{2 \cdot 4 \cdots 2k}. \tag{1.75}$$

This Taylor series converges for $x < 1$, which should be fulfilled if R is sufficiently large, cf. equation (1.73).

Inserting the definition of x into equation (1.74) we can write the Coulomb operator in the general form

$$\frac{1}{r_{12}} = \sum_{n=0}^{\infty} \frac{1}{R^{n+1}} \sum_{m=0}^{n} V_{m,n-m}(\bar{\mathbf{r}}_1, \bar{\mathbf{r}}_2, \hat{\mathbf{R}}). \tag{1.76}$$

Truncating the expansion at $n = p + 1$ and integrating with the charge distributions, we obtain a series of integral approximations

$$\begin{aligned}(ai|bj)^{(p)} = &\sum_{n=2}^{p+1} \frac{1}{R^{n+1}} \sum_{m=1}^{n-1} \int d\mathbf{r}_1 \; \rho_{ai}(\mathbf{r}_1) \\ &\times \int d\mathbf{r}_2 \; \rho_{bj}(\mathbf{r}_2) V_{m,n-m}(\bar{\mathbf{r}}_1, \bar{\mathbf{r}}_2, \hat{\mathbf{R}}).\end{aligned} \tag{1.77}$$

Since our effective charge densities carry no charge, there are no contributions for $n = 0$ and $n = 1$, and the first non-vanishing term is $n = 2$. p is the highest order of multipole operators involved. With $p = 1$ only dipole operators (first moments) are needed, $p = 2$ also includes second moments, and so on.

It is straightforward to write down general expressions for $V_{m,n-m}$, which contain the contributions of powers of $\bar{\mathbf{r}}_1$ and $\bar{\mathbf{r}}_2$ with a fixed total power n (see Appendix B). The simplest approximation is obtained for $p = 1$ ($n = 2$):

$$\begin{aligned} V_{1,1}(\bar{\mathbf{r}}_1, \bar{\mathbf{r}}_2, \hat{\mathbf{R}}) &= -2c_1 \bar{\mathbf{r}}_1 \cdot \bar{\mathbf{r}}_2 - 8c_2(\hat{\mathbf{R}} \cdot \bar{\mathbf{r}}_1)(\hat{\mathbf{R}} \cdot \bar{\mathbf{r}}_2) \\ &= \bar{\mathbf{r}}_1 \cdot \bar{\mathbf{r}}_2 - 3(\hat{\mathbf{R}} \cdot \bar{\mathbf{r}}_1)(\hat{\mathbf{R}} \cdot \bar{\mathbf{r}}_2). \end{aligned} \tag{1.78}$$

Integration over the charge densities yields

$$\begin{aligned} (ai|bj)^{(1)} = \frac{1}{R^3} \big[&\langle a|\mathbf{r}_1|i\rangle \cdot \langle b|\mathbf{r}_2|j\rangle \\ &-3(\hat{\mathbf{R}} \cdot \langle a|\mathbf{r}_1|i\rangle)(\hat{\mathbf{R}} \cdot \langle b|\mathbf{r}_2|j\rangle)\big] . \end{aligned} \tag{1.79}$$

Here we have used that due to the orthogonality of the virtual and occupied orbitals, $\langle a|i\rangle = 0$; the dipole moment integrals are origin-independent, since $\langle a|\bar{\mathbf{r}}_1|i\rangle = \langle a|\mathbf{r}_1 - \mathbf{R}_i|i\rangle = \langle a|\mathbf{r}_1|i\rangle$. $\langle a|\mathbf{r}_1|i\rangle$ denotes the dipole vector $(\langle a|x_1|i\rangle, \langle a|y_1|i\rangle, \langle a|z_1|i\rangle)$, and $\langle a|\mathbf{r}_1|i\rangle \cdot \langle b|\mathbf{r}_2|j\rangle$ the scalar product of the two vectors. This is called the dipole–dipole approximation. Note that we only need to compute and store the integrals for $a \in [i]$ and $b \in [j]$, and therefore the memory demand is low, even if higher multipole orders are included.

In some earlier works [54, 147] also a simplified form of the dipole–dipole approximation

$$(ai|bj) \approx \frac{\sqrt{2}}{R^3} \langle a|\mathbf{r}|i\rangle \cdot \langle b|\mathbf{r}|j\rangle \tag{1.80}$$

has been used. The differences between the results obtained with this or equation (1.79) are rather small. In this work, we will only use equation (1.79) which is formally more accurate.

Equation (1.79) can also be written as

$$(ai|bj)^{(1)} = \sum_{\alpha,\beta} M_{ai}^{(1,\alpha)} A_{\alpha,\beta}^{(1,1)} M_{bj}^{(1,\beta)}, \tag{1.81}$$

where $\alpha, \beta \in \{x, y, z\}$, $M_{ai}^{(1,\alpha)} = \langle a|\hat{\alpha}|i\rangle$ are the dipole integrals, and $\mathbf{A}^{(1,1)}$ is the dipole–dipole *interaction matrix*

$$A_{\alpha,\beta}^{(1,1)}(\hat{\mathbf{R}}) = \delta_{\alpha\beta} - 3\hat{R}_\alpha \hat{R}_\beta. \tag{1.82}$$

This formalism can be extended to any higher order, and the total approximation of the integrals can be written as

$$\begin{aligned} (ai|bj)^{(p)} \approx &\sum_{n=2}^{p+1} \frac{1}{R^{n+1}} \sum_{m=1}^{n-1} \\ &\times \sum_{\mu\nu} M_{ai}^{(m,\mu)}(\mathbf{R}_i) A_{\mu\nu}^{(m,n-m)}(\hat{\mathbf{R}}) M_{bj}^{(n-m,\nu)}(\mathbf{R}_j), \end{aligned} \tag{1.83}$$

where now μ runs over the $(m+1)(m+2)/2$ unique cartesian multipole moment components of order m and $M_{ai}^{(m,\mu)}(\mathbf{R}_i)$ are the integrals over these operator components evaluated at the origin $\mathbf{R}_i$. For example, for $m = 2$ the sum over μ runs over the six components of the second moment operators: xx, xy, xz, yy, yz, zz. The sum over ν is

restricted accordingly. Note that for $p > 1$, this approximation does not include interactions of the highest multipoles with each other. For example, the $p = 3$ approximation includes the dipole–dipole, dipole–quadrupole, quadrupole–quadrupole, and dipole–octupole interactions, but the octupole–octupole interaction contributes only for $p = 4$.

The higher-order multipole moments depend on the origin $\mathbf{R}_i$ at which they are evaluated. Using $\mathbf{R}_i = (X_i, Y_i, Z_i)$ and $\mathbf{r} = (x, y, z)$, the integral $M_{ai}^{(m,\alpha)}(\mathbf{R}_i)$ can be written as

$$M_{ai}^{\{l_x,l_y,l_z\}}(\mathbf{R}_i) = \int (x - X_i)^{l_x}(y - Y_i)^{l_y}(z - Z_i)^{l_z}\rho_{ai}(\mathbf{r})d\mathbf{r}, \tag{1.84}$$

where $\{l_x, l_y, l_z\} \equiv (m, \alpha)$ with $m = l_x + l_y + l_z$ defines the operator component. For example, for the operator xxy, we have $m = 3$ and $l_x = 2$, $l_y = 1$, $l_z = 0$. In order to compute all integrals $(ai|bj)$, we need the multipole operators at all charge centers $\mathbf{R}_i$. Fortunately, if one has computed all multipole operators up to a given order at some origin $\mathbf{R}_0$, they can be shifted to any other position. Multiplying out equation (1.84) yields

$$\begin{aligned} M_{ai}^{\{l_x,l_y,l_z\}}(\mathbf{R}_i) = &\sum_{m_x=0}^{l_x} f_{m_x} \sum_{m_y=0}^{l_y} f_{m_y} \sum_{m_z=0}^{l_z} f_{m_z} \\ &\times M_{ai}^{\{l_x-m_x,l_y-m_y,l_z-m_z\}}(\mathbf{R}_0), \end{aligned} \tag{1.85}$$

where

$$f_{m_x} = \binom{l_x}{m_x} [X_0 - X_i]^{m_x}. \tag{1.86}$$

Similar definitions hold for f_{m_y} and f_{m_z}.

Closed-form expressions for the above formalism up to any order p have been derived and implemented by Hetzer *et al.* [12] and applied in PAO-LMP2 calculations. Increasing the order p improves the accuracy at long range, but leads to faster divergence at short range. Hetzer *et al.* therefore recommended to truncate the expansion at $p = 3$, which gives the best compromise of stability, accuracy, and efficiency. For technical reasons, the general program cannot be used in our current PNO-LMP2 program. We have therefore re-implemented the approximation up to $p = 3$; the required explicit expressions can be found in Appendix B.

A further improvement is possible by splitting the Coulomb operator into a short-range and a long-range part [13]. The integrals over the short range part, which decays quickly, are evaluated exactly. Effective screening techniques can be used to speed up this part of the calculation. The long-range part is treated by multipole approximations, which are then always convergent, and also the charge-transfer and exchange-type integrals can be included. The description of this method is beyond the scope of the current chapter and we refer to the original publication [13] for further details.

1.8.2 Approximations of Distant Pair Energies

In the following, we will assume that $|a\rangle$ and $|b\rangle$ are pseudo-canonical, with $|a\rangle \equiv |a^i\rangle$ and $|b\rangle \equiv |b^j\rangle$. It is possible to use either PC-PAO or PC-OSV domains, but except

Table 1.5 PAO-LMP2 intermolecular interaction energy of the ethylene dimer (in mE_h) computed at various multipole orders. The two molecules are displaced by R_{displ} (in Å) perpendicular to the molecular planes. The last line shows the PAO-LMP2 result without multipole approximation.

	R_{displ}		
p	4	5	6
1	−1.1991	−0.3500	−0.1232
2	−1.6055	−0.4335	−0.1447
3	−1.9825	−0.4913	−0.1569
4	−2.3366	−0.5121	−0.1593
5	−3.2181	−0.5363	−0.1608
Exact	−2.0689	−0.5257	−0.1613

Basis set: aug-cc-pVTZ.

for Table 1.5 we will only present results obtained with PC-OSVs using a threshold $T_{\text{OSV}} = 10^{-9}$.

Using the multipole approximations described in the previous section, the semi-canonical LMP2 pair energies (cf. equation 1.20) can be evaluated on the fly without storing the integrals. This is very fast, even for very large molecules. It is therefore convenient to compute the pair energies for all pairs for which $R_{ij} > R_{\text{min}}$ (using e.g., $R_{\text{min}} = 3\ a_0$) and then select those for which $E_{ij}^{\text{sc}} < T_{\text{dist}}$ as distant pairs. All remaining pairs are fully included in the LMP2 calculation. The approximated distant pair energies are summed up to the total distant pair energy $E_{\text{dist}}^{\text{sc}}$, which is added to the final LMP2 energy. The default threshold for selecting distant pairs is $T_{\text{dist}} = 10^{-6}\ E_{\text{h}}$.

Alternatively, a better approximation is obtained by storing the integrals $(ai|bj)$, and optimizing the corresponding amplitudes and pair energies iteratively along with all other pairs. For the multipole approximation of distant pairs, we use asymmetric OSV domains $a \in [i]_{\text{OSV}}$ and $b \in [j]_{\text{OSV}}$, as explained above. Each of these OSV domains typically comprise 100–200 orbitals, and in this large basis a full optimization of the OSV amplitudes would be very expensive. However, one can use the semi-canonical OSV distant pair amplitudes to determine for each distant pair PNO domains $[i]_{\text{PNO}}$ and $[j]_{\text{PNO}}$, and in most cases, only three to six orbitals in these domains are sufficient to recover more than 99.9% of the OSV distant pair energy. The additional cost for including the distant pairs in the iterative LMP2 optimization then becomes quite small. More details have been given elsewhere [203].

The corresponding distant pair energy will be denoted $E_{\text{dist}}^{\text{it}}$. Table 1.5 shows the convergence of the PAO-LMP2 interaction energy with the multipole order p for the ethylene dimer. The two molecules are parallel to each other and displaced by R_{displ} (in Å) perpendicular to the molecular planes. The domains in each C_2H_4 molecule include all PAOs at the corresponding molecule (`IEXT=2`), and all intermolecular pairs are treated as distant. The amplitudes are optimized iteratively. The table demonstrates that the multipole expansion diverges at high orders at $R_{\text{displ}} = 4$ Å, but converges nicely for $R_{\text{displ}} = 6$ Å. As already pointed out in Ref. [12], the dipole–dipole approximation

Table 1.6 PNO-LMP2 distant pair energies (in mE_h) with different distant pair approximations. The numbers over the columns are the multipole orders p used. NOEXCH means that all integrals are computed exactly, but charge-transfer and exchange-type integrals are neglected for distant pairs. FULL means that no distant pair approximations have been applied.

		Semi-canonical			Iterative				
Molecule	**Distant pairs**	**1**	**2**	**3**	**1**	**2**	**3**	**NOEXCH**	**FULL**
$T_{dist} = 10^{-5}\ E_h$									
Ester	1157	−2.39	−3.08	−3.47	−2.80	−3.62	−4.08	−4.27	−5.10
Precursor	1661	−2.96	−3.69	−4.01	−3.42	−4.29	−4.67	−4.80	−5.61
Auamin	4812	−10.08	−12.79	−13.58	−11.45	−14.31	−15.54	−15.56	−18.30
$T_{dist} = 10^{-6}\ E_h$									
Ester	598	−0.18	−0.21	−0.22	−0.21	−0.25	−0.26	0.27	−0.31
Precursor	951	−0.31	−0.36	−0.36	−0.36	−0.42	−0.42	0.43	−0.47
Auamin	2355	−0.88	−1.00	−1.02	−1.01	−1.15	−1.18	−1.19	−1.28

Basis set: VTZ-F12, IEXT=2.

significantly underestimates the interaction energy; even for $R_{\text{displ}} = 6$ Å, the error still amounts to −24%. This error is reduced to −10% and −3% for $p = 2$ and $p = 3$, respectively. Even for $R_{\text{displ}} = 4$ Å, the error for $p = 3$ is only −4%.

Distant pair energies computed with the semi-canonical (non-iterative) and iterative multipole approximation for larger molecules are presented in Table 1.6 for $p = 1, 2, 3$ and distant pair selection thresholds of $T_{\text{dist}} = 10\ \mu E_h$ and $T_{\text{dist}} = 1\ \mu E_h$. In all cases, the distant pairs have been selected using the semi-canonical $p = 1$ pair energies, that is, the number of distant pairs is independent of the approximation applied (with the more accurate $p = 3$ approximation less distant pairs would be selected and the results would become more accurate, but since we intended to compare the pure effect of the integral approximations this has not been used).

For comparison, also distant pair energies computed without multipole approximations are shown. In the first case, denoted NOEXCH, the charge-transfer and exchange type integrals are neglected, exactly as in the multipole approximations, but the remaining dispersion-type integrals are computed exactly (using density fitting). In the second case (FULL), all pairs are fully included in the LMP2 calculation without further approximations. Table 1.6 shows that with a large threshold of 10 μE_h, the approximate distant pair energies are in all cases significantly underestimated. There are three sources of errors: (i) the neglect of charge-transfer and exchange-type excitations for distant pairs (NOEXCH); (ii) the non-iterative semi-canonical approximation (SC) ; and (iii) the multipole approximation for the integrals (MLTP). The largest error (about −15%) arises from the NOEXCH approximation; the error caused by the SC approximation is also significant (−10% to −15%), while the error of the multipole approximation itself decreases quickly with p and is in all cases below 5% for $p = 3$. For example, for the Auamin molecule (cf. Section 1.1) the MLTP errors (relative to NOEXCH) amount to −26.4%, −8.0%, and −0.1% for $p = 1, 2, 3$, respectively. In total, the semi-canonical multipole approximation for $p = 1$ recovers only 55% of the exact LMP2 distant pair energy for Auamin. For the

Table 1.7 Total PNO-LMP2 reaction energies ΔE and distant pair contributions ΔE_{dist} without multipole approximations, and errors of the total reaction energies caused by various multipole approximations. All values in kJ mol^{-1}. The numbers over the columns correspond to the multipole order applied.

	PNO-LMP2		Errors of reaction energies						
	Reaction energies		Semi-canonical			Iterative			
Reaction	ΔE	ΔE_{dist}	1	2	3	1	2	3	NOEXCH
$T_{\text{dist}} = 10^{-5}\ E_{\text{h}}$									
I	−21.0	−3.2	1.8	1.4	1.2	1.5	0.9	0.7	0.5
II	18.2	4.5	−1.1	−0.7	−0.7	−0.6	−0.1	−0.1	−0.3
III	239.7	22.0	−10.2	−7.1	−6.2	−7.9	−4.1	−2.9	−2.9
$T_{\text{dist}} = 3 \times 10^{-6}\ E_{\text{h}}$									
III	239.7	6.9	−2.7	−1.9	−1.8	−1.8	−0.8	−0.6	−0.6
$T_{\text{dist}} = 10^{-6}\ E_{\text{h}}$									
III	239.7	2.0	−0.6	−0.5	−0.4	−0.4	−0.1	−0.1	−0.1

Basis set: VTZ-F12, IEXT=2.

other two molecules, the error is even larger (47% is recovered for the Ester and 53% for the Precursor).

For the smaller threshold (1 μE_{h}), the errors caused by the NOEXCH approximation are reduced, but still amount to about −7% for Auamin and −13% for the Ester. The relative errors of the other approximations are quite similar as for the larger threshold. Of course, the absolute errors are now reduced by one order of magnitude.

The errors in reaction energies caused by the distant pair approximations relative to the full LMP2 values are listed in Table 1.7 for three reactions involving the same molecules and thresholds. For the largest system (reaction **III**), the total contribution of the distant pairs to the dissociation energy amounts to 22 kJ mol^{-1} and 2.0 kJ mol^{-1} for the thresholds of 10 and 1 μE_{h}, respectively. This demonstrates that the numerous but very small energy contributions of distant pairs in large systems are by no means negligible when summed up. The errors in the reaction energies caused by the simple semi-canonical dipole–dipole approximations are −10.2 and −0.6 kJ mol^{-1}, respectively. With the iterative $p = 3$ approximations, these errors are reduced to −2.9 and −0.1 kJ mol^{-1}. Using the small threshold of 1 μE_{h}, the errors of the reaction energies for **I** and **II** are negligibly small (below 0.2 kJ mol^{-1}) and therefore not shown.

We conclude that the simple dipole–dipole approximation should only be applied with a small threshold T_{dist}; our default value of 1 μE_{h} is a safe choice. Larger thresholds should only be used with higher multipole orders (preferably $p = 3$). Including the distant pairs iteratively reduces the errors typically be a factor of 2. However, if *all* distant pairs are included in the iterations, linear scaling is no longer achieved in the LMP2. The linear scaling behavior could be kept by neglecting very distant pairs entirely, or by treating them non-iteratively.

1.9 Local Coupled-Cluster Methods (LCCSD)

The LCCSD wave function is defined as

$$\Psi_{\mathrm{CCSD}} = e^{\hat{T}}|0\rangle \tag{1.87}$$

with the cluster operator

$$\hat{T} = \sum_i \sum_{a\in[i]} t_a^i \hat{E}_i^a + \frac{1}{2}\sum_{ij\in P}\sum_{a,b\in[ij]} T_{ab}^{ij}\hat{E}_i^a\hat{E}_j^b. \tag{1.88}$$

Here a, b are virtual orbitals, which, depending on the method, can be PAOs, OSVs, or PNOs, and $[ij]$ denotes the corresponding pair domains. The singles domains $[i]$ are usually taken to be equal to the domains $[ii]$ of the "diagonal" pairs, but this restriction can also be lifted. The sum over pairs ij can be restricted to a pair list P. It is also possible to subdivide this list into different classes, which are then treated at different computational levels, for example, CCSD, CEPA (coupled electron pair approximation), or LMP2. Such pair approximations will be discussed in Section 1.9.1.

The amplitudes are determined by solving the usual LCCSD amplitude equations. Inserting the ansatz (1.87) into the Schrödinger equation, multiplying from the left with $e^{-\hat{T}}$, and projecting from the left with the reference function and the contravariant configurations yields

$$E_{\mathrm{CCSD}} = \langle 0|e^{-\hat{T}}\hat{H}e^{\hat{T}}|0\rangle, \tag{1.89}$$

$$r_a^i = \left\langle \tilde{\Phi}_i^a|e^{-\hat{T}}\hat{H}e^{\hat{T}}|0\right\rangle = 0, \qquad a\in[i], \tag{1.90}$$

$$R_{ab}^{ij} = \left\langle \tilde{\Phi}_{ij}^{ab}|e^{-\hat{T}}\hat{H}e^{\hat{T}}|0\right\rangle = 0, \qquad a,b\in[ij], \tag{1.91}$$

where the contravariant configurations for the single excitations are $|\tilde{\Phi}_i^a\rangle = \frac{1}{2}\hat{E}_i^a|0\rangle$; for the double excitations, they are defined as in LMP2, cf. equation (1.5). The equations can be solved iteratively exactly as described earlier for LMP2. In each iteration the residuals r_a^i and R_{ab}^{ij} have to be computed, and updates of the amplitudes can be obtained using equation (1.19) (and similarly for the singles amplitudes t_a^i).

The residuals r_a^i and R_{ab}^{ij} can be formulated compactly using amplitude and integral matrices. A proper factorization of these equations is important for efficiency and proper scaling, and various formulations have been described in the literature [18, 54, 198, 199]. For easy reference, the equations as implemented in our program are given in Appendix A.

The local coupled cluster correlation energy can generally (for any CC level) be written as

$$E_{\mathrm{corr}}^{\mathrm{CC}} = \sum_{i\geq j\in P} E_{ij} + E_{\mathrm{sing}} + E_{\mathrm{dist}}. \tag{1.92}$$

The pair energies E_{ij} are defined exactly as in LMP2:

$$E_{ij} = (2-\delta_{ij})\sum_{a,b\in[ij]} K_{ab}^{ij}\tilde{T}_{ab}^{ij}, \tag{1.93}$$

and E_{dist} is the energy contribution of the distant pairs, which can be approximated by the multipole treatment as described in Section 1.8. The singles energy contribution E_{sing} can be computed using "dressed" Fock matrix elements $\bar{f}_a^i$ (see Appendix A for their definition):

$$E_{\text{sing}} = 2 \sum_i \sum_{a \in [i]} t_a^i \bar{f}_a^i. \tag{1.94}$$

This can be seen as an orbital relaxation contribution to the Hartree–Fock energy.

The number of integrals needed in LCCSD is significantly larger than in LMP2. In LMP2, one only needs the integrals $(ai|bj)$ for $a, b \in [ij]$. In LCCSD, all other classes of transformed integrals are also required: 0-external $(ik|jl)$, 1-external $(ai|kl)$, 2-external $(ab|ij)$, and $(ai|bj)$, 3-external $(ab|ck)$, and 4-external $(ac|bd)$. For the 4-external integrals, the domains of all four virtual orbitals are the same, that is, $a, b, c, d \in [ij]$. However, for the other integral classes, the domain restrictions are much more complicated. Consider, for example, the 2-external exchange integrals $K_{cd}^{kl} = (ck|dl)$, which occur in several terms of the LCCSD equations. A typical term is

$$[\mathbf{R}^{ij}]_{ab} = \ldots \sum_{kl} \sum_{c \in [ik]} \sum_{d \in [lj]} [\mathbf{S}\mathbf{T}^{ik}]_{ac} [\mathbf{K}^{kl}]_{cd} [\mathbf{T}^{lj}\mathbf{S}]_{db}, \qquad a, b \in [ij]. \tag{1.95}$$

Let us assume that distant pairs are not included in the LCCSD *ansatz*. This means that ij, ik, and jl must be non-distant pairs, and for each ij, the index k must be "close" to i, and l be "close" to j (here "close" means not distant). This makes the list of operators $\mathbf{K}^{kl}$ that contribute to a pair ij asymptotically independent of the molecular size. However, the list of kl can be larger than the list of pairs ij. For a given kl, the indices c, d of K_{cd}^{kl} are restricted to $c \in [ik]$, $d \in [jl]$ for all i, j that are "close" to k and l, respectively. This also limits these indices to a number which is asymptotically independent of the molecular size. Thus, the total number of integrals as well as the computational effort will scale linearly with molecular size, but (i) the prefactors may be huge and (ii) the linear scaling regime be reached very late.

If the PAO basis is used (PAO-LCCSD), the dimension of the matrices $\mathbf{K}^{kl}$ can never become larger than the number of AOs (basis functions). However, in the PNO case (PNO-LCCSD) the total number of PNOs can be much larger than the number of AOs. Since the PNOs are different for each pair, one has to compute a huge number of blocks $\mathbf{K}^{kl}_{[ik,jl]}$, where $[ik, jl]$ denotes the domains of the indices c, d, respectively. However, the PNO domains are typically an order of magnitude smaller than in the PAO case, and therefore the total number of integrals in the PNO basis is usually comparable to that in the PAO basis. The most essential advantage of using PNOs is the small size of the matrix dimensions. Since the matrix multiplications scale cubically with the domain sizes, the evaluation of the above terms is in the PNO basis 2–3 orders of magnitude faster than in the PAO basis.

Similar considerations hold for the overlap matrices. Indicating again the domains of the indices of all matrices in square brackets, our example can be written as

$$\mathbf{R}^{ij}_{[ij,ij]} = \ldots \sum_{kl} \mathbf{S}_{[ij,ik]} \mathbf{T}^{ik}_{[ik,ik]} \mathbf{K}^{kl}_{[ik,lj]} \mathbf{T}^{lj}_{[lj,lj]} \mathbf{S}_{[lj,ij]}. \tag{1.96}$$

This means that one has to compute and store large lists of overlap and integral blocks. The blocks of the overlap matrices are addressed using two pair labels (e.g., ij, ik), the

ones for the integrals by three pair labels kl, ik, lj. Efficient index packing and binary search algorithms are used to retrieve individual blocks. Similar considerations are possible for each individual term in the LCCSD equations.

Despite the enormous savings that are possible by using PNOs, for large molecules and good (at least triple-ζ) basis sets, the total amount of integrals and the computational cost can become exceedingly large if all non-distant pairs are fully included in the LCCSD residual equations. Fortunately, this problem can be alleviated by four further approximations, which take into account the fast decay of various long range contributions:

(i) Treatment of weak pairs at lower computational levels;
(ii) Neglect of terms in the LCCSD equations for weak pairs that cancel at long range;
(iii) Neglect of further integral contributions that decay exponentially with distance;
(iv) Projection approximations.

We refer to (i)–(iii) as "weak pair approximations", and we will briefly discuss these in the following sections.

1.9.1 Weak Pair Approximations

Apart from the distant pair approximations that have been discussed in Section 1.8, a distinction of "strong" and "weak" pairs has been introduced for LCCSD [7, 18, 31]. In these early models, "weak" pair amplitudes and corresponding pair energies were optimized at the LMP2 level and only "strong" pair amplitudes and pair energies were evaluated at the full coupled cluster level, that is, equation (1.92) is replaced by

$$\begin{aligned} E_{\text{corr}}^{\text{LCCSD}} &= E_{\text{sing}} + \sum_{i \geq j \in P_s} E_{ij}^{\text{CC}} + \sum_{i > j \in P_w} E_{ij}^{\text{LMP2}} + E_{\text{dist}} \\ &= E_{\text{sing}} + E_{\text{strong}} + E_{\text{weak}} + E_{\text{dist}} \end{aligned} \tag{1.97}$$

where P_s and P_w denote the lists of strong and weak pairs, respectively. The selection of the pairs in each class can be based either on their LMP2 energy contributions or on distance criteria. The reasoning behind this approximation is that the pair energies decay with R_{ij}^{-6}, and it is assumed that the LMP2 approximation for small weak pair energies does not much affect overall accuracy. Similar approximations were also adopted by Neese *et al.* in their DLPNO-CCSD method [54, 57], but they made the even cruder approximation that weak pair energies are computed using the non-iterative semi-canonical LMP2 approximation.

More recent work has shown, however, that this simple weak pair approximation can lead to unexpectedly large errors [31, 32, 145, 204]. Usually, the total correlation energy is overestimated. This is due to the neglect of the weak pair amplitudes in the residuals for strong pairs, which leads to an overestimation of the strong pair energy. Furthermore, MP2 is well known to overestimate long-range dispersion energies, and therefore the weak pair contribution is often also too large. The first effect can be reduced significantly by including the LMP2 weak pair amplitudes in the LCCSD residuals for strong pairs [26, 31]. But even this approximation may not be sufficient, in particular for systems with many aromatic rings and strong long-range dispersion interactions. An extreme case is the Auamin reaction, as will be demonstrated further below. Since

Table 1.8 Summary of pair classes and pair approximations.

Pair class	Energy criterion	Approximation of residual	Amplitudes included	
			Linear terms	Non-linear terms
Strong	$E_{ij}^{\mathrm{LMP2}} \geq T_{\mathrm{close}}$	Full LCCSD	Up to weak	Up to weak
Close	$T_{\mathrm{close}} > E_{ij}^{\mathrm{LMP2}} \geq T_{\mathrm{weak}}$	Approx. LCCSD[a]	Up to weak	Strong+close
Weak	$T_{\mathrm{weak}} > E_{ij}^{\mathrm{LMP2}} \geq T_{\mathrm{dist}}$	Approx. CEPA-2[a]	Up to weak	–
Distant	$T_{\mathrm{dist}} > E_{ij}^{\mathrm{SC-LMP2d}}$	LMP2(multipole)[b]	–	–

Basis set: VDZ-F12, $T_{\mathrm{LMO}} = 0.2$, $T_{\mathrm{PNO}}^{\mathrm{occ}} = 10^{-8}$.
[a] Approximations described in Section 1.9.2.
[b] LMP2 with non-iterative multipole approximation.

this system is not untypical for "real-life chemistry," it is important to apply higher-order approximations for weak pairs.

In order to keep the computational effort tractable we have therefore split the weak pair class further into "close" and "weak" pairs, leading to the final hierarchy of strong, close, weak, and distant pairs. The classification of the pairs is based on their LMP2 pair energies. A summary of the thresholds and approximations for each class is given in Table 1.8. The default values of the thresholds are (in E_{h}): $T_{\mathrm{dist}} = 10^{-6}$, $T_{\mathrm{weak}} = 10^{-5}$, $T_{\mathrm{close}} = 10^{-4}$. In addition, the non-linear terms in the LCCSD equations can be neglected for weak pairs.

The residuals for close and weak pairs employ approximations in which terms that cancel at long-range are neglected. These approximations will be outlined in the next section.

1.9.2 Long-Range Cancellations of Terms in the LCCSD Equations

In order to devise accurate weak pair approximations, it is important to consider the spatial decay properties of individual terms in the coupled-cluster equations [32, 204]. The contribution of individual terms in the residual to a pair energy can be obtained by using

$$\mathbf{R}^{ij} = \mathbf{K}^{ij} + \mathbf{O}^{ij}, \tag{1.98}$$

where $\mathbf{O}^{ij}$ is the part of the residual which depends on the amplitudes. For the converged LCCSD wave function the residuals vanish, and $\mathbf{K}^{ij} = -\mathbf{O}^{ij}$. Thus, we can rewrite the pair energies in equation (1.93) as

$$E_{ij} = -(2 - \delta_{ij}) \sum_{ab \in [ij]} O_{ab}^{ij} \tilde{T}_{ab}^{ij}. \tag{1.99}$$

The amplitudes $\tilde{T}_{ab}^{ij}$ decay asymptotically with R^{-3}, where R is the distance between the charge centers of orbitals i and j as defined in Section 1.8. There are also faster decaying contributions which contribute at shorter distances, but these contributions will be neglected in the following discussion.

Consider, for example, the contribution of 4-external integrals

$$R_{ab}^{ij} \mathrel{+}= \sum_{cd} (ac|bd) T_{cd}^{ij}. \tag{1.100}$$

As we have seen in Section 1.8, for large R only amplitudes where c is close to i and d is close to j will be significant. Due to the exponential decay of the integrals $(ac|bd)$ with the distances R_{ac} and R_{bd}, it follows that a must also be close to i and b close to j. The largest contributions will arise from $(aa|bb)T_{ab}^{ij}$. Since the charge distributions ρ_{aa} and ρ_{bb} carry charges of 1 (assuming normalized orbitals), the integral $(aa|bb)$ decays as R^{-1}, the residual contribution as R^{-4}, and the energy contribution with R^{-7}. It turns out, however, that these rather slowly decaying terms in the residual equations cancel at long range with other terms. In the following, this will be exemplified for the coupled-cluster doubles (CCD) residual [32].

The linear CCD terms containing slowly decaying integrals are

$$\begin{aligned} R_{ab}^{ij} \mathrel{+}= & \sum_{cd} (ac|bd) T_{cd}^{ij} + \sum_{kl} (ik|lj) T_{ab}^{kl} \\ & - \sum_{kc} \left[T_{ac}^{kj} (cb|ik) + (ac|kj) T_{cb}^{ik} \right]. \end{aligned} \tag{1.101}$$

Equation (1.101) can be split into differently decaying parts

$$R_{ab}^{ij} \mathrel{+}= \mathcal{O}(R^{-4}) + \mathcal{O}(R^{-5}) + \mathcal{O}(R^{-6}), \tag{1.102}$$

where

$$\mathcal{O}(R^{-4}) = T_{ab}^{ij} \left[(aa|bb) + (ii|jj) - (aa|jj) - (ii|bb) \right], \tag{1.103}$$

$$\begin{aligned} \mathcal{O}(R^{-5}) = & \sum_{c \neq b} T_{ac}^{ij} [(aa|cb) - (ii|cb)] + \sum_{c \neq a} [(ac|bb) - (ac|jj)] T_{cb}^{ij} \\ & + \sum_{l \neq j} T_{ab}^{il} [(ii|lj) - (aa|lj)] + \sum_{k \neq i} [(ik|jj) - (ik|bb)] T_{ab}^{kj}. \end{aligned} \tag{1.104}$$

At long-range, the positive and negative contributions in the $\mathcal{O}(R^{-4})$ and $\mathcal{O}(R^{-5})$ parts will cancel, leading to an overall R^{-6} decay for a given pair residual R_{ab}^{ij}, and therefore an overall R^{-9} decay of the contribution to the pair energy E_{ij}. Very similar considerations can be made for the additional terms in the CCSD residual equations. It can be shown that at long range all terms which contain integrals that decay with R^{-1} or R^{-2} cancel in any coupled cluster theory that respects the particle-hole symmetry.

The canceling contributions can be neglected in the close and weak pair residuals, leading to our approximate coupled-cluster treatment for those pairs [32]. The greatest advantage of this approximation is that the 4-external integrals $(ab|cd)$ are not needed for close and weak pairs. Furthermore, the summation $\sum_{kl} (ik|lj) T_{ab}^{kl}$ can be restricted to contributions where ik and jl are strong pairs. This leads to a balanced treatment of terms that are related by the particle-hole symmetry, and, in fact, we found that it improves the accuracy. More generally, approximations in further terms (e.g., those involving single excitations) should always treat contributions that are related by particle-hole symmetries on equal footing.

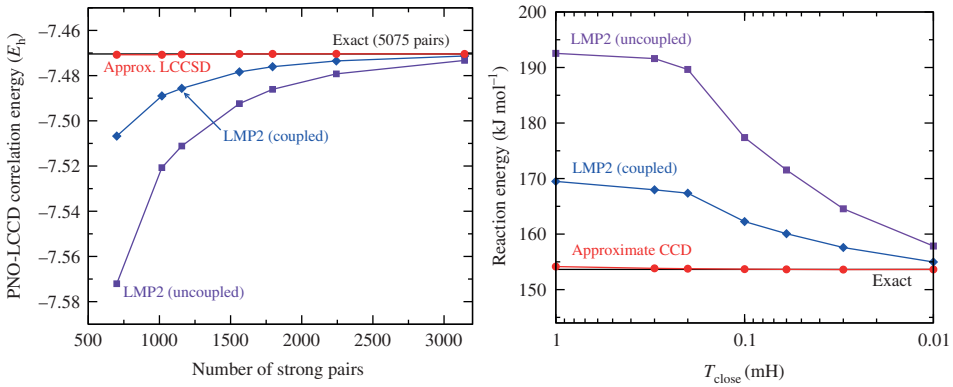


Figure 1.6 Effect of close pair approximations on the correlation and dissociation energies of Auamin. In both cases, distant pairs were excluded from the LCCD ($T_{dist} = 10^{-6}$), and no weak pair approximations were used ($T_{weak} = T_{dist}$). *Left panel*: Correlation energy as a function of the number of strong pairs. The remaining pairs are treated as close pairs. The data points correspond to the thresholds in the other right panel. *Right panel*: Dissociation energy (in kJ mol^{-1}) as a function of T_{close}. Basis set: VDZ-F12, `IEXT=1`. *Source*: Schwilk *et al.* 2015 [32]. Reproduced with permission of AIP Publishing.

In addition, the non-linear terms can be neglected for weak pairs. This corresponds to a linearized coupled-cluster or CEPA-0 method. We use CEPA-2, which differs from CEPA-0 by terms $-E_{ij} \cdot T^{ij}_{ab}$ in the residual R^{ij}_{ab}. Since the weak pair energies are small, the differences of CEPA-2 and CEPA-0 are tiny. Table 1.8 summarizes these approximations.

Figure 1.6 demonstrates for PNO-LCCD how these approximations converge with the thresholds that determine the pair classes. The left panel shows the convergence of the correlation energy of Auamin as a function of the number of strong pairs, and the right panel shows the corresponding convergence of the reaction (dissociation) energy. The data points in the left panel are located at the same thresholds as shown in the right panel, and so this also shows how the number of strong pairs depends on the threshold T_{close}. All remaining pairs (except distant pairs) have been treated as close pairs. For the cases denoted LMP2 (uncoupled) and LMP2 (coupled), the close pair amplitudes and pair energies were optimized in the preceding PNO-LMP2 calculation. In the "uncoupled" case, these are entirely neglected in the residuals for strong pairs, while in the "coupled case," they are included in the residuals (but not reoptimized). These figures demonstrate that in this case, large errors are caused by the use of LMP2 amplitudes and pair energies, and these errors decay very slowly with the threshold T_{close} (similar results are obtained if a distance criterion is used). For the largest threshold ($T_{close} = 1\,mE_h$), the reaction energy is overestimated by nearly 40 kJ mol^{-1}. This is about half of the difference between the pure PNO-LMP2 and PNO-LCCD (without close or weak pair approximations) reaction energies (LMP2 overestimates the reaction energy by about 65 kJ mol^{-1} relative to LCCD). The error is more than halved if the LMP2 amplitudes are included in LCCD residuals for strong pairs. Note that this improvement is solely due to the strong pair energy, and this demonstrates that long-range couplings are very important. Even for the smallest threshold of $T_{close} = 0.01\,mE_h$, the error of LMP2 (uncoupled) still amounts to 5 kJ mol^{-1}. These errors are dramatically

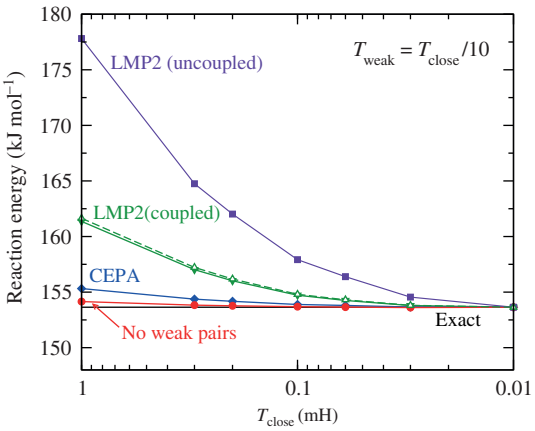


Figure 1.7 Effect of weak pair approximations on the dissociation energy of Auamin (in kJ mol^{-1}) as a function of T_{close}, $T_{weak} = T_{close}/10$. LMP2 (coupled), LMP2 (uncoupled), and approximate LCCD determine how the close pair amplitudes are optimized (see text). Basis set: VDZ-F12, `IEXT=1`. *Source*: Schwilk *et al.* 2015 [32]. Reproduced with permission of AIP Publishing.

reduced if the approximate coupled-cluster method is used for the close pairs. In this case, the error for $T_{close} = 1\,\mathrm{m}E_h$ is reduced to about 2 kJ mol^{-1} and becomes entirely negligible for $T_{close} \leq 0.3\,\mathrm{m}E_h$.

Figure 1.7 demonstrates the effect of the additional weak pair approximation. For simplicity, we have chosen fixed ratios T_{close}/T_{weak} equal to 10, and varied T_{close}. In this case, the close pairs are treated by approximate LCCD, and the weak pairs either by LMP2 (uncoupled), LMP2 (coupled), or CEPA. In the CEPA case, the weak pair amplitudes are included in the strong and close pair residuals, corresponding to LMP2 (coupled). The red curve corresponds to the approximate LCCD curve in the right panel of figure 1.6. The finding is that treating weak pairs by CEPA strongly reduces the error relative to LMP2 (coupled), and for $T_{close} \leq 0.3\,\mathrm{m}E_h$ the error is below 1 kJ mol^{-1}.

Similar results have also been obtained for reactions **I** and **II**. The effects are qualitatively similar, but smaller in magnitude. Details can be found in the supplementary material of Ref. [32]. That the approximate coupled cluster treatment of close and weak pairs also works well if singles are included will be demonstrated in Section 1.11.2 for LCCSD-F12.

1.9.3 Projection Approximations

A further problem in PNO-LCCSD is the large number of integral blocks that have to be computed and stored, see for example equation (1.96) discussed above. Neese *et al.* [48, 49, 54] proposed projection approximations, in which an orbital in a particular domain, for example, $|a^{ik}\rangle$, is projected onto another domain, for example, $[kl]_{PNO}$. This leads to the expansion

$$|a^{ik}\rangle \approx |\tilde{a}^{ik}\rangle = \sum_{c\in[kl]_{PNO}} |c^{kl}\rangle\langle c^{kl}|a^{ik}\rangle = \sum_{c\in[kl]_{PNO}} |c^{kl}\rangle S^{kl,ik}_{ca}. \tag{1.105}$$

It is easily shown that this also minimizes the square deviation $\langle a^{ik} - \tilde{a}^{ik}|a^{ik} - \tilde{a}^{ik}\rangle$. The term in equation (1.96) then becomes

$$R^{ij}_{[ij,ij]} = \ldots \sum_{kl} \mathbf{S}_{[ij,ik]}\mathbf{T}^{ik}_{[ik,ik]}\mathbf{S}_{[ik,kl]}\mathbf{K}^{kl}_{[kl,kl]}\mathbf{S}_{[kl,lj]}\mathbf{T}^{lj}_{[lj,lj]}\mathbf{S}_{[lj,ij]}. \tag{1.106}$$

The number of integrals $\mathbf{K}^{kl}_{[kl,kl]}$ is drastically smaller than the number of all integrals $\mathbf{K}^{kl}_{[ik,lj]}$, but more matrix multiplications and additional S-matrix blocks are needed. Overall, the reduction of data is very significant, and the CPU time is comparable (due to savings in the integral transformation). The projection approximation might look rather crude since the domain $[kl]$ at best partly spans the domains $[ik]$ and $[jl]$. However, we have implemented this approximation optionally for all terms that are quadratic in the amplitudes, and found that the errors are surprisingly small. Detailed tests will be presented elsewhere [205].

Similar projection approximations can be applied to 3-external integrals [54, 57]. For example, the linear contribution of the singles amplitudes to the doubles residual is approximated as

$$R^{ij}_{ab} += \sum_{c\in[j]} (a^{ij}i|b^{ij}c^{j})t^{j}_{c} \approx \sum_{c\in[ij]} (a^{ij}i|b^{ij}c^{ij}) \left[\sum_{d\in[j]} S^{ij,j}_{cd} t^{j}_{d}\right]. \tag{1.107}$$

This should be a good approximation, since in the PAO basis the singles domain $[i]$ is contained in the pair domain $[ij]$ (which is the union of $[i]$ and $[j]$). It is not guaranteed that $[i]_{\mathrm{PNO}}$ is contained in $[ij]_{\mathrm{PNO}}$, but the error will become smaller with decreasing PNO threshold and zero if $T^{\mathrm{occ}}_{\mathrm{PNO}} = 0$. A similar approximation is also possible for the linear 3-external doubles contribution in the singles residual. In fact, we found that the error caused by these approximations is negligible. The big advantage is that only 3-index integrals need to be computed and stored in which all three virtual orbitals belong to the same PNO domain, which leads to significant savings in the memory usage and the CPU time.

In the contributions $\mathbf{T}^{ik}\mathbf{K}(\mathbf{E}^{kj})$ to the doubles residuals (see Appendix A), the 3-external integral contractions

$$\sum_{c\in[j]} (a^{ik}k|b^{ij}c^{j})t^{j}_{c} \approx \sum_{c\in[ij]} (a^{ik}k|b^{ij}c^{ij}) \left[\sum_{d\in[j]} S^{ij,j}_{cd} t^{j}_{d}\right] \tag{1.108}$$

occur. The 3-external integrals $(a^{ik}k|b^{ij}c^{ij})$ still contain two different domains (apart from the third index k). Neese *et al.* have also projected $|a^{ik}\rangle$ to domain $[ij]$. However, this changes the decay behavior of the integrals, since $|a^{ik}\rangle$ contains contributions close to k, but this may not be the case for $|a^{ij}\rangle$, and therefore this approximation might introduce larger errors.

In our current program, the latter approximation and the evaluation and storage of the large sets of 3-external integrals in equation (1.108) is avoided by computing the term as $K^{k\tilde{j}}_{a^{ik}b^{ij}} = (a^{ik}k|b^{ij}\tilde{j})$ where

$$|\tilde{j}\rangle = \sum_{c\in[j]_{\mathrm{PNO}}} |c^{j}\rangle t^{j}_{c} = \sum_{\mu}^{\mathrm{AO}} |\mu\rangle \bar{t}^{j}_{\mu}, \tag{1.109}$$

$$\bar{t}^{i}_{\mu} = \sum_{r\in[j]_{\mathrm{PAO}}} P_{\mu r} \sum_{c\in[j]_{\mathrm{PNO}}} \tilde{V}^{j}_{rc} t^{j}_{c}. \tag{1.110}$$

The integrals can then be computed by a partial integral transformation, just as the integrals K^{kj}_{ab}. However, the transformation must be done in each CCSD iteration. Similarly,

the matrix $\tilde{\mathbf{G}}$, which contains slowly decaying terms (see Appendix A), is computed in each iteration in the AO basis and then transformed to the LMO/PNO basis. This proceeds in close analogy to the computation of a Fock matrix, and local density-fitting approximations can be used to achieve linear scaling of the exchange contribution [206]. Overall, this introduces contributions that scale cubically with the molecular size, but with a very small prefactor.

1.10 Triple Excitations

Local methods to compute the perturbative (T) correction for LCCSD have been described for PAO [16, 17, 19] OSV [167], and PNO [55] methods. Using PAO or OSV virtual orbitals, it is straightforward to define triples domains [*ijk*], which are the union of the three orbital domains. It has been found that the list of triples *ijk* can be restricted so that at least one of the pairs *ij*, *ik*, or *jk* is a strong pair, and the others are strong or close pairs. Furthermore, only strong and close pair amplitudes need to be included in the triples calculation [16, 17]. This leads to linear scaling, and often the calculation of the triples correction takes much less time than the preceding LCCSD calculation. Since in a local orbital basis the Fock matrix is not diagonal, an iterative solution of the triples amplitude equations is in principle required, just as for LMP2. However, it was found that, in most cases, a semi-canonical non-iterative energy correction is accurate enough [16, 17]. Full iterative solutions are also available [17, 19], but much more expensive. The treatment of triples in PNO methods is more involved, since the union of the three pair domains is non-orthogonal, large, and not well suitable. Riplinger *et al.* have proposed to use so-called "triples-natural orbitals" [55]. A detailed description of these methods is beyond the scope of the current article, and the reader is referred to the original publications.

1.11 Local Explicitly Correlated Methods

Electron correlation methods generally suffer from the problem of slow basis set convergence, and very large basis sets are often required to obtain converged results. The slow convergence is due to the fact that the expansion in products of limited 1-electron functions (orbitals) do not describe well the shape of the wave function at small to intermediate values of interelectron distance r_{12}, which should satisfy the electronic wave function cusp condition [207, 208]:

$$\left.\frac{\partial \Psi}{\partial r_{12}}\right|_{r_{12}=0} = \frac{1}{2}\Psi(r_{12}=0). \tag{1.111}$$

This problem can be avoided by including terms in the wave function that depend explicitly on r_{12} and thus can describe the cusp properly [209]. Early implementations used a linear R_{12} correlation factor, and a number of so-called R12-methods were developed [97–108]. It was found later that a Slater-type function $F_{12} \sim \exp(-\gamma r_{12})$ yields much better basis set convergence and numerical stability [109]. This family of methods is called the F12 methods [109–153].

In this section, we will summarize the essential theory in local MP2-F12 and CCSD-F12 methods [142–148] as implemented in Molpro. We will focus on the approximations most suitable for efficient, parallel implementations for PNO based local correlation methods, namely the 3*A and the CCSD-F12x (x = a, b) approximations.

1.11.1 PNO-LMP2-F12

The first-order MP2-F12 wave function can be written as

$$\Psi^{(1)} = \frac{1}{2}\sum_{i,j}^{\text{val}}\left(\sum_{a,b}^{\text{virt}}|\Phi_{ij}^{ab}\rangle T_{ab}^{ij} + \sum_{\alpha,\beta}^{\text{complete}}|\Phi_{ij}^{\alpha\beta}\rangle T_{\alpha\beta}^{ij}\right) \tag{1.112}$$

with

$$T_{\alpha\beta}^{ij} = \sum_{kl}^{\text{val}}\left\langle\Phi_{ij}^{\alpha\beta}|\hat{Q}_{12}F_{12}|kl\right\rangle T_{kl}^{ij}, \tag{1.113}$$

and α, β denote a formally complete orthonormal orbital basis.

$$F_{12} = -\frac{1}{\gamma}e^{-\gamma r_{12}} \tag{1.114}$$

is the correlation factor, which depends on a length-scale parameter γ. For valence-shell correlation $\gamma = 1\,a_0^{-1}$ is usually a good choice. $\hat{Q}_{12}$ is a projector that keeps the explicitly correlated terms orthogonal to the reference Hartree–Fock functions as well as to the conventional configurations $|\Phi_{ij}^{ab}\rangle$. The projector can be chosen from several different forms [118]:

$$\textit{Ansatz}\ \mathbf{1}\text{:}\quad \hat{Q}_{12} = (1-\hat{r}_1)(1-\hat{r}_2), \tag{1.115}$$

$$\textit{Ansatz}\ \mathbf{2}\text{:}\quad \hat{Q}_{12} = (1-\hat{o}_1)(1-\hat{o}_2), \tag{1.116}$$

$$\textit{Ansatz}\ \mathbf{3}\text{:}\quad \hat{Q}_{12} = (1-\hat{o}_1)(1-\hat{o}_2) - \hat{v}_1\hat{v}_2, \tag{1.117}$$

where $\hat{o} = \sum_m |m\rangle\langle m|$, $\hat{v} = \sum_a |a\rangle\langle a|$, and $\hat{r} = \hat{o} + \hat{v}$ are 1-electron projection operators onto the occupied, virtual, and full orbital spaces, respectively, and the subscripts refer to the electron coordinates on which they act. *Ansatz* **1** is unsatisfactory since it neglects the configurations in which one electron is excited to a virtual orbital and the other to an orbital outside of the MO basis. *Ansätze* **2** and **3** are equivalent before further approximations are introduced. *Ansatz* **3** leads to simpler working equations and is used in our work as well as in most other implementations.

The Hylleraas functional for MP2-F12 can be obtained by inserting equation (1.112) into equation (1.3):

$$E_2 = \sum_{i,j}^{\text{val}}\sum_{a,b}^{\text{virt}}\left(K_{ab}^{ij} + R_{ab}^{ij}\right)\tilde{T}_{ab}^{ij} + \sum_{i,j}^{\text{val}}\sum_{k,l}^{\text{val}}\left(V_{kl}^{ij} + R_{kl}^{ij}\right)\tilde{T}_{kl}^{ij}, \tag{1.118}$$

where

$$V_{kl}^{ij} = \left\langle kl|F_{12}\hat{Q}_{12}r_{12}^{-1}|ij\right\rangle, \tag{1.119}$$

$$R_{kl}^{ij} = V_{kl}^{ij} + \left\langle\tilde{\Phi}_{ij}^{kl}|\hat{H}^{(0)} - E^{(0)}|\Psi^{(1)}\right\rangle. \tag{1.120}$$

The contravariant configurations $|\tilde{\Phi}_{ij}^{kl}\rangle$ and amplitudes $\tilde{T}_{kl}^{ij}$ are defined in analogy of those described in Section 1.3. For optimized amplitudes the residuals R_{ab}^{ij} and R_{kl}^{ij} must vanish. The explicit forms of the residuals are [118]

$$R_{ab}^{ij} = K_{ab}^{ij} + f_{ac}T_{cb}^{ij} + T_{ac}^{ij}f_{cb} - f_{io}T_{ab}^{oj} - T_{ab}^{io}f_{oj} + T_{mn}^{ij}C_{ab}^{mn} \tag{1.121}$$

and

$$R_{kl}^{ij} = V_{kl}^{ij} + B_{kl,mn}T_{mn}^{ij} - S_{kl,mn}(f_{io}T_{mn}^{oj} + T_{mn}^{io}f_{oj}) + C_{ab}^{kl}T_{ab}^{ij}, \tag{1.122}$$

where i, j, k, l, m, n, o denote valence orbitals and the summations over repeated dummy indices are implied. The matrix elements are defined as

$$B_{kl,mn} = \langle kl|F_{12}\hat{Q}_{12}(\hat{f}_1 + \hat{f}_2)\hat{Q}_{12}F_{12}|mn\rangle\,, \tag{1.123}$$

$$S_{kl,mn} = \langle kl|F_{12}\hat{Q}_{12}F_{12}|mn\rangle\,, \tag{1.124}$$

$$C_{ab}^{kl} = \langle kl|F_{12}\hat{Q}_{12}(\hat{f}_1 + \hat{f}_2)|ab\rangle\,. \tag{1.125}$$

Up to this point, no approximations are introduced within the second-order Møller-Plesset treatment. However, expanding the projector in equations (1.123) through (1.125) leads to 3- and 4-electron integrals such as

$$\left\langle ij|r_{12}^{-1}\hat{o}_1F_{12}|kl\right\rangle = \sum_{m}^{\text{occ}} \left\langle ijm|r_{12}^{-1}F_{32}|mkl\right\rangle\,. \tag{1.126}$$

The many-electron integrals can be avoided by applying resolutions of the identity (RI) on electron 2 in the operator $\hat{o}_1$:

$$\hat{o}_1 \rightarrow \hat{o}_1\hat{u}_2, \tag{1.127}$$

where $\hat{u} = |\alpha\rangle\langle\alpha|$. Equation (1.126) can then be factorized as

$$\left\langle ij|r_{12}^{-1}\hat{o}_1F_{12}|kl\right\rangle = \sum_{m}^{\text{occ}}\sum_{\alpha}^{\text{complete}} \left\langle ij|r_{12}^{-1}|m\alpha\right\rangle\langle m\alpha|\hat{F}_{12}|kl\rangle\,. \tag{1.128}$$

Note that it is common to use the so-called "physicist's notation" for the 2-electron integrals in F12 theory, that is, $\langle ij|r_{12}^{-1}|m\alpha\rangle = (im|j\alpha)$. The RI is exact when an infinite basis $|\alpha\rangle$ is used. In practice, the RI is approximated by an auxiliary basis set. With this approximation, the projector (*Ansatz* **3**) can be written as

$$\begin{aligned}\hat{Q}_{12} = 1 &- \sum_{a,b}^{\text{virt}} |ab\rangle\langle ab| + \sum_{m,n}^{\text{occ}} |mn\rangle\langle mn| \\ &- \sum_{m}^{\text{occ}}\sum_{\alpha}^{\text{RI}} (|m\alpha\rangle\langle m\alpha| + |\alpha m\rangle\langle \alpha m|)\,.\end{aligned} \tag{1.129}$$

In most canonical F12 methods, a complementary auxiliary basis set (CABS) approach [112] is used, in which the operator $\hat{u}$ in equation (1.127) is written as a sum of the contributions from the orbital basis and the auxiliary basis. The CABS approach leads to simpler equations in canonical F12 methods but is less well suited in local methods, since due to the necessary orthogonalization steps, it is more difficult to apply local RI approximations. However, when using the union of the AO basis and the auxiliary basis

as the RI basis, equation (1.129) is equivalent to the projector in the CABS formulation. For example, this can be achieved by using the union of the correlation consistent orbital basis sets and the corresponding `OPTRI` auxiliary bases [154].

In the PNO-LMP2-F12 method, we introduce domain approximations on the projector:

$$\hat{Q}_{12}^{ij} = 1 - \sum_{a,b\in[ij]_{\mathrm{PNO}}} |ab\rangle\langle ab| + \sum_{m,n\in[ij]_{\mathrm{LMO}}} |mn\rangle\langle mn| - \sum_{m\in[ij]_{\mathrm{LMO}},\bar{\alpha}\in[ij]_{\mathrm{RI}}} \left(|m\bar{\alpha}\rangle\langle m\bar{\alpha}| + |\bar{\alpha}m\rangle\langle\bar{\alpha}m|\right), \tag{1.130}$$

where $[ij]_{\mathrm{PNO}}$, $[ij]_{\mathrm{LMO}}$, and $[ij]_{\mathrm{RI}}$ denote domains of orthonormal PNOs, LMOs, and RI functions for an LMO pair ij, respectively. The RI orbitals $\bar{\alpha}$ are orthogonalized for each domain $[ij]_{\mathrm{RI}}$ separately, that is,

$$|\bar{\alpha}\rangle = \sum_{\beta\in[ij]_{\mathrm{RI}}} |\beta\rangle \left[\mathbf{S}_{\mathrm{RI}}^{-1/2}\right]_{\beta\alpha}. \tag{1.131}$$

The projector is pair-specific. Limiting $a, b \in [ij]_{\mathrm{PNO}}$ in equation (1.130) ensures that only doubly excited configurations included in the PNO-LMP2 first-order wave function are projected out from the explicitly correlated part. The contributions of the remaining parts of the virtual orbital space (outside the domains) are implicitly approximated by the F12 terms, and this leads to a reduction of the domain errors by typically one order of magnitude [142, 143, 145–148]. Thus, as will be demonstrated later, smaller domains can be used in explicitly correlated methods.

The domain approximations in the summations over the LMOs and the RI basis are applied to reduce the scaling of the method. They do cause slight errors in projecting out the contributions of the occupied-occupied block. However, the integrals such as $\langle ij|\hat{F}_{12}|m\alpha\rangle$, which occur in equations (1.134) and (1.135) below, decay exponentially with the distance between the LMOs i and m as well as with the distances between the LMO j and the RI basis functions α (and similarly with i and j exchanged). As a result, LMOs m and RI functions α will contribute significantly only if they are spatially close to either i or j, and the domain approximations lead to only small errors [145, 148].

As proposed by Ten-no [109, 110], the F12 amplitudes T_{kl}^{ij} can be determined from the first-order wave function cusp conditions and then take the fixed values

$$T_{kl}^{ij} = \frac{3}{8}\delta_{ik}\delta_{jl} + \frac{1}{8}\delta_{il}\delta_{jk}. \tag{1.132}$$

The fixed amplitudes have the advantage that no amplitude equations have to be solved for the F12 correction. In combination with $\gamma = 1\,a_0^{-1}$, this approximation leads to negligible errors in treating valence–valence correlations, although in treating core and core–valence correlations in heavy atoms, different geminal exponents are required [138].

Straightforward insertion of the projector $\hat{Q}^{ij}$ into the expressions for $B_{kl,mn}$ (equation 1.123) and C_{ab}^{kl} (equation 1.125) leads to RI approximations for products of the Fock operator and the F12 correlation factor. These may be slowly convergent, in particular for the contribution of the kinetic energy operators $\hat{t}_1$ and $\hat{t}_2$ in the Fock operators $\hat{f}_1$ and $\hat{f}_2$. To reduce this problem, various commutator approximations have been proposed [107, 114], which involve matrix elements over commutators such as $[\hat{t}_{12}, \hat{F}_{12}]$,

where $\hat{t}_{12} = \hat{t}_1 + \hat{t}_2$. Historically, these approximations are denoted A, B, C. Approximations B and C are formally most accurate and equivalent for complete RI basis sets. Approximation A is simplified and does not lead to exactly the same result. Optionally, further simplifications can be achieved by assuming that the extended Brillouin condition (EBC) $f_{ax} = 0$ is valid, were x denotes orbitals in the complementary auxiliary space (i.e., outside the orbital basis). This approximation is indicated by a star (*). For a more complete discussion, see for example Refs. [107, 118].

We use the 3*A approximation [118] in our LMP2-F12 and LCCSD-F12 methods. This is the simplest of all approximations, but extensive benchmarks have shown that it yields excellent results. The EBC approximation leads to $C_{ab}^{kl} = 0$, and this decouples the F12 contribution from the standard LMP2 amplitude equations. Furthermore, the exchange commutator terms $[\hat{k}_1 + \hat{k}_2, F_{12}]$ are neglected. The most important advantage of approximation A* is that the entire theory depends only linearly on the size of the RI basis. Furthermore, no RI approximations involving Fock matrices occur, and therefore local RI approximations can be introduced most easily.

Combined with the fixed amplitudes, the computation of F12 corrections are non-iterative and completely decoupled from the PNO-LMP2 calculations. The F12 residual equation (1.122) becomes

$$R_{kl}^{ij} = V_{kl}^{ij} + B_{kl,mn} T_{mn}^{ij}. \tag{1.133}$$

When using fixed amplitudes, these F12 residuals do not vanish and should be included explicitly in the energy expression, that is, a Hylleraas functional should be used (since this depends only quadratically on the differences between the fixed and optimized amplitudes). Due to the δ-factors in equation (1.132), the summations over kl and mn in equations (1.118) and (1.133) are removed, and the only quantities required for the F12 energy corrections are (for details see Refs. [118, 144, 148]):

$$\begin{aligned} V_{ij}^{ij} = \left\langle ij | r_{12}^{-1} F_{12} | ij \right\rangle &+ \sum_{m,n \in [ij]_{\mathrm{LMO}}} K_{mn}^{ij} F_{mn}^{ij} - \sum_{a,b \in [ij]_{\mathrm{PNO}}} K_{ab}^{ij} F_{ab}^{ij} \\ &- \sum_{m \in [ij]_{\mathrm{LMO}}} \sum_{\alpha \in [ij]_{\mathrm{RI}}} \left(K_{\alpha m}^{ij} \bar{F}_{\alpha m}^{ij} + K_{\alpha m}^{ji} \bar{F}_{\alpha m}^{ji} \right), \end{aligned} \tag{1.134}$$

$$\begin{aligned} B_{ij,ij} = \langle ij | [\hat{F}_{12}, \hat{t}_{12}] \hat{F}_{12} | ij \rangle &+ \sum_{m,n \in [ij]_{\mathrm{LMO}}} U_{mn}^{ij} F_{mn}^{ij} - \sum_{a,b \in [ij]_{\mathrm{PNO}}} U_{ab}^{ij} F_{ab}^{ij} \\ &- \sum_{m \in [ij]_{\mathrm{LMO}}} \sum_{\alpha \in [ij]_{\mathrm{RI}}} \left(U_{\alpha m}^{ij} \bar{F}_{\alpha m}^{ij} + U_{\alpha m}^{ji} \bar{F}_{\alpha m}^{ji} \right), \end{aligned} \tag{1.135}$$

and similar quantities V_{ji}^{ij} and $B_{ij,ji}$. In the above equations, we used the notations $K_{mn}^{ij} = \langle ij | r_{12}^{-1} | mn \rangle$, $F_{mn}^{ij} = \langle ij | \hat{F}_{12} | mn \rangle$, and $U_{mn}^{ij} = \langle ij | [\hat{F}_{12}, \hat{t}_{12}] | mn \rangle$ (and similarly with mn replaced by αm or ab). $\bar{F}_{\alpha m}^{ij}$ is introduced to account for the nonorthogonality of the RI basis functions with the overlap matrix $S_{\alpha\beta} = \langle \alpha | \beta \rangle$. It is obtained by solving the linear equations

$$F_{\alpha m}^{ijp} = \sum_{\beta \in [ij]_{\mathrm{RI}}} S_{\alpha\beta} \bar{F}_{\beta m}^{ijp}. \tag{1.136}$$

Since all domain sizes are asymptotically independent of the molecular size, and the number of pairs *ij* scales linearly with the molecular size (with pair approximations applied, cf. Section 1.8), the number of integrals required for computing the F12 correction also scales linearly.

The approximation 3*A leads to a slight overestimation of the correlation energies, but the impact on energy differences such as reaction energies is minor [118, 133, 210, 211]. The 3*A approximation does not require double RIs, and efficient domain approximations can be easily applied without introducing significant errors. Recently, more rigorous treatments of MP2-F12 in local or fragmentation methods have been used by others [152, 153], but there is no evidence yet that these methods are more efficient or more accurate than the 3*A approximation we used.

Figures 1.8 and 1.9 demonstrate the convergence of the PNO-LMP2 and PNO-LMP2-F12 correlation energies of adrenaline as a function of the PAO extension parameter `IEXT` and the PNO domain thresholds, respectively. It can be seen that the F12 correction improves the convergence with the domain sizes dramatically. Most importantly, with F12 much smaller PAO domains are necessary to reach convergence, and `IEXT=1` is sufficient. Later, it will be demonstrated that this also holds for LCCSD-F12 and much larger molecules. The reduction of the PAO domain size is very important for the efficiency, since all integrals are first computed in the PAO basis and then transformed to the PNO basis. Similarly, the convergence with the PNO domain thresholds is also strongly improved, cf. Figure 1.9. The left panel shows the convergence as a function of $T^{\mathrm{occ}}_{\mathrm{PNO}}$ without the additional completeness criterion $T^{\mathrm{en}}_{\mathrm{PNO}}$, while in the right panel, $T^{\mathrm{en}}_{\mathrm{PNO}} = 0.997$ has been used. Accordingly, about 99.7% of the correlation energy is recovered even with the largest threshold $T^{\mathrm{occ}}_{\mathrm{PNO}} = 10^{-6}$. With the same thresholds, PNO-LMP2-F12 yields already 99.96% of the canonical MP2-F12 value. Note the

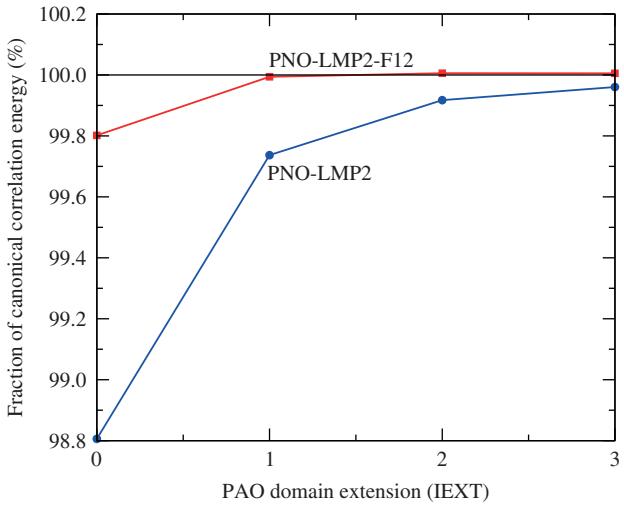


Figure 1.8 PNO-LMP2 and PNO-LMP2-F12 correlation energies of adrenaline relative to the canonical values (in percent) as a function of the PAO domain extenion parameter `IEXT` (see text). The PNO occupation number threshold $T_{\mathrm{PNO}} = 10^{-10}$ and the completeness criterion $T^{\mathrm{en}}_{\mathrm{PNO}} = 0.997$ have been used. Basis set: VTZ-F12.

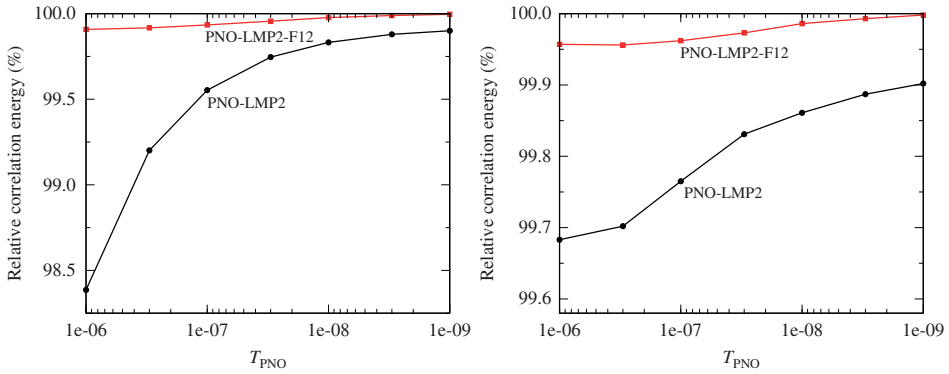


Figure 1.9 PNO-LMP2 and PNO-LMP2-F12 correlation energies of adrenaline relative to the canonical values (in percent) as a function of the PNO threshold T_{PNO}. *Left panel*: PNO domain selection using the natural occupation number threshold T_{PNO} only. *Right panel*: In addition, the completeness criterion $T^{en}_{PNO} = 0.997$ has been used (see text). `IEXT=2`, basis set: VTZ-F12.

different scales of the left and right panels of figure 1.9. It should be noted that the additional PNO domain error can also be corrected quite efficiently by adding the difference of the semi-canonical PAO-LMP2 (or OSV-LMP2) and PNO-LMP2 correlation energies to the LMP2 or LCCSD correlation energies, as done in the PNO methods of Neese *et al.* [48–57]. However, in contrast to the F12 treatment, this does not correct for errors caused by the incomplete PAO domains nor for the basis set incompleteness error.

Absolute PNO-LMP2 and PNO-LMP2-F12 correlation energies for various PAO domain sizes are presented in Table 1.9 for adrenaline and some other molecules. These calculations confirm that with PNO-LMP2-F12, `IEXT=1` is sufficient to reach $\geq$ 99.96% of the canonical MP2-F12 correlation energy, while with the same domains, PNO-LMP2 only yields 99.0–99.5% of the canonical MP2 correlation energy. Note also the large differences between the absolute values of the PNO-LMP2 and PNO-LMP2-F12 correlation energies. This is due to the basis set incompleteness error, which is greatly reduced by the F12 correction. The PNO-LMP2-F12 correlation energies for the VDZ-F12 basis are slightly larger than those obtained with the cc-pVTZ-F12 (VTZ-F12) basis. This is due to the well-known overshooting of the 3*A approximation.

A comparison of the MP2 and MP2-F12 reaction energies of our three benchmark reactions with their local counterparts is presented in Table 1.10. While the MP2 and PNO-LMP2 differ significantly (in particular for reaction **III**), the MP2-F12 and PNO-LMP2-F12 results are in very close agreement. This table also demonstrates the effect of the additional completeness energy criterion T^{en}_{PNO} for the PNO domain selection. For reaction **III**, this increases the PNO-LMP2 reaction energy by 2.1 kJ mol^{-1}, which is mainly attributed to long-range effects. This effect is reduced to 0.5 kJ mol^{-1} by the F12 treatment. Note that for reaction **I,** the canonical MP2 overestimates the correlation effect relative to the MP2-F12 result (which is in close agreement with the extrapolated MP2 complete basis set (CBS) limit, cf. Ref. [147]). This is attributed to intramolecular basis set superposition errors (BSSE). These are reduced by LMP2 [14, 212], and indeed the PNO-LMP2/VTZ-F12 result is much closer to the CBS limit than the MP2 one.

Table 1.9 PNO-LMP2 and PNO-LMP2-F12 correlation energies using various PAO domain sizes (basis set: VDZ-F12, $T_{\mathrm{LMO}} = 0.2$, $T_{\mathrm{PNO}}^{\mathrm{occ}} = 10^{-8}$). The fraction of correlation energy relative to the canonical values is given in parenthesis. `IEXT=Full` corresponds to the canonical MP2-F12 calculation.

	VDZ-F12				VTZ-F12			
IEXT	PAO	PNO	LMP2	LMP2-F12	PAO	PNO	LMP2	LMP2-F12
Naphtalene								
0	61	53.1	−1.434336 (97.799)	−1.754813 (99.787)	108	84.6	−1.607515 (98.820)	−1.751784 (99.793)
1	144	67.1	−1.459509 (99.516)	−1.758781 (100.013)	257	101.9	−1.622407 (99.736)	−1.755287 (99.993)
2	246	69.8	−1.464503 (99.856)	−1.759206 (100.037)	441	105.9	−1.624709 (99.877)	−1.755356 (99.997)
Full	338		−1.466615 (100.000)	−1.758552 (100.000)	674	0.0	−1.626705 (100.000)	−1.755415 (100.000)
Adrenaline								
0	49	44.1	−2.173019 (97.721)	−2.708837 (99.780)	88	70.4	−2.457964 (98.759)	−2.701751 (99.785)
1	121	56.4	−2.211627 (99.458)	−2.714507 (99.989)	216	86.7	−2.480927 (99.682)	−2.706874 (99.974)
2	223	60.2	−2.219818 (99.826)	−2.715291 (100.017)	402	91.7	−2.485388 (99.861)	−2.707183 (99.986)
Full	458		−2.223690 (100.000)	−2.714817 (100.000)	923		−2.488848 (100.000)	−2.707570 (100.000)
Testosterone								
0	48	38.9	−3.301752 (96.725)	−4.110938 (99.764)	85	61.3	−3.734627 (98.395)	−4.103197 (99.793)
1	133	51.4	−3.380683 (99.037)	−4.119281 (99.967)	239	77.5	−3.776146 (99.489)	−4.110686 (99.975)
2	286	55.4	−3.401254 (99.640)	−4.120945 (100.007)	517	82.5	−3.786582 (99.764)	−4.110783 (99.978)
Full	882		−3.413553 (100.000)	−4.120653 (100.000)	1617		−3.795542 (100.000)	−4.111706 (100.000)
Progesterone								
0	48	38.7	−3.591953 (96.754)	−4.466493 (99.761)	86	60.9	−4.059920 (98.412)	−4.458090 (99.792)
1	132	51.0	−3.676732 (99.038)	−4.475547 (99.963)	238	76.8	−4.104467 (99.491)	−4.466212 (99.974)
2	282	54.8	−3.698765 (99.631)	−4.477428 (100.005)	510	81.6	−4.115578 (99.761)	−4.466408 (99.978)
Full	960	0.0	−3.712464 (100.000)	−4.477214 (100.000)	1759		−4.125452 (100.000)	−4.467379 (100.000)

Table 1.10 Reaction energies (in kJ mol^{-1}) for the androstendione (**I**), testosterone (**II**), and gold (**III**) reactions.

Method	$T^{\text{en}}_{\text{PNO}}$	Reaction I	Reaction II	Reaction III
HF		−4.9	−26.8	91.9
MP2		22.4	−23.0	255.9
PNO-LMP2	0	17.5	−20.4	237.4
PNO-LMP2	0.997	18.2	−20.9	239.5
HF+CABS		−5.8	−26.2	92.2
MP2-F12		18.8	−19.7	253.0
PNO-LMP2-F12	0	18.5	−19.9	251.6
PNO-LMP2-F12	0.997	18.6	−19.9	252.1

Basis set: VTZ-F12, $T^{\text{occ}}_{\text{PNO}} = 10^{-8}$, `IEXT=2`, $T_{\text{dist}} = 10^{-6}$. The iterative multipole approximation with $p = 3$ has been used. HF+CABS includes the CABS singles correction [120,123] to the Hartree-Fock energy.

1.11.2 PNO-LCCSD-F12

The CCSD-F12 wave function is defined as

$$\Psi_{\text{CCSD-F12}} = \exp\left(\hat{T}_1 + \hat{T}_2\right)|0\rangle\,, \tag{1.137}$$

where the excitation operators are defined as

$$\hat{T}_1 = \sum_{i}^{\text{val}} \sum_{a}^{\text{virt}} t^i_a \hat{E}^a_i, \tag{1.138}$$

$$\hat{T}_2 = \frac{1}{2} \sum_{i,j}^{\text{val}} \sum_{a,b}^{\text{virt}} T^{ij}_{ab} \hat{E}^{ab}_{ij} + \frac{1}{2} \sum_{i,j}^{\text{val}} \sum_{\alpha,\beta}^{\text{complete}} \sum_{k,l}^{\text{val}} T^{ij}_{kl} \langle kl|F_{12}\hat{Q}_{12}|\alpha\beta\rangle \hat{E}^{\alpha\beta}_{ij}. \tag{1.139}$$

These operators differ from the CCSD ones (cf. Section 1.9) by the additional F12 term. The F12 operator, projector, and amplitudes are the same as defined in Section 1.11.1.

A formally complete treatment of the CCSD-F12 method introduces terms in which the unity operator in the projector must be approximated with a double RI, practically limiting its application to very small molecules. In the PNO-LCCSD-F12 method we use the so-called CCSD-F12x (x = a, b) approximations [120,133], in which only contributions that are linear in the F12 amplitudes are considered (beyond LMP2-F12). Furthermore, there are no contributions to the residuals that require double RI approximations. The CCSD-F12x method has been extensively benchmarked, and is found to give similar or even better results than more complete treatments [115, 129]. This is due to certain systematic error cancellations and the avoidance of multiple RI approximations [133]. In addition, we also use the approximation 3*A and fixed amplitudes in PNO-LCCSD-F12. The PNO-LCCSD-F12x and the PNO-LCCSD residual equations then differ only slightly:

$$\Delta r^i_a = \sum_{j}^{ij\in P_s} \sum_{b\in[ij]_{\text{PNO}}} S^{i,ij}_{ab} \left(2\tilde{V}^{ij}_{bj} - \tilde{V}^{ji}_{bj}\right) \quad \forall a \in [ii]_{\text{PNO}}, \tag{1.140}$$

and

$$\Delta R^{ij}_{ab} = \tilde{V}^{ij}_{ab} - \sum_{k\in[ij]_{\mathrm{LMO}}} \left[\tilde{V}^{ij}_{ak} (\mathbf{S}^{ij,k}\mathbf{t}^k)_b + (\mathbf{S}^{ij,k}\mathbf{t}^k)_a \tilde{V}^{ij}_{bk} \right] \quad \forall i,j \in P_s, \quad \forall a,b \in [ij]_{\mathrm{PNO}}, \tag{1.141}$$

where

$$S^{ij,k}_{ab} = \langle a^{ij} | b^{kk} \rangle , \tag{1.142}$$

$$\tilde{V}^{ij}_{ab} = \left\langle ab | r_{12}^{-1} Q^{ij}_{12} F_{12} | \tilde{ij} \right\rangle . \tag{1.143}$$

The quantity $\tilde{V}^{ij}_{ak}$ is defined in a similar way. The modified kets

$$|\tilde{ij}\rangle = \frac{3}{8} |ij\rangle + \frac{1}{8} |ji\rangle \tag{1.144}$$

account for the fixed amplitudes defined in equation (1.132). We treat the F12 correction at the CCSD-F12*x* level only for strong pairs *ij*. For close and weak pairs, the F12 corrections at the MP2-F12 level are included, and previous benchmark calculations [133] have shown that this simple treatment is a surprisingly good approximation. We note that in equation (1.140), a projection approximation has been used to project the contributions of $\tilde{V}^{ij}_{bj}$ from PNO domain $b \in [ij]$ to the singles domain $a \in [i]$.

The PNO-LCCSD-F12a energy expression then differs from the PNO-LCCSD one (cf. equation 1.97) only by adding the MP2-F12 energy correction $\Delta E^{\mathrm{MP2}}_{\mathrm{F12}}$:

$$E^{\mathrm{LCCSD-F12a}}_{\mathrm{corr}} = E^{\mathrm{LCCSD}}_{\mathrm{corr}} + \Delta E^{\mathrm{MP2}}_{\mathrm{F12}}. \tag{1.145}$$

But note that due to the additional terms in the residuals, the amplitudes are different, and therefore the $E^{\mathrm{LCCSD}}_{\mathrm{corr}}$ contribution is different than for LCCSD. The F12b approximation adds further terms which introduce an additional coupling with the conventional amplitudes:

$$E^{\mathrm{LCCSD-F12b}}_{\mathrm{corr}} = E^{\mathrm{LCCSD-F12a}}_{\mathrm{corr}} + \sum_{i\geq j\in P_s} (2-\delta_{ij}) \sum_{a,b\in[ij]_{\mathrm{PNO}}} \left[\left(2D^{ij}_{ab} - D^{ji}_{ab} \right) \tilde{V}^{ij}_{ab} + \left(2\tilde{V}^{ij}_{aj} - \tilde{V}^{ji}_{aj} \right) (\mathbf{S}^{ij,i}\mathbf{t}^i)_a + \left(2\tilde{V}^{ji}_{bi} - \tilde{V}^{ij}_{bi} \right) (\mathbf{S}^{ij,j}\mathbf{t}^j)_b \right], \tag{1.146}$$

where

$$[\mathbf{D}^{ij}]_{ab} = [\mathbf{T}^{ij}]_{ab} + [\mathbf{S}^{ij,i}\mathbf{t}^i]_a [\mathbf{S}^{ij,j}\mathbf{t}^j]_b, \quad a,b \in [ij]. \tag{1.147}$$

The F12b approximation is more rigorous than F12a. Nevertheless, it has been found that the F12a approximation sometimes gives more accurate energy differences if small AO basis sets are used. This is due to a systematic overestimation of the F12a energy correction, which favorably compensates for basis set incompleteness errors. For accurate calculations with larger basis sets (triple-ζ and larger), the F12b approximation should be used [133].

The quantity $\tilde{V}_{ab}^{ij}$ is computed as [143, 145]

$$\tilde{V}_{ab}^{ij} = \langle ab|r_{12}^{-1}F_{12}|\tilde{ij}\rangle - \sum_{c,d\in[ij]_{\mathrm{PNO}}} K_{ab}^{cd}\tilde{F}_{cd}^{ij} - \sum_{m,n\in[ij]_{\mathrm{LMO}}} K_{ab}^{mn}\tilde{F}_{mn}^{ij} - \sum_{m\in[ij]_{\mathrm{LMO}},c\in[ij]_{\mathrm{PNO}}} \left(K_{ab}^{mc}\tilde{F}_{mc}^{ij} + K_{ab}^{cm}\tilde{F}_{cm}^{ij}\right), \quad (1.148)$$

where

$$\tilde{F}_{xy}^{ij} = \langle xy|F_{12}|\tilde{ij}\rangle, \quad (x, y \text{ representing PNOs or LMOs}) \quad (1.149)$$

and the other 2-electron integrals are defined as in section 1.11.1. The $\tilde{V}_{ak}^{ij}$ operators can be computed in a similar fashion.

In equations (1.140) through (1.148), we have applied similar domain approximations as in the PNO-LMP2-F12 method. In addition, the last summation in equation (1.148), which should strictly run over the complete virtual space (including the CABS part), is restricted to the PNOs in the domain $[ij]_{\mathrm{PNO}}$ [143, 145]. This avoids very expensive contributions of 3-external integrals involving the CABS space. Furthermore, the F12 terms are only added to the CCSD residual equations for strong pairs, and the F12 corrections for the close and weak pairs are thus limited to the MP2-F12 level. These approximations significantly reduce the computational cost of the PNO-LCCSD-F12 corrections, since all 3- and 4-external integrals required for the F12 terms are also needed for the PNO-LCCSD calculations. The effect of the approximations on the accuracy has been shown to be small [143, 145].

In the PNO-LCCSD-F12 method, all summations are restricted to domains that asymptotically have a constant size. Using the local density-fitting technique for the integral evaluations and transformations to be discussed in the following section, the method scales linearly with the molecule size. With our present implementation, the inclusion of the F12 terms increases the overall computational time of a PNO-LCCSD calculation only by 10–20%. More than 50% of this is due to the MP2-F12 correction. The cost of LCCSD-F12a and LCCSD-F12b is virtually the same. As will be demonstrated in the following, the F12 corrections very much improve the results and should therefore always be included.

Table 1.11 shows the computed reaction energies for our three benchmark reactions for PNO-LMP2, PNO-LMP2-F12, PNO-LCCSD, and PNO-LCCSD-F12 using the VDZ-F12 and VTZ-F12 basis sets. For simplicity, the prefix PNO- is omitted. In order to minimize the effect of DF and RI approximations, the aug-cc-pVTZ auxiliary basis sets (cf. Section 1.2) have been used for both orbital basis sets. The F12 corrections have a significant effect on the reaction energies and lead to much better convergence with the basis set. Furthermore, using the F12 correction, the PAO domain size (`IEXT=1` or `IEXT=2`) has a much smaller effect on the explicitly correlated results than without the F12 correction. Thus, it may often be sufficient to use `IEXT=1` in LCCSD-F12 calculations, which saves considerable time and memory. In Table 1.11 also different LCCSD-F12 approximations are compared: LCCSD+ΔF12 means that the F12 correction computed at the PNO-LMP2-F12 level is simply added to the PNO-LCCSD result. F12a and F12b additionally include couplings between the LCCSD amplitudes and the F12 terms (see above). As expected, the (absolute) F12 corrections systematically decrease

Table 1.11 Reaction energies (in kJ mol^{-1}) for the androstendione (**I**), testosterone (**II**), and gold (**III**) reactions for different values of `IEXT` and two basis sets.

Reaction	Basis	LMP2	LMP2-F12	LCCSD	LCCSD+ΔF12	LCCSD-F12a	LCCSD-F12b
`IEXT=1`							
I	VDZ-F12	12.3	18.9	13.9	20.4	20.1	18.9
	VTZ-F12	15.4	18.2	16.4	19.2	18.9	18.4
II	VDZ-F12	−18.3	−19.3	−22.7	−23.8	−23.9	−23.9
	VTZ-F12	−20.4	−19.7	−26.4	−25.7	−25.7	−25.7
III	VDZ-F12	214.4	249.8	153.3	188.6	188.1	185.1
	VTZ-F12	234.1	250.6	171.6	188.1	187.5	185.6
`IEXT=2`							
I	VDZ-F12	17.8	19.2	19.2	20.5	20.2	19.1
	VTZ-F12	18.2	18.6	18.8	19.3	19.1	18.7
II	VDZ-F12	−20.2	−19.8	−24.5	−24.1	−24.3	−24.3
	VTZ-F12	−20.9	−19.9	−26.8	−25.7	−25.8	−25.8
III	VDZ-F12	225.2	253.0	162.4	190.2	189.7	186.6
	VTZ-F12	239.5	252.1	176.2	188.7	188.3	186.5

$T_{close} = 10^{-4}$, $T_{weak} = 10^{-5}$, $T_{dist} = 10^{-6}$. The CABS singles corrections are included in all F12 results. SCS-LMP2 distant pair energies obtained using the iterative multipole approximation ($p = 3$) were used in the LCCSD and LCCSD-F12 calculations.

in the order ΔF12>F12a>F12b. It is known from conventional coupled cluster calculations that the basis set effect is usually somewhat smaller at the CCSD than at the MP2 level, and this effect is reflected in the current results. Overall, the final LCCSD-F12b reaction energies are least sensitive to the basis set, and we therefore believe that the LCCSD-F12b/VTZ-F12 results are most accurate. Except for reaction **III**, the differences between the F12a and F12b results are negligible. For reaction **III** the difference still amounts to about 2 kJ mol^{-1}. This can be seen as a measure of the uncertainty. In this very difficult case, the LMP2-F12 and LCCSD-F12b results differ by 65 kJ mol^{-1}, and the F12b correction amounts to 10.3 kJ mol^{-1} (`IEXT=2`, VTZ-F12).

Figure 1.10 shows the convergence of the LCCSD-F12b correlation energy of Auamin (left panel) and of the reaction energy (right panel) as a function of the close and weak pair thresholds T_{close} and T_{weak}. We have chosen ratios of T_{close}/T_{weak} to be 10, 30, or $T_{weak} = T_{dist}$ (no weak pairs). The variations of the reaction energies caused by the close pair approximation below a threshold of $T_{close} = 3 \times 10^{-4}\ E_h$ are smaller than 0.5 kJ mol^{-1}, while for this threshold the correlation energy of the Auamin molecule differs by only 0.15 mE_h from the converged value. The weak pair CEPA approximation somewhat increases the errors, but for a threshold of $T_{weak} = 3 \times 10^{-5}\ E_h$ the additional error is still below 1 kJ mol^{-1}.

In summary, the benchmarks presented in this and previous sections have shown that it is possible to control all local approximations, and to converge the results toward the canonical values. Of course a direct comparison with the canonical results is only

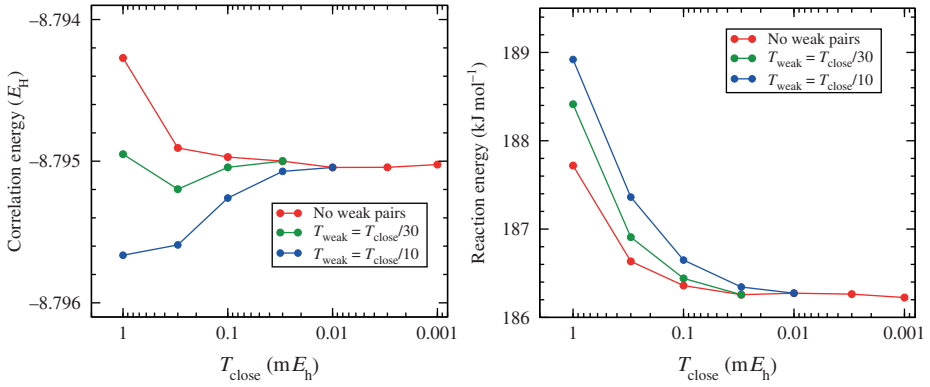


Figure 1.10 Convergence of the PNO-LCCSD-F12a absolute energies for the Auamin molecule (left) and reaction energies for reaction **III** (right) depending on T_{close} and T_{weak} pair selection thresholds. Basis set: VTZ-F12 (for Au cc-pVTZ-PP), $T_{dist}3\,10^{-6}E_h$, distant pair energies computed with the iterative multipole approximation p=3, `IEXT=1`.

possible for rather small molecules. For large molecules, the only way to check the convergence is to lower the thresholds, as has been shown in figure 1.10 for close and weak pair approximations. If tight close and weak pair thresholds are applied, it appears likely that the canonical CCSD-F12 results (which are impossible to compute) would not differ more than 1–2 kJ mol^{-1} from the PNO-LCCSD-F12 values. Since the implementation of our PNO-LCCSD-F12 method has been completed very recently, further benchmarks and improvements are still under way. The results will be presented in a future publication.

1.12 Technical Aspects

1.12.1 Local Density Fitting

Density fitting (DF) is a widely used approximation for the evaluation of 2-electron integrals in electron correlation methods. The principle of DF is to use an auxiliary basis to approximate the 1-electron charge densities in equation (1.11):

$$\rho_{ai}(\mathbf{r}) = \phi_a(\mathbf{r})\phi_i(\mathbf{r}) \approx \tilde{\rho}_{ai} = \sum_A^{\text{fit}} d_{ai}^A \phi_A(\mathbf{r}), \tag{1.150}$$

and similar for ρ_{bj}. Equation (1.11) then becomes

$$(ai|bj) \approx \sum_{A,B}^{\text{fit}} d_{ai}^A d_{bj}^B \int_{\mathbb{R}^3} \mathrm{d}\mathbf{r}_1 \int_{\mathbb{R}^3} \mathrm{d}\mathbf{r}_2 \phi_A(\mathbf{r}_1)\phi_B(\mathbf{r}_2) = \sum_{A,B}^{\text{fit}} d_{ai}^A d_{bj}^B (A|B). \tag{1.151}$$

As shown by Dunlap *et al.* [213], the density-fitting coefficient d_{ai}^A can be obtained by minimizing

$$\Delta_{ai} = \int_{\mathbb{R}^3} \mathrm{d}\mathbf{r}_1 \int_{\mathbb{R}^3} \mathrm{d}\mathbf{r}_2 [\rho_{ai}(\mathbf{r}_1) - \tilde{\rho}_{ai}(\mathbf{r}_1)] \frac{1}{r_{12}} [\rho_{ai}(\mathbf{r}_2) - \tilde{\rho}_{ai}(\mathbf{r}_2)], \tag{1.152}$$

which is equivalent to solving a linear equation system

$$(A|ai) = \sum_{B}^{\text{fit}} (A|B) d_{ai}^{A}, \tag{1.153}$$

where $(A|ai)$ is a 3-index, 2-electron integral

$$(A|ai) = \int_{\mathbb{R}^3} \mathrm{d}\mathbf{r}_1 \int_{\mathbb{R}^3} \mathrm{d}\mathbf{r}_2 \phi_A(\mathbf{r}_1) \frac{1}{r_{12}} \rho_{ai}(\mathbf{r}_2) = (ai|A). \tag{1.154}$$

Similarly, we have

$$(A|bj) = \sum_{B}^{\text{fit}} (A|B) d_{bj}^{A}. \tag{1.155}$$

Inserting equation (1.155) into equation (1.151) gives a simplified equation for the 2-electron integrals

$$(ai|bj) \approx \sum_{A}^{\text{fit}} d_{ai}^{A} (A|bj) = \sum_{A,B} (A|ai) [\mathbf{J}^{-1}]_{AB} (B|bj), \qquad [\mathbf{J}]_{AB} = (A|B). \tag{1.156}$$

The density-fitting technique significantly reduces the computational cost of canonical MP2 calculations without introducing significant errors. In local methods, an additional advantage is that the summations over the fitting functions can be limited to those close to the orbitals i and j, which reduces the scaling of the method. In the PNO-LMP2 and PNO-LCCSD methods, we restrict the summations over the fitting functions to domains $[ij]_{\text{fit}}$, determined in a similar fashion as for the domains $[ij]_{\text{PAO}}$ (see Section 1.6.2). The parameters for extending the fitting domains are denoted `IDFDOM` and `RDFDOM` (corresponding to `IEXT` and `REXT`, respectively). Our benchmark calculations show that using the default values `IDFDOM=3` and `RDFDOM=7` (all distances in a_0 and with `IEXT=2` and `REXT=5`) usually lead to negligible errors in PNO-LMP2 calculations [147, 148]. Even smaller domains `IDFDOM=2` and `RDFDOM=5` give satisfactory results when explicit correlation is included, and these values were used for PNO-LCCSD and PNO-LCCSD-F12 calculations.

The 3-index integrals can only be evaluated in the AO basis and must be transformed to the LMO or PNO bases in our local correlation methods. In the PNO-LMP2 method, only 2-external K_{ab}^{ij} integrals in pseudo-canonical PAO and OSV bases are needed. We first transform the 3-index integrals to the LMO and PAO bases

$$(A|\mu i) = \sum_{\nu}^{\text{AO}} (A|\mu\nu) L_{\nu i}, \tag{1.157}$$

$$(A|\tilde{r}i) = \sum_{\mu}^{\text{AO}} (A|\mu i) P_{\mu\tilde{r}}. \tag{1.158}$$

The $K_{\tilde{r}\tilde{s}}^{ij}$ integrals are then assembled pairwise

$$K_{\tilde{r}\tilde{s}}^{ij} = \sum_{A,B \in [ij]_{\text{fit}}} (A|\tilde{r}i) [\mathbf{J}^{-1}]_{AB} (B|\tilde{s}j) \tag{1.159}$$

before they are transformed to the PC-PSV basis as

$$K^{ij}_{a^{ij}b^{ij}} = \sum_{r,s\in[ij]_{\mathrm{PAO}}} \tilde{V}^{ij}_{ra^{ij}} K^{ij}_{\tilde{r}\tilde{s}} \tilde{V}^{ij}_{sb^{ij}}. \tag{1.160}$$

Due to the large number of fitting functions, this strategy is found to be more efficient than transforming the 3-index integrals to the PC-PSV basis [147]. To achieve linear scaling, the sparsity of the LMO and PAO expansion coefficients must be exploited to limit the summations in equations (1.157) and (1.158).

The PNO-LCCSD method requires a number of different types of integrals and the strategy described above for transforming the $K^{ij}_{a^{ij}b^{ij}}$ integrals may not be optimal. For example, the 4-external integrals $(a^{ij}b^{ij}|c^{ij}d^{ij})$ are assembled after transforming 3-index integrals to the PNO basis

$$(a^{ij}b^{ij}|c^{ij}d^{ij}) = \sum_{A,B\in[ij]_{\mathrm{fit}}} (A|a^{ij}b^{ij})(\mathbf{J}^{-1})_{AB}(B|c^{ij}d^{ij}). \tag{1.161}$$

The reason for transforming to the PNO basis before the assembly step is performed is that the number of the 4-external integrals scales with the fourth power in the number of the virtual orbitals per pair, and the memory and CPU requirements for assembling them in the PAO basis would be much larger. Furthermore, a transformation of the 4-index integrals from the PAO to the PNO basis is avoided.

For integrals other than the Coulomb integrals, it is essential to use the robust fitting formula [108, 214] to ensure sufficient accuracy. For example, in our PNO-LMP2-F12 method, local density fitting of an F12 integral takes the form

$$\begin{aligned} F^{ij}_{\tilde{r}\tilde{s}} \approx & \sum_{A\in[i]_{\mathrm{fit}}} d^{A}_{\tilde{r}i}(A|F_{12}|\tilde{s}j) + \sum_{B\in[j]_{\mathrm{fit}}} (B|F_{12}|\tilde{r}i) d^{B}_{\tilde{s}j} \\ & - \sum_{A\in[i]_{\mathrm{fit}}} \sum_{B\in[j]_{\mathrm{fit}}} d^{A}_{\tilde{r}i}(A|F_{12}|B) d^{B}_{\tilde{s}j}. \end{aligned} \tag{1.162}$$

The robust fitting formula ensures that the errors of the integrals are quadratic in the fitting errors. Equation (1.162) can also be used in assembling the Coulomb integrals. However, if we use the union of fitting domains $A, B \in [ij]_{\mathrm{fit}}$ and replace the kernel F_{12} with r_{12}^{-1}, the last two terms in equation (1.162) cancel out, and the equation reduces to equation (1.159). In other words, the simple local fitting formula (1.159) is robust for Coulomb integrals. We note that the F12-specific commutator integrals take a more complicated form [108].

The local DF method ensures that the integral evaluation and transformation in our PNO methods asymptotically scale linearly with the size of the molecule. There is a non-negligible overhead due to the pairwise linear equation system solving, and therefore there is a certain molecular size below which local DF will be more expensive than the standard DF procedure. The overhead is partially compensated in a parallel environment, since in a standard DF method, high parallel efficiency is more difficult to achieve due to increased I/O. More details about the parallelization of the program will be given in the following section.

1.12.2 Parallelization

Our PNO methods are parallelized with the help of MPI and the Global Arrays (GA) toolkit [215]. The GA toolkit provides a portable one-sided remote memory access interface so that a process can access remote data without intervening the corresponding remote process. Currently, we do not use shared memory parallelization.

We use static as well as dynamic parallelization techniques. Static parallelization means that predetermined tasks are allocated to certain processors (processing cores). This is used, for example, in the iterative solution of the LMP2 or LCCSD equations, where groups of pair residuals are assigned to each processor. After computing the residuals, each processor updates the amplitudes for the corresponding pairs and copies them to a GA. Subsequently, other processors read from this GA all amplitudes which are needed in their residuals and which are not local to them. Thus, communication and synchronization is necessary only once per iteration after the amplitudes have been copied to the GA.

This static parallelization strategy is especially useful when calculated quantities (e.g., integrals or amplitudes) can remain local to the processors during a procedure, and only little communication of data is necessary. In order to minimize the memory demands, the group of pairs allocated to one processing core should share as many data as possible. Furthermore, the total amount of memory (and/or CPU time) on each compute core should be similar, that is, a good load balancing should be achieved. The optimal distribution of pairs to the processors is a highly non-trivial task. We use the METIS graph partitioning program [216] for this purpose, but even then the load balancing is often not optimal, and therefore dynamic parallelization may be advantageous, even if this leads to more communication.

In the dynamic parallelization model, the tasks are allocated to the processors on a first-come-first-serve basis. This is achieved using a task list and a shared counter, which is incremented whenever a task is allocated to a processor. In order to obtain optimal load balancing, larger tasks should be processed first and small ones at the end. This model yields a very good load balancing, provided that the number of tasks is significantly larger than the number of processing cores. An example is the evaluation and the transformation of the 2-electron integrals. We first compute all required 3-index PAO/LMO integrals sets such as $(A|ij)$, $(A|\tilde{r}i)$, and $(A|\tilde{r}\tilde{s})$ and store them in GAs. This step is parallelized over blocks of fitting functions A to avoid redundancies in the evaluation of the AO integrals $(A|\mu\nu)$. In the following step, the different types of 4-index integrals are assembled and transformed to the PC-PNO basis. This step is parallelized over LMO pairs, and the 3-index integrals are retrieved from the GAs as required. The resulting 4-index PC-PNO integrals are also stored in GAs and retrieved when needed in the calculations of the residuals. An exception is the calculation of the F12 correction in the PNO-LMP2-F12 method, in which the individual contributions are computed on the fly from the assembled 4-index integrals, and the integrals are then discarded immediately.

Our PNO methods are designed to minimize computational redundancy by computing (nearly) all types of 3-index and 4-index integrals only once for the whole molecule in a PNO-LCCSD-F12 calculation. This leads to minimum CPU-time but requires a lot of communication of 3-index and 4-integrals between the processors (via the GAs). The communication overhead is reasonably small if a fast network (e.g., InfiniBand) is available. It is also possible to minimize the communication at the prize of redundant

integral evaluations. For example, in LMP2 one can compute groups of operators $\mathbf{K}^{ij}$ on different processors, without any communication. This requires redundant calculations of the 3-index integrals. Using our compute cluster with a few hundred CPU cores and QDR-InfiniBand connections between the nodes, this is much slower than the dynamical calculation. However, this may not be true when massively parallel computers or a slow network connection is used.

1.13 Comparison of Local Correlation and Fragment Methods

In fragmentation methods [60–87, 151], the correlation of electrons in subsets of LMOs or LMO pairs is treated independently in different fragments or increments. Various ways to choose these fragments (or increments) and to assemble the total correlation energy have been proposed, and this is the subject of other chapters in this book. One possibility is to assemble the total correlation energy using pair energies E_{ij} obtained in different fragments. This is for example the case in the "Divide-Expand-Consolidate" (DEC) approach [66–74]. Alternatively, the correlation energy can also be rewritten as a sum of orbital contributions E_i, which are computed in independent fragments. This is for example used in the Cluster in Molecules (CIM) approach [75–85, 151]. Incremental methods [88–96] are somewhat different and use a many-body expansion. It is also possible to split the preceding HF calculation into fragments [60–65], but this is more difficult and has to take the electrostatic interactions with the environment into account. Furthermore, it may be necessary to introduce artificial "link atoms" in order to saturate each fragment. Here we will only discuss the case that a single HF calculation is carried out for the whole system, just as in local correlation methods.

In order to obtain an accurate value for a particular pair energy E_{ij} in a fragment, the interaction with neighboring pairs must be taken into account. We can distinguish between "primary" pairs, which are those for which the pair energies are computed and used in the final energy assembly, and "secondary" pairs, whose amplitudes are needed to get accurate residuals for the primary pairs, but which do not directly contribute to the energy of the fragment. Similarly, if the correlation energy is expressed as a sum of orbital contributions, one can distinguish between "central MOs" and "buffer" or "environmental" MOs [79, 81]. In any case, each group of primary pairs needs an interaction region of secondary pairs around it. The number of primary and secondary pairs together (or the number of LMOs in a fragment) determines the total size and cost of each fragment calculation. The interaction regions of different fragments overlap strongly, and this leads to a high redundancy in fragmentation treatments. The advantage, however, is that the fragments can be treated independently, and thousands of fragments can be computed in parallel on a supercomputer. Furthermore, conventional (non-local) methods can be used. For this, one can determine a single PAO domain for each fragment and then use the pseudo-canonical orbitals of this domain as virtual space for the fragment. No further domain or pair approximations are applied, and this makes such methods technically much simpler than the local correlation treatments as described in this chapter.

The most important question is how big the interaction regions have to be in order to obtain accurate correlation energies, since the cost of a CCSD calculation for a single fragment scales with $\mathcal{O}(\mathcal{N}^6)$, where $\mathcal{N}$ is a measure of the fragment size (e.g., the number of correlated orbitals in it, including the buffer region). If triples are included, the

scaling is even $\mathcal{O}(\mathcal{N}^7)$. If all fragments would be calculated in parallel on a supercomputer, the total elapsed time would depend on the time needed for the largest fragment.

The smallest fragments one can think of are obtained if each one contains only a single primary pair ij. Our local correlation treatment allows us to estimate the size of the interaction regions that are needed to describe the pair energies E_{ij} accurately, at least on the average. The size of the fragments depends on the number of amplitude matrices $\mathbf{T}^{ik}$ and $\mathbf{T}^{jk}$ that are taken into account in the computation of the residual $\mathbf{R}^{ij}$. This number depends on the distant pair threshold T_{dist} in our PNO-LCCSD method.

In Figure 1.11, the dependence of the PNO-LCCSD reaction energy of the three benchmark reactions is shown as a function of T_{dist}. Either distant pairs are neglected entirely or an LMP2 correction for distant pairs is added. When the distant pairs are entirely neglected, the convergence with decreasing threshold T_{dist} is very slow. The LMP2 correction somewhat improves the accuracy, but overshoots significantly, as has been shown earlier for PNO-LCCD. Significantly better results are obtained by using spin-component scaled LMP2 (SCS-LMP2) [217] for the distant pair correction. This is consistent with the well-known fact that SCS-LMP2 avoids the overestimation of dispersion interactions by LMP2. But for the Auamin reaction, the error still amounts to about 2 kJ mol^{-1} if a threshold of $T_{\text{dist}} = 10^{-5}\,E_{\text{h}}$ is used. It should be noted that for distant pairs, when the charge-transfer and exchange contributions are neglected (`NOEX` approximation), the SCS-LMP2 pair correlation energies are obtained simply by scaling the LMP2 ones with a factor of $23/30 = 0.766$.

Table 1.12 shows the average and maximum numbers of LMOs k that occur in $\mathbf{T}^{ik}$ and $\mathbf{T}^{jk}$ contributing to a residual $\mathbf{R}^{ij}$ as a function of two thresholds: T_{primary} and $T_{\text{secondary}}$. T_{primary} determines the selection of primary pairs, while $T_{\text{secondary}}$ controls the selection of the secondary pairs for each primary pair (Figure 1.11 corresponds to $T_{\text{dist}} = T_{\text{secondary}} = T_{\text{primary}}$). We restrict here $T_{\text{secondary}} \leq T_{\text{primary}}$. These thresholds determine the minimum fragment size that would be necessary for a fragment calculation with comparable accuracy. Naturally, the number of LMOs k increases with decreasing threshold T_{primary}, since for small thresholds more pairs with distant orbitals i and j are included. For the molecules shown in Table 1.12, with the smallest considered threshold of $T_{\text{primary}} = 3 \times 10^{-6}$, the largest fragment comprises the whole molecule. Even with a threshold of $T_{\text{primary}} = 3 \times 10^{-5}$, the largest fragments still comprise 60–100 LMOs. Unfortunately, conventional CCSD or even CCSD(T) calculations of this size with reasonable basis sets are extremely challenging at present, and this limits the accuracy or applicability of fragmentation approaches.

On the other hand, in local correlation methods, only a non-redundant set of integrals and residuals is computed. Furthermore, the CPU time per residual is greatly reduced through the use of domain and pair approximations. Therefore, such calculations should be much faster than fragmentation calculations. However, the size of molecules that can be treated is mainly limited by the required memory and/or disk space. Our methods are very well parallelized, and in order to avoid I/O bottlenecks, currently all data is kept in distributed memory (global arrays or distributed local data). The number of computer nodes that are necessary for a particular calculation depends on the memory per node, the size of the molecule, and the basis set. The molecular size that can be handled is in principle scalable with the number of nodes, but in practice, some quantities such as overlap or Fock matrices must be kept locally on each node. This currently limits the

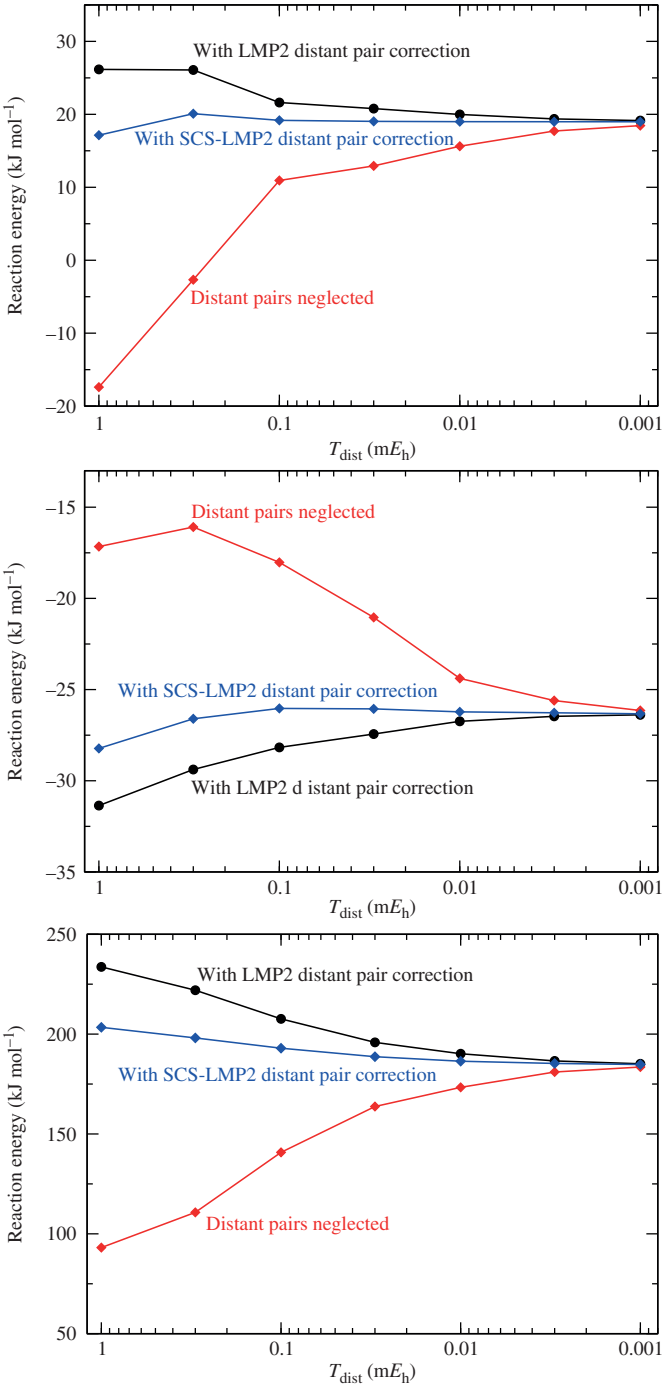


Figure 1.11 LCCSD-F12 reaction energies for the reactions **I** (top), **II** (middle), and **III** (bottom) as a function of the distant pair threshold T_{dist}. All pairs which have LMP2 pair energies $\geq T_{dist}$ are included. The remaining pairs are either neglected or treated by LMP2. Basis set: VTZ-F12, `IEXT=1`.

Table 1.12 The average (n_k^{avg}) and the maximum (n_k^{max}) numbers of LMOs that are associated with an LMO pair *ij* with the restriction that the pair energies $E_{ij} \geq T_{primary}$ (shown in the table header), and $E_{ik} \geq T_{secondary}$ or $E_{kj} \geq T_{secondary}$.

		3×10^{-4}		3×10^{-5}		3×10^{-6}	
Molecule	$T_{secondary}$	n_k^{avg}	n_k^{max}	n_k^{avg}	n_k^{max}	n_k^{avg}	n_k^{max}
Auamin	3×10^{-4}	24.5	55				
	3×10^{-5}	49.4	100	56.3	102		
	3×10^{-6}	81.5	122	87.9	122	91.7	122
Precursor	3×10^{-4}	22.7	38				
	3×10^{-5}	37.7	64	41.1	71		
	3×10^{-6}	51.7	78	54.8	78	58.0	78
Auamin2s	3×10^{-4}	23.8	56				
	3×10^{-5}	41.5	68	45.9	71		
	3×10^{-6}	58.7	76	61.9	76	63.8	76
Ester	3×10^{-4}	22.6	41				
	3×10^{-5}	39.0	56	42.2	64		
	3×10^{-6}	50.5	66	53.5	69	55.7	69

applicability of our method to molecular sizes of a few hundred atoms. The memory problem can be alleviated by storing data on disks, but then parallelization becomes much less efficient and the overall elapsed time will become the bottleneck. Nevertheless, Neese and coworkers have presented some impressive calculations with more than 20,000 basis functions and 1000 atoms (for linear alkane chains).

A way forward to treat "very" large molecules is to combine the ideas of local correlation and fragmentation methods. Of course, it would be immediately possible to use local correlation methods for each fragment.

1.14 Summary

In this chapter, we have reviewed important aspects of local correlation methods, namely the construction of most suitable local orbital spaces, the choice of domains, and pair approximations for weak and distant pairs. We have shown that all approximations can be well controlled by a few parameters, and for medium-sized molecules (up to about 100 atoms), it is possible to reduce the errors caused by local approximations to the mE_h scale for absolute energies and below 1 kJ mol^{-1} for relative energies. By including explicitly correlated terms in the wave function, basis set incompleteness errors are also strongly reduced, and better than quintuple-ζ quality results are obtained with triple-ζ basis sets. This makes it possible to compute highly accurate coupled-cluster energies for much larger molecules than can be treated by conventional coupled-cluster methods.

Without an F12 treatment, basis set incompleteness errors are in many cases much larger than those caused by local approximations, and therefore it is strongly recommended to always use the explicitly correlated variants. With our new PNO-LCCSD-F12 method, the additional cost is small, usually less than 20% of the total computation time, but the improvements of the results are drastic. Besides the reduction of basis set errors, also the errors caused by the local domain approximation are strongly reduced by the F12 terms. The reason is twofold: first, intramolecular basis superposition errors (BSSE) can be significant in canonical calculations unless very large basis sets are used. The local domain approximation strongly reduces these errors [14, 147, 212], which leads to smaller absolute values of the correlation energy, and so apparently to domain errors. These decay slowly with increasing domain sizes, since then the BSSE is recovered. This view is corroborated by the finding that the convergence of relative energies and other properties toward the CBS limit is often significantly better for local than for canonical methods [25, 147, 218, 219]. The BSSE effects are strongly reduced by the explicit correlation treatment, and this contributes to the reduction of the (apparent) domain errors. The second reason for the reduction of these errors is that the F12 terms in the wave function can implicitly approximate the energy contributions of the orbitals that are omitted in the domain approximation.

In many early papers on local correlation methods, it was assumed that the largest errors arise from the domain approximation, and that the effect of pair approximations is small. In our current methods, it is likely that the opposite is true. The F12 corrections reduce the domain errors typically by one order of magnitude (see above). Furthermore, much larger PAO domains can now be used than in early PAO-LCCSD programs. With triple-ζ basis sets, our current default PAO domains comprise 300–600 PAOs per pair. Solving the PAO-LCCSD amplitude equations with such large domains would be extremely demanding. However, the domain sizes are reduced by a factor of 5–10 (even more for weak pairs) when PNOs are used, and this dramatically reduces the CPU and memory demands. The integrals are still computed in the PAO basis using large domains, but transformed on the fly to the much smaller pair-specific PNO domains. Thus, 4-index quantities in the PAO basis are never stored. For example, the number of 4-external integrals depends on the fourth power of the domain sizes, and is therefore in the PNO basis 3–4 orders of magnitude smaller than in the PAO basis. This makes it possible to keep all quantities such as integrals, amplitudes, and intermediates in distributed high-speed memory, which is a prerequisite for efficient parallelization.

Despite this improvement, PNO-LCCSD calculations without further approximations still become prohibitively expensive for very large molecules. This is due to the fact that the number of pairs increases quadratically with the number of correlated electrons. Even if distant pairs with energy contributions $\leq 10^{-6}\ E_\mathrm{h}$ are treated by the multipole approximation, there may still be a very large number of "weak" pairs with individually small energy contributions of $10^{-6} \leq E_{ij} \leq 10^{-4}\ E_\mathrm{h}$. The sum of these pair energies is significant and also important in order to obtain accurate relative energies. Approximating the amplitudes and energies of weak pairs by LMP2, as was done in the older PAO-LCCSD methods developed in our group [7, 18, 31], and also adopted in the DLPNO-LCCSD methods of Riplinger *et al.* [54, 57], may unfortunately lead to unexpectedly large errors. There are two sources for these errors. First, long-range correlation effects are significantly overestimated by MP2. This effect can be significantly reduced by using SCS-MP2 pair energies, but tests have shown that the accuracy is still unsatisfactory

for weak pairs. Second, it is very important to include the amplitudes of the weak pairs into the strong-pair residuals, that is, to account for the coupling of strong and weak pairs accurately. Without this, the strong pair energies are overestimated. Using LMP2 amplitudes for the weak pairs is insufficient to remove this error.

It is therefore important to apply higher-order approximations for simplifying the treatment of close and weak pairs. We have shown that an approximate CCSD treatment [32, 204, 205], in which terms that cancel at long-range are neglected, leads to excellent results, and nevertheless to a significant reduction of the computational effort and storage demands. Most importantly, the expensive class of 4-external integrals is then needed only for the strong pairs. Furthermore, a linearized coupled-cluster (CEPA) treatment is sufficient for weak pairs.

The finding that the neglect of weak pairs in LCCSD treatments causes large errors is also highly relevant for fragmentation methods. It means that the fragments must be very large in order to obtain converged results. Even in the extreme case that each fragment is used to compute only a single pair energy, the necessary fragment sizes may comprise 100 or more LMOs. Conventional calculations of this size may be extremely expensive, if possible at all.

The computational cost and storage demands of local correlation methods increase at least linearly with the molecular size. It is difficult to avoid the storage of some quantities that scale quadratically on each computing core, as for example the Fock and overlap matrices in the full PAO basis, and this becomes a limiting factor for calculations with more than $\approx 10,000$ basis functions. Furthermore, due to the relatively slow decay of some singles terms it is advantageous to compute in each iteration a "dressed" Fock matrix that depends on the singles amplitudes. This part requires some operations that scale cubically with the molecular size, though with a very low prefactor. The applicability of our current program is mainly limited by the memory demands. Since the data is distributed over many processors, the method is well suited for small compute clusters as available in many groups. Currently, it allows accurate LCCSD-F12 calculations for molecules with 100–200 atoms in a few hours of elapsed time using 100–200 compute cores. A perturbative correction for triple excitations is still under development.

Calculations for larger molecules would be possible by combining local correlation and fragmentation methods. The overall memory and storage demands then become independent of the molecular size, at the prize of introducing a lot of redundancy. We believe, however, that for the simulation of most real chemistry problems, calculations for molecules with more that 100–200 atoms are hardly necessary. One should also keep in mind that in large systems, dynamical and entropic effects become increasingly important, and therefore single-point calculations loose their justification. The environment in large systems can be taken into account by QM/MM methods or other embedding techniques. Local correlation methods in combination with QM/MM approaches have for example been successfully used to study some enzyme reactions [29, 220–222]. Local correlation methods also allow treating the active region of a reaction at a high level [e.g., LCCSD(T)], and a larger environment at a lower level, for example, LMP2 [30]. This can save a huge amount of computer time without losing much accuracy.

Finally, it should be mentioned that the implementation of analytical energy gradients for high-level local correlation methods is very challenging. Efficient analytical energy gradients are available for PAO-LMP2 [23, 223] and Laplace-transformed LMP2 methods [42], but these still cannot compete with the speed of DFT gradient calculations.

Although rather straightforward in principle [224], a manual implementation of LCCSD gradients would be cumbersome. This is particularly true for PNO-based methods, since various auxiliary conditions, which are related to the PNO definition, must be taken into account. The implementation of such complex methods can be facilitated using tools like the integrated tensor framework (ITF) of Knizia [182, 225], which has recently been extended to local PAO, OSV, and PNO methods by Kats [34, 176]. This is a program which can directly execute a long sequence of tensor expressions, which are provided in a readable formula file. The expressions can be generated and factorized with the help of computer algebra programs. However, such gradient calculations would at least be twice as expensive as an energy calculation. They could be used for accurate geometry optimizations of medium-sized molecules, but it is unlikely that in the near future high-level wave function methods can be applied for direct dynamics calculations for large systems.

Appendix A: The LCCSD Equations

In the following, summations over repeated indices are implied. r, s, t, u will denote non-orthogonal virtual orbitals (e.g., PAOs or PNOs), and $\mathbf{S}$ their overlap matrix $S_{rs} = \langle r|s\rangle$. We define amplitude and integral matrices (upper case bold face letters)

$$[\mathbf{T}^{kl}]_{rs} = T^{kl}_{rs}, \qquad \tilde{\mathbf{T}}^{kl} = 2\mathbf{T}^{kl} - \mathbf{T}^{lk} \tag{A.1}$$

$$[\mathbf{D}^{ij}]_{rs} = T^{ij}_{rs} + t^i_r t^j_s, \qquad \tilde{\mathbf{D}}^{kl} = 2\mathbf{D}^{kl} - \mathbf{D}^{lk} \tag{A.2}$$

$$[\mathbf{K}^{kl}]_{rs} = (rk|ls), \qquad \mathbf{L}^{kl} = 2\mathbf{K}^{kl} - \mathbf{K}^{lk} \tag{A.3}$$

$$[\mathbf{J}^{kl}]_{rs} = (rs|kl), \qquad [\mathbf{F}]_{rs} = F_{rs} \tag{A.4}$$

as well as vectors (lower case bold face letters)

$$[\mathbf{t}^i]_r = t^i_r, \tag{A.5}$$

$$[\mathbf{k}^{kli}]_r = (rk|li), \qquad \mathbf{l}^{kli} = 2\mathbf{k}^{kli} - \mathbf{k}^{lki} \tag{A.6}$$

$$[\bar{\mathbf{k}}^{kli}]_r = [\mathbf{k}^{kli} + \mathbf{K}^{kl}\mathbf{t}^i]_r, \quad \bar{\mathbf{l}}^{kli} = \mathbf{l}^{kli} + \mathbf{L}^{kl}\mathbf{t}^i, \tag{A.7}$$

$$[\mathbf{f}^k]_r = F_{rk}. \tag{A.8}$$

The dimension of all these matrices and vectors corresponds to the virtual space (or, in practice, domains in the virtual space). The domains are implied by the superscripts of the residual and amplitude matrices or vectors, and will not be shown explicitly. The following contractions of amplitudes and integrals will be used and have to be computed in each iteration:

$$[\mathbf{K}(\mathbf{D}^{ij})]_{rs} = (rt|su)D^{ij}_{tu} \tag{A.9}$$

$$[\mathbf{K}(\mathbf{D}^{ij})^k]_r = [\mathbf{K}(\mathbf{D}^{ij})]_{rk} = (rt|ku)D^{ij}_{tu} \tag{A.10}$$

$$[\mathbf{J}(\mathbf{E}^{ik})]_{rs} = (rs|it)t^k_t, \tag{A.11}$$

$$[\mathbf{K}(\mathbf{E}^{ik})]_{rs} = (ri|st)t^k_t, \tag{A.12}$$

$$[\tilde{\mathbf{G}}]_{rs} = [2(rs|ku) - (rk|su)]t^k_u. \tag{A.13}$$

Note that in previous papers [18, 31], we denoted the latter matrix as $[\mathbf{G}(\mathbf{E})]_{rs}$. This notation stems from the formal definition $[\mathbf{E}^{ik}]_{tu} = \delta_{ti} t^k_u$ and $[\mathbf{G}(\mathbf{E})]_{rs} = \sum_k [2\mathbf{J}(\mathbf{E}^{kk}) - \mathbf{K}(\mathbf{E}^{kk})]_{rs}$. Here we will use the simplified notation.

In the calculation of $\mathbf{D}^{ij}$ in the PNO basis, the singles must be projected

$$D^{ij}_{a^{ij}b^{ij}} = T^{ij}_{a^{ij}b^{ij}} + \langle a^{ij}|c^{ii}\rangle t^i_{c^{ii}} t^j_{d^{jj}} \langle d^{jj}|b^{ij}\rangle. \tag{A.14}$$

In terms of these quantities, the singles and the doubles residuals are

$$\mathbf{r}^i = \tilde{\mathbf{f}}^i + \bar{\mathbf{F}}^\dagger \mathbf{t}^i - \mathbf{S}\mathbf{T}^{kl}\mathbf{l}^{lki} + \mathbf{S}\tilde{\mathbf{T}}^{ik}\bar{\mathbf{f}}^k + \mathbf{K}(\tilde{\mathbf{T}}^{ik})^k - \beta_{ik}\mathbf{S}\mathbf{t}^k, \tag{A.15}$$

$$\mathbf{R}^{ij} = \mathbf{K}^{ij} + \mathbf{K}(\mathbf{D}^{ij}) + \alpha_{ij,kl}\mathbf{S}\mathbf{D}^{kl}\mathbf{S} + \mathbf{G}^{ij} + \mathbf{G}^{ji\dagger}, \tag{A.16}$$

$$\begin{aligned}\mathbf{G}^{ij} = {} & \mathbf{K}(\mathbf{E}^{ij}) + \mathbf{S}\mathbf{T}^{ij}\mathbf{X} + \mathbf{S}\left[\tilde{\mathbf{T}}^{ik}\mathbf{Y}^{kj} - \frac{1}{2}\mathbf{T}^{ki}\mathbf{Z}^{kj}\right] - (\mathbf{S}\mathbf{T}^{ki}\mathbf{Z}^{kj})^\dagger \\ & - \left[\mathbf{K}(\mathbf{D}^{ij})^k + \bar{\mathbf{k}}^{ikj} + \mathbf{J}^{jk}\mathbf{t}^i\right](\mathbf{S}\mathbf{t}^k)^\dagger - \beta_{ik}[\mathbf{S}\mathbf{T}^{kj}\mathbf{S}]\end{aligned} \tag{A.17}$$

with the intermediates

$$\alpha_{ij,kl} = (ik|jl) + \mathbf{t}^{i\dagger}\mathbf{k}^{klj} + \mathbf{t}^{j\dagger}\mathbf{k}^{lki} + tr(\mathbf{D}^{ij}\mathbf{K}^{lk}), \tag{A.18}$$

$$\beta_{ik} = f_{ik} + \mathbf{t}^{i\dagger}\mathbf{f}^k + \mathbf{t}^{j\dagger}\bar{\mathbf{l}}^{lki} + tr(\mathbf{L}^{kl}\mathbf{T}^{li}), \tag{A.19}$$

$$\tilde{\mathbf{f}}^i = \mathbf{f}^i + (2\mathbf{K}^{ik} - \mathbf{J}^{ik})\mathbf{t}^k, \tag{A.20}$$

$$\bar{\mathbf{f}}^k = \mathbf{f}^k + \mathbf{L}^{kl}\mathbf{t}^l, \tag{A.21}$$

$$\bar{\mathbf{F}} = \mathbf{F} + \tilde{\mathbf{G}} - \mathbf{L}^{lk}\mathbf{T}^{kl}\mathbf{S}, \tag{A.22}$$

$$\mathbf{X} = \bar{\mathbf{F}} - \bar{\mathbf{f}}^k(\mathbf{S}\mathbf{t}^k)^\dagger, \tag{A.23}$$

$$\mathbf{Y}^{kj} = \mathbf{K}^{kj} + \mathbf{K}(\mathbf{E}^{kj}) - \frac{1}{2}\left[\mathbf{J}^{kj} + \mathbf{J}(\mathbf{E}^{kj}) + \bar{\mathbf{l}}^{klj}(\mathbf{S}\mathbf{t}^l)^\dagger\right] + \frac{1}{4}\mathbf{L}^{kl}\tilde{\mathbf{T}}^{lj}\mathbf{S}, \tag{A.24}$$

$$\mathbf{Z}^{kj} = \mathbf{J}^{kj} + \mathbf{J}(\mathbf{E}^{kj}) - \frac{1}{2}\mathbf{K}^{lk}\mathbf{T}^{jl}\mathbf{S} - \bar{\mathbf{k}}^{lkj}(\mathbf{S}\mathbf{t}^l)^\dagger. \tag{A.25}$$

In a canonical CCSD or in a PAO-LCCSD program, the intermediates $\mathbf{X}$, $\mathbf{Y}^{kj}$, and $\mathbf{Z}^{kj}$ can be precomputed and then multiplied from the left with the appropriate amplitude matrices (in the PAO case the intermediates $\mathbf{Y}^{kj}$ and $\mathbf{Z}^{kj}$ are stored using united domains, see Ref. [147] for details). This leads to the smallest number of matrix multiplications. In a PNO-LCCSD method, this is not possible, since the left indices of the intermediates depend on the pair with which they are multiplied, and therefore each term in the intermediates must be recomputed for each i.

In our program, $\tilde{\mathbf{G}}$ is computed in each iteration in the full AO basis similar to a Fock matrix and subsequently transformed to the LMO/PAO|PNO basis. The intermediates $\bar{\mathbf{f}}^k$, $\tilde{\mathbf{f}}^i$, and β_{ik} can then be simplified to

$$\bar{f}^k_r = f^k_r + \tilde{G}_{rk}, \tag{A.26}$$

$$\tilde{f}^k_r = f^k_r + \tilde{G}_{kr}, \tag{A.27}$$

$$\beta_{ik} = f_{ik} + \tilde{G}_{ik} + \mathbf{t}^{i\dagger}\bar{\mathbf{f}}^k + tr(\mathbf{L}^{kl}\mathbf{T}^{li}). \tag{A.28}$$

This also avoids summations over slowly decaying terms. Furthermore, the singles energy contribution can be compactly written as

$$E_{\text{sing}} = \mathbf{t}^{k\dagger}(\mathbf{f}^k + \mathbf{L}^{kl}\mathbf{t}^l) = \mathbf{t}^{k\dagger}\bar{\mathbf{f}}^k. \tag{A.29}$$

Note that all terms are now expressed by a "dressed" Fock matrix $\mathbf{F}_{\mathrm{AO}} + \tilde{\mathbf{G}}_{\mathrm{AO}}$. We compute the two contributions separately. $\mathbf{F}_{\mathrm{AO}}$ is taken from the preceding HF calculation, which uses the JKFIT auxiliary basis, while $\tilde{\mathbf{G}}_{\mathrm{AO}}$ is computed in each iteration using the MP2FIT auxiliary basis (for consistency with other terms). The sum of both contributions is subsequently transformed to the appropriate LMO/PAO spaces.

Appendix B: Derivation of the Interaction Matrices

The powers of x defined in equation (1.73) are

$$x = (\hat{\mathbf{r}} \cdot \hat{\mathbf{r}}) + 2(\hat{\mathbf{r}} \cdot \hat{\mathbf{R}}), \tag{B.1}$$

$$x^2 = (\hat{\mathbf{r}} \cdot \hat{\mathbf{r}})^2 + 4(\hat{\mathbf{r}} \cdot \hat{\mathbf{R}})^2 + 4(\hat{\mathbf{r}} \cdot \hat{\mathbf{r}})(\hat{\mathbf{r}} \cdot \hat{\mathbf{R}}), \tag{B.2}$$

$$x^3 = (\hat{\mathbf{r}} \cdot \hat{\mathbf{r}})^3 + 8(\hat{\mathbf{r}} \cdot \hat{\mathbf{R}})^3 + 6(\hat{\mathbf{r}} \cdot \hat{\mathbf{r}})^2(\hat{\mathbf{r}} \cdot \hat{\mathbf{R}}) + 12(\hat{\mathbf{r}} \cdot \hat{\mathbf{r}})(\hat{\mathbf{r}} \cdot \hat{\mathbf{R}})^2, \tag{B.3}$$

$$\begin{aligned} x^4 = {} & (\hat{\mathbf{r}} \cdot \hat{\mathbf{r}})^4 + 16(\hat{\mathbf{r}} \cdot \hat{\mathbf{R}})^4 + 24(\hat{\mathbf{r}} \cdot \hat{\mathbf{r}})^2(\hat{\mathbf{r}} \cdot \hat{\mathbf{R}})^2 \\ & + 8(\hat{\mathbf{r}} \cdot \hat{\mathbf{r}})^4(\hat{\mathbf{r}} \cdot \hat{\mathbf{R}}) + 32(\hat{\mathbf{r}} \cdot \hat{\mathbf{r}})(\hat{\mathbf{r}} \cdot \hat{\mathbf{R}})^3. \end{aligned} \tag{B.4}$$

The different interactions are obtained by replacing $\hat{\mathbf{r}}$ by the appropriate $-\bar{\mathbf{r}}_1/R$ or $\bar{\mathbf{r}}_2/R$. Whenever $(\bar{\mathbf{r}}_1 \cdot \bar{\mathbf{r}}_2)$ occurs, a factor of 2 applies, since the contributions of $(\bar{\mathbf{r}}_1 \cdot \bar{\mathbf{r}}_2)$ and $(\bar{\mathbf{r}}_2 \cdot \bar{\mathbf{r}}_1)$ are the same. Similarly, appropriate factors apply for powers of $(\hat{\mathbf{r}} \cdot \hat{\mathbf{R}})$. This yields for the dipole—dipole interaction:

$$\begin{aligned} V_{1,1} &= -2c_1(\bar{\mathbf{r}}_1 \cdot \bar{\mathbf{r}}_2) - 8c_2(\bar{\mathbf{r}}_1 \cdot \hat{\mathbf{R}})(\bar{\mathbf{r}}_2 \cdot \hat{\mathbf{R}}) \\ &= \bar{\mathbf{r}}_1 \cdot \bar{\mathbf{r}}_2 - 3(\bar{\mathbf{r}}_1 \cdot \hat{\mathbf{R}})(\bar{\mathbf{r}}_2 \cdot \hat{\mathbf{R}}). \end{aligned} \tag{B.5}$$

Using the factors $c_1 = -\frac{1}{2}$, $c_2 = \frac{3}{8}$, $c_3 = -\frac{5}{16}$, $c_4 = \frac{35}{128}$, the terms describing the interaction of higher moments are derived similarly. The results are summarized in the following. The interaction potentials in equation (1.77) are

Dipole–Quadrupole:

$$\begin{aligned} V_{1,2} &= -8c_2(\bar{\mathbf{r}}_1 \cdot \bar{\mathbf{r}}_2)(\bar{\mathbf{r}}_2 \cdot \hat{\mathbf{R}}) - 4c_2(\bar{\mathbf{r}}_2 \cdot \bar{\mathbf{r}}_2)(\bar{\mathbf{r}}_1 \cdot \hat{\mathbf{R}}) - 24c_3(\bar{\mathbf{r}}_1 \cdot \hat{\mathbf{R}})(\bar{\mathbf{r}}_2 \cdot \hat{\mathbf{R}})^2 \\ &= -3(\bar{\mathbf{r}}_1 \cdot \bar{\mathbf{r}}_2)(\bar{\mathbf{r}}_2 \cdot \hat{\mathbf{R}}) - \frac{3}{2}(\bar{\mathbf{r}}_2 \cdot \bar{\mathbf{r}}_2)(\bar{\mathbf{r}}_1 \cdot \hat{\mathbf{R}}) + \frac{15}{2}(\bar{\mathbf{r}}_1 \cdot \hat{\mathbf{R}})(\bar{\mathbf{r}}_2 \cdot \hat{\mathbf{R}})^2; \end{aligned} \tag{B.6}$$

Quadrupole–Quadrupole:

$$\begin{aligned} V_{2,2} = {} & 2c_2\left[2(\bar{\mathbf{r}}_1 \cdot \bar{\mathbf{r}}_2)(\bar{\mathbf{r}}_1 \cdot \bar{\mathbf{r}}_2) + (\bar{\mathbf{r}}_1 \cdot \bar{\mathbf{r}}_1)(\bar{\mathbf{r}}_2 \cdot \bar{\mathbf{r}}_2)\right] \\ & + 12c_3\left[(\bar{\mathbf{r}}_1 \cdot \bar{\mathbf{r}}_1)(\bar{\mathbf{r}}_2 \cdot \bar{\mathbf{r}})^2 + (\bar{\mathbf{r}}_2 \cdot \bar{\mathbf{r}}_2)(\bar{\mathbf{r}}_1 \cdot \bar{\mathbf{r}})^2\right] \\ & + 48c_3(\bar{\mathbf{r}}_1 \cdot \hat{\mathbf{R}})(\bar{\mathbf{r}}_1 \cdot \bar{\mathbf{r}}_2)(\bar{\mathbf{r}}_2 \cdot \hat{\mathbf{R}}) + 96c_4(\bar{\mathbf{r}}_1 \cdot \hat{\mathbf{R}})^2(\bar{\mathbf{r}}_2 \cdot \hat{\mathbf{R}})^2 \\ = {} & \frac{3}{2}(\bar{\mathbf{r}}_1 \cdot \bar{\mathbf{r}}_2)(\bar{\mathbf{r}}_1 \cdot \bar{\mathbf{r}}_2) + \frac{3}{4}(\bar{\mathbf{r}}_1 \cdot \bar{\mathbf{r}}_1)(\bar{\mathbf{r}}_2 \cdot \bar{\mathbf{r}}_2) \\ & - \frac{15}{4}\left[(\bar{\mathbf{r}}_1 \cdot \bar{\mathbf{r}}_1)(\bar{\mathbf{r}}_2 \cdot \hat{\mathbf{R}})^2 + (\bar{\mathbf{r}}_2 \cdot \bar{\mathbf{r}}_2)(\bar{\mathbf{r}}_1 \cdot \hat{\mathbf{R}})^2\right] \\ & - 15(\bar{\mathbf{r}}_1 \cdot \hat{\mathbf{R}})(\bar{\mathbf{r}}_1 \cdot \bar{\mathbf{r}}_2)(\bar{\mathbf{r}}_2 \cdot \hat{\mathbf{R}}) + \frac{105}{4}(\bar{\mathbf{r}}_1 \cdot \hat{\mathbf{R}})^2(\bar{\mathbf{r}}_2 \cdot \hat{\mathbf{R}})^2; \end{aligned} \tag{B.7}$$

Octupole–Dipole:

$$\begin{aligned} V_{1,3} &= -4c_2\ (\bar{\mathbf{r}}_1\cdot\bar{\mathbf{r}}_2)(\bar{\mathbf{r}}_2\cdot\bar{\mathbf{r}}_2) \\ &\quad -24c_3\left[(\bar{\mathbf{r}}_1\cdot\bar{\mathbf{r}}_2)(\bar{\mathbf{r}}_2\cdot\hat{\mathbf{R}})^2-(\bar{\mathbf{r}}_1\cdot\hat{\mathbf{R}})(\bar{\mathbf{r}}_2\cdot\bar{\mathbf{r}}_2)(\bar{\mathbf{r}}_2\cdot\hat{\mathbf{R}})\right] \\ &\quad -64c_4(\bar{\mathbf{r}}_2\cdot\hat{\mathbf{R}})^3(\bar{\mathbf{r}}_1\cdot\hat{\mathbf{R}}) \\ &= -\frac{3}{2}(\bar{\mathbf{r}}_1\cdot\bar{\mathbf{r}}_2)(\bar{\mathbf{r}}_2\cdot\bar{\mathbf{r}}_2)+\frac{15}{2}\left[(\bar{\mathbf{r}}_1\cdot\bar{\mathbf{r}}_2)(\bar{\mathbf{r}}_2\cdot\hat{\mathbf{R}})^2+(\bar{\mathbf{r}}_1\cdot\hat{\mathbf{R}})(\bar{\mathbf{r}}_2\cdot\bar{\mathbf{r}}_2)(\bar{\mathbf{r}}_2\cdot\hat{\mathbf{R}})\right] \\ &\quad -\frac{35}{2}(\bar{\mathbf{r}}_2\cdot\hat{\mathbf{R}})^3(\bar{\mathbf{r}}_1\cdot\hat{\mathbf{R}})\Big]. \end{aligned} \tag{B.8}$$

The remaining two interactions are obtained using

$$V_{2,1}(\bar{\mathbf{r}}_1,\bar{\mathbf{r}}_2,\hat{\mathbf{R}}) = -V_{1,2}(\bar{\mathbf{r}}_2,\bar{\mathbf{r}}_1,\hat{\mathbf{R}}), \tag{B.9}$$

$$V_{3,1}(\bar{\mathbf{r}}_1,\bar{\mathbf{r}}_2,\hat{\mathbf{R}}) = V_{1,3}(\bar{\mathbf{r}}_2,\bar{\mathbf{r}}_1,\hat{\mathbf{R}}). \tag{B.10}$$

In order to obtain the interaction matrices, one has to expand the scalar products and collect the contributions of $\bar{\mathbf{r}}_1$ and $\bar{\mathbf{r}}_2$. In the following, $\alpha,\beta,\gamma,\mu,\nu\in\{x,y,z\}$. For example,

$$(\bar{\mathbf{r}}_1\cdot\bar{\mathbf{r}}_2)^2=\sum_{\alpha\beta}(\alpha_1\beta_1)(\alpha_2\beta_2)=\sum_{\alpha\le\beta}\frac{2}{l_\alpha!l_\beta!}(\alpha_1\beta_1)(\alpha_2\beta_2).$$

The factor $2/(l_\alpha!l_\beta!)=2-\delta_{\alpha\beta}$ occurs since we restrict the summations in equation (1.83) to the unique second-moment operators, that is, $\alpha\le\beta$ (the l_α, l_β are defined as explained below equation (1.84)). Similarly, for third moments, there may be up to $3!=6$ equal contributions, and factors of $6/(l_\alpha!l_\beta!l_\gamma!)$ arise.

The interaction matrices up to $p=3$ read explicitly:

$$A^{(1,1)}_{\alpha,\beta}=\delta_{\alpha\beta}-3\hat{R}_\alpha\hat{R}_\beta, \tag{B.11}$$

$$\begin{aligned} A^{(2,1)}_{\alpha\beta,\gamma} &= \frac{1}{l_\alpha l_\beta}\left[15\hat{R}_\alpha\hat{R}_\beta\hat{R}_\gamma-3(\hat{R}_\alpha\delta_{\beta\gamma}+\hat{R}_\beta\delta_{\alpha\gamma}+\hat{R}_\gamma\delta_{\alpha\beta})\right], \\ A^{(1,2)}_{\gamma,\alpha\beta} &= -A^{(2,1)}_{\alpha\beta,\gamma}, \qquad \alpha\le\beta, \end{aligned} \tag{B.12}$$

$$\begin{aligned} A^{(2,2)}_{\alpha\beta,\mu\nu} &= \frac{1}{l_\alpha!l_\beta!l_\mu!l_\nu!}\Big[3(\delta_{\alpha\mu}\delta_{\beta\nu}+\delta_{\alpha\nu}\delta_{\beta\mu}+\delta_{\alpha\beta}\delta_{\mu\nu}) \\ &\quad -15\,(\delta_{\alpha\beta}\hat{R}_\mu R_\nu+\delta_{\alpha\mu}\hat{R}_\beta R_\nu+\delta_{\alpha\nu}\hat{R}_\beta R_\mu \\ &\quad +\delta_{\beta\mu}\hat{R}_\alpha\hat{R}_\nu+\delta_{\beta\nu}\hat{R}_\alpha\hat{R}_\mu+\delta_{\mu\nu}\hat{R}_\alpha\hat{R}_\beta) \\ &\quad +105\,\hat{R}_\alpha\hat{R}_\beta\hat{R}_\mu\hat{R}_\nu\Big] \qquad \alpha\le\beta,\mu\le\nu, \end{aligned} \tag{B.13}$$

$$A^{(3,1)}_{\alpha\beta\gamma,\mu}=A^{(2,2)}_{\alpha\beta,\gamma\mu}, \tag{B.14}$$

$$A^{(1,3)}_{\mu,\alpha\beta\gamma}=A^{(3,1)}_{\alpha\beta\gamma,\mu}, \quad \alpha\le\beta\le\gamma. \tag{B.15}$$

The interaction matrices for the quadrupole–quadrupole and octupole–dipole interactions are formally identical but differ by the prefactors and index restrictions.

Acknowledgments

This work has been funded by the ERC Advanced Grant 320723 (ASES).

References

1 Pulay, P. (1983) Localizability of dynamic electron correlation. *Chem. Phys. Lett.*, **100**, 151–154.
2 Saebø, S. and Pulay, P. (1985) Local configuration-interaction: An efficient approach for larger molecules. *Chem. Phys. Lett.*, **113**, 13–18.
3 Pulay, P. and Saebø, S. (1986) Orbital-invariant formulation and second-order gradient evaluation in Møller-Plesset perturbation theory. *Theor. Chim. Acta*, **69**, 357–368.
4 Saebø, S. and Pulay, P. (1987) Fourth-order Møller-Plesset perturbation theory in the local correlation treatment. I. Method. *J. Chem. Phys.*, **86**, 914–922.
5 Saebø, S. and Pulay, P. (1988) The local correlation treatment. II. Implementation and tests. *J. Chem. Phys.*, **88**, 1884–1890.
6 Saebø, S. and Pulay, P. (1993) Local treatment of electron correlation. *Annu. Rev. Phys. Chem.*, **44**, 213–236.
7 Hampel, C. and Werner, H.J. (1996) Local treatment of electron correlation in coupled cluster theory. *J. Chem. Phys.*, **104**, 6286–6297.
8 Maslen, P.E. and Head-Gordon, M. (1998) Non-iterative local second order Moller-Plesset theory. *Chem. Phys. Lett.*, **283**, 102–180.
9 Maslen, P.E. and Head-Gordon, M. (1998) Noniterative local second order Moller-Plesset theory: Convergence with local correlation space. *J. Chem. Phys.*, **109**, 7093–7099.
10 Ayala, P.Y. and Scuseria, G.E. (1999) Linear scaling second-order Møller-Plesset theory in the atomic orbital basis for large molecular systems. *J. Chem. Phys.*, **110**, 3660–3671.
11 Scuseria, G.E. and Ayala, P.Y. (1999) Linear scaling coupled cluster and perturbation theories in the atomic orbital basis. *J. Chem. Phys.*, **111**, 8330–8343.
12 Hetzer, G., Pulay, P., and Werner, H.J. (1998) Multipole approximation of distant pair energies in local MP2 calculations. *Chem. Phys. Lett.*, **290**, 143–149.
13 Hetzer, G., Schütz, M., Stoll, H., and Werner, H.J. (2000) Low-order scaling local correlation methods II: Splitting the Coulomb operator in linear scaling local second-order Møller-Plesset perturbation theory. *J. Chem. Phys.*, **113**, 9443–9455.
14 Schütz, M., Rauhut, G., and Werner, H.J. (1998) Local treatment of electron correlation in molecular clusters: Structures and stabilities of $(H_2O)_n$, $n = 2$–4. *J. Phys. Chem. A*, **102**, 5997–6003.
15 Schütz, M., Hetzer, G., and Werner, H.J. (1999) Low-order scaling local electron correlation methods. I. Linear scaling local MP2. *J. Chem. Phys.*, **111**, 5691–5705.
16 Schütz, M. and Werner, H.J. (2000) Local perturbative triples correction (T) with linear cost scaling. *Chem. Phys. Lett.*, **318**, 370–378.
17 Schütz, M. (2000) Low-order scaling local electron correlation methods. III. Linear scaling local perturbative triples correction (T). *J. Chem. Phys.*, **113**, 9986–10001.

18 Schütz, M. and Werner, H.J. (2001) Low-order scaling local electron correlation methods. IV. Linear scaling local coupled-cluster (LCCSD). *J. Chem. Phys.*, **114**, 661–681.
19 Schütz, M. (2002) Linear scaling local connected triples beyond local (T): Local CCSDT-1b with O(N) scaling. *J. Chem. Phys.*, **116**, 8772–8785.
20 Schütz, M. (2002) A new, fast, semi-direct implementation of linear scaling local coupled cluster theory. *Phys. Chem. Chem. Phys.*, **4**, 3941–3947.
21 Schütz, M. and Manby, F.R. (2003) Linear scaling local coupled cluster theory with density fitting. I : 4-external integrals. *Phys. Chem. Chem. Phys.*, **5**, 3349–3358.
22 Werner, H.J., Manby, F.R., and Knowles, P. (2003) Fast linear scaling second-order Møller-Plesset perturbation theory (MP2) using local and density fitting approximations. *J. Chem. Phys.*, **118**, 8149–8160.
23 Schütz, M., Werner, H.J., Lindh, R., and Manby, F.R. (2004) Analytical energy gradients for local second-order Møller-Plesset perturbation theory using density fitting approximations. *J. Chem. Phys.*, **121**, 737–750.
24 Auer, A. and Nooijen, M. (2006) Dynamically screened local correlation method using enveloping localized orbitals. *J. Chem. Phys.*, **125**, 024 104.
25 Hrenar, T., Rauhut, G., and Werner, H.J. (2006) Impact of local and density fitting approximations on harmonic vibrational frequencies. *J. Phys. Chem. A*, **110**, 2060–2064.
26 Werner, H.J. and Pflüger, K. (2006) On the selection of domains and orbital pairs in local correlation treatments. *Ann. Reports Comput. Chem.*, **2**, 53–80.
27 Mata, R. and Werner, H.J. (2006) Calculation of smooth potential energy surfaces using local electron correlation methods. *J. Chem. Phys.*, **125**, 184110.
28 Mata, R. and Werner, H.J. (2007) Local correlation methods with a natural localized molecular orbital basis. *Mol. Phys.*, **105**, 2753–2761.
29 Mata, R.A., Werner, H.J., Thiel, S., and Thiel, W. (2008) Towards accurate barriers for enzymatic reactions: QM/MM case study on *p*-hydroxybenzoate hydroxylase. *J. Chem. Phys.*, **128**, 025104.
30 Mata, R., Werner, H.J., and Schütz, M. (2008) Correlation regions within a localized molecular orbital approach. *J. Chem. Phys.*, **128**, 144106.
31 Werner, H.J. and Schütz, M. (2011) An efficient local coupled cluster method for accurate thermochemistry of large systems. *J. Chem. Phys.*, **135**, 144116.
32 Schwilk, M., Usvyat, D., and Werner, H.J. (2015) Communication: Improved pair approximations in local coupled-cluster methods. *J. Chem. Phys.*, **142**, 121102.
33 Köppl, C. and Werner, H.J. (2015) On the use of Abelian point group symmetry in density-fitted local MP2 using various types of virtual orbitals. *J. Chem. Phys.*, **142**, 164108.
34 Kats, D. and Manby, F.R. (2013) Sparse tensor framework for implementation of general local correlation methods. *J. Chem. Phys.*, **138**, 144101.
35 Kats, D. (2014) Speeding up local correlation methods. *J. Chem. Phys.*, **141**, 244101.
36 Russ, N.J. and Crawford, T.D. (2004) Local correlation in coupled cluster calculations of molecular response properties. *Chem. Phys. Lett.*, **400**, 104–111.
37 Maslen, P.E., Dutoi, A.D., Lee, M.S., Shao, Y., and Head-Gordon, M. (2005) Accurate local approximations to the triples correlation energy: Formulation, implementation and tests of 5th-order scaling models. *Mol. Phys.*, **103**, 425–437.

JWST817-c01 JWST817-Gordon May 18, 2017 12:57 Printer Name: Trim: 244mm × 170mm

38 DiStasio, R.A., Jung, Y.S., and Head-Gordon, M. (2005) A resolution-of-the-identity implementation of the local triatomics-in-molecules model for second-order Møller-Plesset perturbation theory with application to alanine tetrapeptide conformational energies. *J. Chem. Theory Comput.*, **1**, 862–876.

39 Subotnik, J.E. and Head-Gordon, M. (2005) A local correlation model that yields intrinsically smnooth potential-energy surfaces. *J. Chem. Phys.*, **123**, 064108.

40 Lawler, K.V., Parkhill, J.A., and Head-Gordon, M. (2008) Penalty functions for combining coupled-cluster and perturbation amplitudes in local correlation methods with optimized orbitals. *Mol. Phys.*, **106**, 2309–2324.

41 Schweizer, S., Kussmann, J., Doser, B., and Ochsenfeld, C. (2008) Linear-scaling Cholesky decomposition. *J. Comp. Chem.*, **29**, 1004–1010.

42 Schweizer, S., Doser, B., and Ochsenfeld, C. (2008) An atomic orbital-based reformulation of energy gradients in second-order Møller-Plesset perturbation theory. *J. Chem. Phys.*, **128**, 154101.

43 Doser, B., Lambrecht, D.S., Kussmann, J., and Ochsenfeld, C. (2009) Linear-scaling atomic orbital-based second-order Møller–Plesset perturbation theory by rigorous integral screening criteria. *J. Chem. Phys.*, **130**, 064107.

44 Doser, B., Zienau, J., Clin, L., Lambrecht, D.S., and Ochsenfeld, C. (2010) A linear-scaling MP2 method for large molecules by rigorous integral-screening criteria. *Z. Phys. Chem.*, **224**, 397–412.

45 Kats, D. and Schütz, M. (2009) A multistate local coupled cluster CC2 response method based on the Laplace transform. *J. Chem. Phys.*, **131**, 124117.

46 Freundorfer, K., Kats, D., Korona, T., and Schütz, M. (2010) Local CC2 response method for triplet states based on Laplace transform: Excitation energies and first-order properties. *J. Chem. Phys.*, **133**, 244110.

47 Maschio, L. (2011) Local MP2 with density fitting for periodic systems: A parallel implementation. *J. Chem. Theory Comput.*, **7**, 2818–2830.

48 Neese, F., Wennmohs, F., and Hansen, A. (2009) Efficient and accurate local approximations to coupled-electron pair approaches: An attempt to revive the pair natural orbital method. *J. Chem. Phys.*, **130**, 114108.

49 Neese, F., Hansen, A., and Liakos, D.G. (2009) Efficient and accurate approximations to the local coupled cluster singles doubles method using a truncated pair natural orbital basis. *J. Chem. Phys.*, **131**, 064103.

50 Hansen, A., Liakos, D.G., and Neese, F. (2011) Efficient and accurate local single reference correlation methods for high-spin open-shell molecules using pair natural orbitals. *J. Chem. Phys.*, **135**, 214102.

51 Liakos, D.G., Hansen, A., and Neese, F. (2011) Weak molecular interactions studied with parallel implementations of the local pair natural orbital coupled pair and coupled cluster methods. *J. Chem. Theory Comput.*, **7**, 76–87.

52 Izsak, R., Hansen, A., and Neese, F. (2012) The resolution of identity and chain of spheres approximations for the LPNO-CCSD singles Fock term. *Mol. Phys.*, **110**, 2413–2417.

53 Schmitz, G., Helmich, B., and Hättig, C. (2013) A O(N-3) scaling PNO-MP2 method using a hybrid OSV-PNO approach with an iterative direct generation of OSVs. *Mol. Phys.*, **111**, 2463–2476.

54 Riplinger, C. and Neese, F. (2013) An efficient and near linear scaling pair natural orbital based local coupled cluster method. *J. Chem. Phys.*, **138**, 034106.
55 Riplinger, C., Sandhoefer, B., Hansen, A., and Neese, F. (2013) Natural triple excitations in local coupled cluster calculations with pair natural orbitals. *J. Chem. Phys.*, **139**, 134101.
56 Pinski, P., Riplinger, C., Valeev, E.F., and Neese, F. (2015) Sparse maps—A systematic infrastructure for reduced-scaling electronic structure methods. I. An efficient and simple linear scaling local MP2 method that uses an intermediate basis of pair natural orbitals. *J. Chem. Phys.*, **143**, 034108.
57 Riplinger, C., Pinski, P., Becker, U., Valeev, E.F., and Neese, F. (2016) Sparse maps—A systematic infrastructure for reduced-scaling electronic structure methods. II. Linear scaling domain based pair natural orbital coupled cluster theory. *J. Chem. Phys.*, **144**, 024109.
58 Maurer, S.A., Clin, L., and Ochsenfeld, C. (2014) Cholesky-decomposed density MP2 with density fitting: Accurate MP2 and double-hybrid DFT energies for large systems. *J. Chem. Phys.*, **140**, 224112.
59 Schurkus, H.F. and Ochsenfeld, C. (2016) Communication: An effective linear-scaling atomic-orbital reformulation of the random-phase approximation using a contracted double-Laplace transformation. *J. Chem. Phys.*, **144**, 031101.
60 Fedorov, D.G. and Kitaura, K. (2005) Coupled-cluster theory based upon the fragment molecular-orbital method. *J. Chem. Phys.*, **123**, 134103.
61 Fedorov, A., Couzijn, E.P.A., Nagornova, N.S., Boyarkin, O.V., Rizzo, T.R., and Chen, P. (2010) Structure and bonding of isoleptic coinage metal (Cu, Ag, Au) dimethylaminonitrenes in the gas phase. *J. Am. Chem. Soc.*, **132**, 13789–13798.
62 Hughes, T.F., Flocke, N., and Bartlett, R.J. (2008) Natural linear-scaled coupled-cluster theory with local transferable triple excitations: Applications to peptides. *J. Phys. Chem. A*, **112**, 5994–6003.
63 Gordon, M.S., Mullin, J.M., Pruitt, S.R., Roskop, L.B., Slipchenko, L.V., and Boatz, J.A. (2009) Accurate methods for large molecular systems. *J. Phys. Chem. B*, **113**, 9646–9663.
64 Gordon, M.S., Fedorov, D.G., Pruitt, S.R., and Slipchenko, L.V. (2012) Fragmentation methods: A route to accurate calculations on large systems. *Chem. Rev.*, **112**, 632–672.
65 Findlater, A.D., Zahariev, F., and Gordon, M.S. (2015) Combined fragment molecular orbital cluster in molecule approach to massively parallel electron correlation calculations for large systems. *J. Phys. Chem. A*, **119**, 3587–3593.
66 Ziółkowski, M., Jansìk, B., Kjærgaard, T., and Jørgensen, P. (2010) Linear scaling coupled cluster method with correlation energy based error control. *J. Chem. Phys.*, **133**, 014107.
67 Kristensen, K., Ziółkowski, M., Jansìk, B., Kjærgaard, T., and Jørgensen, P. (2011) A locality analysis of the divide-expand-consolidate coupled cluster amplitude equations. *J. Chem. Theory Comput.*, **7**, 1677–1694.
68 Høyvik, I.M., Kristensen, K., Jansìk, B., and Jørgensen, P. (2012) The divide-expand-consolidate family of coupled cluster methods: Numerical illustrations using second order Møller-Plesset perturbation theory. *J. Chem. Phys.*, **136**, 014105.
69 Kristensen, K., Jørgensen, P., Jansìk, B., Kjærgaard, T., and Reine, S. (2012) Molecular gradient for second-order Møller-Plesset perturbation theory using the divide-expand-consolidate (DEC) scheme. *J. Chem. Phys.*, **137**, 114102.

JWST817-c01 JWST817-Gordon May 18, 2017 12:57 Printer Name: Trim: 244mm × 170mm

70 Kristensen, K., Kjærgaard, T., Høyvik, I.M., Ettenhuber, P., Jørgensen, P., Jansik, B., Reine, S., and Jakowski, J. (2013) The divide-expand-consolidate MP2 scheme goes massively parallel. *Mol. Phys.*, **111**, 1196–1210.

71 Eriksen, J.J., Baudin, P., Ettenhuber, P., Kristensen, K., Kjærgaard, T., and Jørgensen, P. (2015) Linear-scaling coupled cluster with perturbative triple excitations: The divide–expand–consolidate CCSD(T) model. *J. Chem. Theory Comput.*, **11**, 2984–2993.

72 Baudin, P., Ettenhuber, P., Reine, S., Kristensen, K., and Kjaergaard, T. (2016) Efficient linear-scaling second-order Møller-Plesset perturbation theory: The divide-expand-consolidate RI-MP2 model. *J. Chem. Phys.*, **144**, 054102.

73 Bykov, D., Kristensen, K., and Kjaergaard, T. (2016) The molecular gradient using the divide-expand-consolidate resolution of the identity second-order Møller-Plesset perturbation theory: The DEC-RI-MP2 gradient. *J. Chem. Phys.*, **145**, 024106.

74 Ettenhuber, P., Baudin, P., Kjaergaard, T., Jorgensen, P., and Kristensen, K. (2016) Orbital spaces in the divide-expand-consolidate coupled cluster method. *J. Chem. Phys.*, **144**, 164116.

75 Li, W., Piecuch, P., Gour, J.R., and Li, S. (2009) Local correlation calculations using standard and renormalized coupled-cluster approaches. *J. Chem. Phys.*, **131**, 114109.

76 Li, W. and Piecuch, P. (2010) Improved design of orbital domains within the cluster-in-molecule local correlation framework: Single-environment cluster-in-molecule ansatz and its application to local coupled-cluster approach with singles and doubles. *J. Phys. Chem. A*, **114**, 8644–8657.

77 Li, W. and Piecuch, P. (2010) Multilevel extension of the cluster-in-molecule local correlation methodology: Merging coupled-cluster and Møller-Plesset perturbation theories. *J. Phys. Chem. A*, **114**, 6721–6727.

78 Li, W., Guo, Y., and Li, S. (2012) A refined cluster-in-molecule local correlation approach for predicting the relative energies of large systems. *Phys. Chem. Chem. Phys.*, **14**, 7854–7862.

79 Guo, Y., Li, W., and Li, S. (2014) Improved cluster-in-molecule local correlation approach for electron correlation calculation of large systems. *J. Phys. Chem. A*, **118**, 8996–9004.

80 Li, W., Chen, C., Zhao, D., and Li, S. (2015) LSQC: Low scaling quantum chemistry program. *Int. J. Quantum Chem.*, **115**, 641–646.

81 Li, W., Ni, Z., and Li, S. (2016) Cluster-in-molecule local correlation method for post-Hartree-Fock calculations of large systems. *Mol. Phys.*, **114**, 1447–1460.

82 Rolik, Z. and Kallay, M. (2011) A general-order local coupled-cluster method based on the cluster-in-molecule approach. *J. Chem. Phys.*, **135**, 104111.

83 Rolik, Z., Szegedy, L., Ladjánszki, I., Ladóczki, B., and Kallay, M. (2013) An efficient linear-scaling CCSD(T) method based on local natural orbitals. *J. Chem. Phys.*, **139**, 094105.

84 Kallay, M. (2015) Linear-scaling implementation of the direct random-phase approximation. *J. Chem. Phys.*, **142**, 204105.

85 Nagy, P.R., Samu, G., and Kallay, M. (2016) An integral-direct linear-scaling second-order Møller-Plesset approach. *J. Chem. Theory Comput.*, **12**, 4897–4914.

86 Saha, A. and Raghavachari, K. (2014) Dimers of dimers (DOD): A new fragment-based method applied to large water clusters. *J. Chem. Theory Comput.*, **10**, 58–67.

87 Yoshikawa, T. and Nakai, H. (2015) Linear-scaling self-consistent field calculations based on divide-and-conquer method using resolution-of-identity approximation on graphical processing units. *J. Comput. Chem.*, **36**, 164–170.
88 Stoll, H. (1992) On the correlation energy of graphite. *J. Chem. Phys.*, **97**, 8449–8454.
89 Friedrich, J., Hanrath, M., and Dolg, M. (2007) Fully automated implementation of the incremental scheme: Application to CCSD energies for hydrocarbons and transition metal compounds. *J. Chem. Phys.*, **126**, 154110.
90 Friedrich, J., Hanrath, M., and Dolg, M. (2008) Evaluation of incremental correlation energies for open-shell systems: Application to the intermediates of the 4-exo cyclization, Arduengo carbenes and an anionic water cluster. *J. Phys. Chem. A*, **112**, 8762–8766.
91 Friedrich, J. and Dolg, M. (2008) Implementation and performance of a domain-specific basis set incremental approach for correlation energies: Applications to hydrocarbons and a glycine oligomer. *J. Chem. Phys.*, **129**, 244105.
92 Friedrich, J., Coriani, S., Helgaker, T., and Dolg, M. (2009) Implementation of the incremental scheme for one-electron first-order properties in coupled-cluster theory. *J. Chem. Phys.*, **131**, 154102.
93 Friedrich, J. and Dolg, M. (2009) Fully automated incremental evaluation of MP2 and CCSD(T) energies: Application to water clusters. *J. Chem. Theory Comput.*, **5**, 287–294.
94 Friedrich, J. and Hänchen, J. (2013) Incremental CCSD(T)(F12*)|MP2: A black box method to obtain highly accurate reaction energies. *J. Chem. Theory Comput.*, **9**, 5381–5394.
95 Meitei, O.R. and Hesselmann, A. (2016) Molecular energies from an incremental fragmentation method. *J. Chem. Phys.*, **144**, 084109.
96 Hoyau, S., Maynau, D., and Malrieu, J.P. (2011) A regionally contracted multireference configuration interaction method: General theory and results of an incremental version. *J. Chem. Phys.*, **134**, 054125.
97 Kutzelnigg, W. (1985) r_{12}-Dependent terms in the wave function as closed sums of partial wave amplitudes for large l. *Theor. Chim. Acta*, **68**, 445–469.
98 Klopper, W. and Kutzelnigg, W. (1987) Møller-Plesset calculations taking care of the correlation CUSP. *Chem. Phys. Lett.*, **134**, 17–22.
99 Klopper, W. and Kutzelnigg, W. (1990) MP2-R12 calculations on the relative stability of carbocations. *J. Phys. Chem.*, **94**, 5625.
100 Klopper, W., Röhse, R., and Kutzelnigg, W. (1991) CID and CEPA calculations with linear r_{12} terms. *Chem. Phys. Lett.*, **178**, 455–461.
101 Kutzelnigg, W. and Klopper, W. (1991) Wave functions with terms linear in the interelectronic coordinates to take care of the correlation cusp. I. General theory. *J. Chem. Phys.*, **94**, 1985–2001.
102 Termath, V., Klopper, W., and Kutzelnigg, W. (1991) Wave functions with terms linear in the interelectronic coordinates to take care of the correlation cusp. II. Second-order Møller-Plesset (MP2-R12) calculations on closed-shell atoms. *J. Chem. Phys.*, **94**, 2002–2019.
103 Klopper, W. and Kutzelnigg, W. (1991) Wave functions with terms linear in the interelectronic coordinates to take care of the correlation cusp. III. Second-order Møller-Plesset (MP2-R12) calculations on molecules of first row atoms. *J. Chem. Phys.*, **94**, 2020–2030.

JWST817-c01 JWST817-Gordon May 18, 2017 12:57 Printer Name: Trim: 244mm × 170mm

104 Klopper, W. (1991) Orbital-invariant formulation of the MP2-R12 method. *Chem. Phys. Lett.*, **186**, 583–585.

105 Noga, J., Kutzelnigg, W., and Klopper, W. (1992) CC-R12, a correlation cusp corrected coupled-cluster method with a pilot application to the Be_2 potential curve. *Chem. Phys. Lett.*, **199**, 497–504.

106 Noga, J. and Kutzelnigg, W. (1994) Coupled cluster theory that takes care of the correlation cusp by inclusion of linear terms in the interelectronic coordinates. *J. Chem. Phys.*, **101**, 7738–7762.

107 Klopper, W. and Samson, C.C.M. (2002) Explicitly correlated second-order Møller-Plesset methods with auxiliary basis sets. *J. Chem. Phys.*, **116**, 6397–6410.

108 Manby, F.R. (2003) Density fitting in second-order linear-r_{12} Møller-Plesset perturbation theory. *J. Chem. Phys.*, **119**, 4607–4613.

109 Ten-no, S. (2004) Initiation of explicitly correlated Slater-type germinal theory. *Chem. Phys. Lett.*, **398**, 56–61.

110 Ten-no, S. (2004) Explicitly correlated second order perturbation theory: Introduction of a rational generator and numerical quadratures. *J. Chem. Phys.*, **121**, 117–129.

111 May, A.J. and Manby, F.R. (2004) An explicitly correlated second order Møller-Plesset theory using a frozen Gaussian geminal. *J. Chem. Phys.*, **121**, 4479–4485.

112 Valeev, E.F. (2004) Improving on the resolution of the identity in linear R12 ab initio theories. *Chem. Phys. Lett.*, **395**, 190–195.

113 Tew, D.P. and Klopper, W. (2005) New correlation factors for explicitly correlated electronic wave functions. *J. Chem. Phys.*, **123**, 074101.

114 Kedžuch, S., Milko, M., and Noga, J. (2005) Alternative formulation of the matrix elements in MP2-R12 theory. *Int. J. Quantum Chem.*, **105**, 929–936.

115 Fliegl, H., Klopper, W., and Hättig, C. (2005) Coupled-cluster theory with simplified linear-r_{12} corrections: The CCSD(R12) model. *J. Chem. Phys.*, **122**, 084107.

116 Fliegl, H., Hättig, C., and Klopper, W. (2006) Inclusion of the (T) triples correction into the linear-r12 corrected coupled-cluster model CCSD(R12). *Int. J. Quantum Chem.*, **106**, 2306–2317.

117 Manby, F.R., Werner, H.J., Adler, T.B., and May, A.J. (2006) Explicitly correlated local second-order perturbation theory with a frozen geminal correlation factor. *J. Chem. Phys.*, **124**, 094103.

118 Werner, H.J., Adler, T.B., and Manby, F.R. (2007) General orbital invariant MP2-F12 theory. *J. Chem. Phys.*, **126**, 164102.

119 Noga, J., Kedžuch, S., and Šimunek, J. (2007) Second order explicitly correlated R12 theory revisited: A second quantization framework for treatment of the operators' partitionings. *J. Chem. Phys.*, **127**, 034106.

120 Adler, T.B., Knizia, G., and Werner, H.J. (2007) A simple and efficient CCSD(T)-F12 approximation. *J. Chem. Phys.*, **127**, 221106.

121 Ten-no, S. (2007) A simple F12 geminal correction in multi-reference perturbation theory. *Chem. Phys. Lett.*, **447**, 175–179.

122 Tew, D.P., Klopper, W., Neiss, C., and Hättig, C. (2007) Quintuple-zeta quality coupled-cluster correlation energies with triple-zeta basis sets. *Phys. Chem. Chem. Phys.*, **9**, 1921–1930.

123 Knizia, G. and Werner, H.J. (2008) Explicitly correlated RMP2 for high-spin open-shell reference states. *J. Chem. Phys.*, **128**, 154103.

124 Shiozaki, T., Kamiya, M., Hirata, S., and Valeev, E.F. (2008) Explicitly correlated coupled-cluster singles and doubles method based on complete diagrammatic equations. *J. Chem. Phys.*, **129**, 071101.

125 Shiozaki, T., Kamiya, M., Hirata, S., and Valeev, E.F. (2008) Equations of explicitly-correlated coupled-cluster methods. *Phys. Chem. Chem. Phys.*, **10**, 3358–3370.

126 Noga, J., Kedžuch, S., Šimunek, J., and Ten-no, S. (2008) Explicitly correlated coupled cluster F12 theory with single and double excitations. *J. Chem. Phys.*, **128**, 174103.

127 Tew, D.P., Klopper, W., and Hättig, C. (2008) A diagonal orbital-invariant explicitly correlated coupled-cluster method. *Chem. Phys. Lett.*, **452**, 326–332.

128 Valeev, E.F. (2008) Coupled-cluster methods with perturbative inclusion of explicitly correlated terms: A preliminary investigation. *Phys. Chem. Chem. Phys.*, **10**, 106–113.

129 Valeev, E.F. and Crawford, T.D. (2008) Simple coupled-cluster singles and doubles method with perturbative inclusion of triples and explicitly correlated geminals: The CCSD(T)$_{\overline{R12}}$ model. *J. Chem. Phys.*, **128**, 244113.

130 Torheyden, M. and Valeev, E.F. (2008) Variational formulation of perturbative explicitly-correlated coupled-cluster methods. *Phys. Chem. Chem. Phys.*, **10**, 3410.

131 Bokhan, D., Ten-no, S., and Noga, J. (2008) Implementation of the CCSD(T)-F12 method using cusp conditions. *Phys. Chem. Chem. Phys.*, **10**, 3320–3326.

132 Köhn, A., Richings, G.W., and Tew, D.P. (2008) Implementation of the full explicitly correlated coupled-cluster singles and doubles model CCSD-F12 with optimally reduced auxiliary basis dependence. *J. Chem. Phys.*, **129**, 201103.

133 Knizia, G., Adler, T.B., and Werner, H.J. (2009) Simplified CCSD(T)-F12 methods: Theory and benchmarks. *J. Chem. Phys.*, **130**, 054104.

134 Shiozaki, T., Kamiya, M., Hirata, S., and Valeev, E.F. (2009) Higher-order explicitly correlated coupled-cluster methods. *J. Chem. Phys.*, **130**, 054101.

135 Bokhan, D., Bernadotte, S., and Ten-no, S. (2009) Implementation of the CCSD(T)(F12) method using numerical quadratures. *Chem. Phys. Lett.*, **469**, 214–218.

136 Bischoff, F.A., Wolfsegger, S., Tew, D.P., and Klopper, W. (2009) Assessment of basis sets for F12 explicitly-correlated molecular electronic-structure methods. *Mol. Phys.*, **107**, 963–975.

137 Hättig, C., Tew, D.P., and Köhn, A. (2010) Accurate and efficient approximations to explicitly correlated coupled-cluster singles and doubles, CCSD-F12. *J. Chem. Phys.*, **132**, 231102.

138 Werner, H.J., Knizia, G., and Manby, F.R. (2011) Explicitly correlated coupled cluster methods with pair-specific geminals. *Mol. Phys.*, **109**, 407–417.

139 Shiozaki, T., Knizia, G., and Werner, H.J. (2011) Explicitly correlated multireference configuration interaction: MRCI-F12. *J. Chem. Phys.*, **134**, 034113.

140 Werner, H.J. and Manby, F.R. (2006) Explicitly correlated second-order perturbation theory using density fitting and local approximations. *J. Chem. Phys.*, **124**, 054114.

141 Manby, F.R., Werner, H.J., Adler, T.B., and May, A.J. (2006) Explicitly correlated local second-order perturbation theory with a frozen geminal correlation factor. *J. Chem. Phys.*, **124**, 094103.

142 Werner, H.J. (2008) Eliminating the domain error in local explicitly correlated second-order Møller-Plesset perturbation theory. *J. Chem. Phys.*, **129**, 101103.

JWST817-c01 JWST817-Gordon May 18, 2017 12:57 Printer Name: Trim: 244mm × 170mm

143 Adler, T.B. and Werner, H.J. (2009) Local explicitly correlated coupled-cluster methods: Efficient removal of the basis set incompleteness and domain errors. *J. Chem. Phys.*, **130**, 241101.

144 Adler, T.B., Werner, H.J., and Manby, F.R. (2009) Local explicitly correlated second-order perturbation theory for the accurate treatment of large molecules. *J. Chem. Phys.*, **130**, 054106.

145 Adler, T.B. and Werner, H.J. (2011) An explicitly correlated local coupled cluster method for calculations of large molecules close to the basis set limit. *J. Chem. Phys.*, **135**, 144117.

146 Krause, C. and Werner, H.J. (2012) Comparison of explicitly correlated local coupled-cluster methods with various choices of virtual orbitals. *Phys. Chem. Chem. Phys.*, **14**, 7591–7604.

147 Werner, H.J., Knizia, G., Krause, C., Schwilk, M., and Dornbach, M. (2015) Scalable electron correlation methods. I. PNO-LMP2 with linear scaling in the molecular size and near-inverse-linear scaling in the number of processors. *J. Chem. Theory Comput.*, **11**, 484–507.

148 Ma, Q. and Werner, H.J. (2015) Scalable electron correlation methods. II. Parallel PNO-LMP2-F12 with near linear scaling in the molecular size. *J. Chem. Theory Comput.*, **11**, 5291–5304.

149 Tew, D.P., Helmich, B., and Hättig, C. (2011) Local explicitly correlated second-order Moller-Plesset perturbation theory with pair natural orbitals. *J. Chem. Phys.*, **135**, 074107.

150 Hättig, C., Tew, D.P., and Helmich, B. (2012) Local explicitly correlated second- and third-order Møller-Plesset perturbation theory with pair natural orbitals. *J. Chem. Phys.*, **136**, 204105.

151 Li, W. (2013) Linear scaling explicitly correlated MP2-F12 and ONIOM methods for the long-range interactions of the nanoscale clusters in methanol aqueous solutions. *J. Chem. Phys.*, **138**, 014106.

152 Wang, Y.M., Hättig, C., Reine, S., Valeev, E., Kjaergaard, T., and Kristensen, K. (2016) Explicitly correlated second-order Møller-Plesset perturbation theory in a divide-expand-consolidate (DEC) context. *J. Chem. Phys.*, **144**, 204112.

153 Pavošević, F., Pinski, P., Riplinger, C., Neese, F., and Valeev, E.F. (2016) Sparse maps—A systematic infrastructure for reduced-scaling electronic structure methods. IV. Linear-scaling second-order explicitly correlated energy with pair natural orbitals. *J. Chem. Phys.*, **144**, 144109.

154 Peterson, K.A., Adler, T.B., and Werner, H.J. (2008) Systematically convergent basis sets for explicitly correlated wavefunctions: The atoms H, He, B-Ne, and Al-Ar. *J. Chem. Phys.*, **128**, 084102.

155 Hill, J.G., Peterson, K.A., Knizia, G., and Werner, H.J. (2009) Extrapolating MP2 and CCSD explicitly correlated correlation energies to the complete basis set limit with first and second row correlation consistent basis sets. *J. Chem. Phys.*, **131**, 194105.

156 Edmiston, C. and Krauss, M. (1965) Configuration-interaction calculation of H_3 and H_2. *J. Chem. Phys.*, **42**, 1119–1120.

157 Meyer, W. (1971) Ionization energies of water from PNO-CI calculations. *Int. J. Quantum Chem.*, **5**, 341–348.

158 Meyer, W. (1973) PNO-CI Studies of electron correlation effects. I. Configuration expansion by means of nonorthogonal orbitals, and application to the ground state and ionized states of methane. *J. Chem. Phys.*, **58**, 1017–1035.

159 Ahlrichs, R., Driessler, F., Lischka, H., Staemmler, V., and Kutzelnigg, W. (1975) PNO-CI (pair natural orbital configuration interaction) and CEPA-PNO (coupled electron pair approximation with pair natural orbitals) calculations of molecular systems. II. The molecules BeH_2, BH, BH_3, CH_4, CH_3^-, NH_3 (planar and pyramidal), H_2O, OH_3^+, HF and the Ne atom. *J. Chem. Phys.*, **62**, 1235–1247.

160 Taylor, P.R., Bacskay, G., Hush, N., and Hurley, A. (1976) The coupled-pair approximation in a basis of independent-pair natural orbitals. *Chem. Phys. Lett.*, **41**, 444–449.

161 Taylor, P.R. (1981) A rapidly convergent CI expansion based on several reference configurations, using optimized correlating orbitals. *J. Chem. Phys.*, **74**, 1256–1270.

162 Staemmler, V. and Jaquet, R. (1981) CEPA calculations on open-shell molecules. I. Outline of the method. *Theor. Chim. Acta.*, **59**, 487–500.

163 Fink, R. and Staemmler, V. (1993) A multi-configuration reference CEPA method based on pair natural orbitals. *Theor. Chem. Acc.*, **87**, 129–145.

164 Yang, J., Kurashige, Y., and Manby, F.R. (2011) Tensor factorizations of local second-order Møller–Plesset theory. *J. Chem. Phys.*, **134**, 044123.

165 Kurashige, Y., Yang, J., Chan, G.K.L., and Manby, F.R. (2012) Optimization of orbital-specific virtuals in local Møller-Plesset perturbation theory. *J. Chem. Phys.*, **136**, 124106.

166 Yang, J., Chan, G.K.L., Manby, F.R., Schütz, M., and Werner, H.J. (2012) The orbital-specific-virtual local coupled cluster singles and doubles method. *J. Chem. Phys.*, **136**, 144105.

167 Schütz, M., Yang, J., Chan, G.K.L., Manby, F.R., and Werner, H.J. (2013) The orbital-specific virtual local triples correction: OSV-L(T). *J. Chem. Phys.*, **138**, 054109.

168 Walter, D., Venkatnathan, A., and Carter, E. (2003) Local correlation in the virtual space in multireference singles and doubles configuration interaction. *J. Chem. Phys.*, **118**, 8127–8139.

169 Chwee, T.S., Szilva, A.B., Lindh, R., and Carter, E.A. (2008) Linear scaling multireference singles and doubles configuration interaction. *J. Chem. Phys.*, **128**, 224106.

170 Chwee, T.S. and Carter, E.A. (2010) Density fitting of two-electron integrals in local multireference single and double excitation configuration interaction calculations. *Mol. Phys.*, **108**, 2519–2526.

171 Chwee, T.S. and Carter, E.A. (2010) Cholesky decomposition within local multireference singles and doubles configuration interaction. *J. Chem. Phys.*, **132**, 074104.

172 Krisiloff, D.B. and Carter, E.A. (2012) Approximately size extensive local multireference singles and doubles configuration interaction. *Phys. Chem. Chem. Phys.*, **14**, 7710–7717.

173 Krisiloff, D.B., Krauter, C.M., Ricci, F.J., and Carter, E.A. (2015) Density fitting and cholesky decomposition of the two-electron integrals in local multireference configuration interaction theory. *J. Chem. Theory Comput.*, **11**, 5242–5251.

174 Demel, O., Pittner, J., and Neese, F. (2015) A local pair natural orbital-based multireference Mukherjee's coupled cluster method. *J. Chem. Theory Comput.*, **11**, 3104–3114.

175 Guo, Y., Sivalingam, K., Valeev, E.F., and Neese, F. (2016) Sparse maps—A systematic infrastructure for reduced-scaling electronic structure methods. III. Linear-scaling

JWST817-c01 JWST817-Gordon May 18, 2017 12:57 Printer Name: Trim: 244mm × 170mm

multireference domain-based pair natural orbital N-electron valence perturbation theory. *J. Chem. Phys.*, **144**, 094111.

176 Menezes, F., Kats, D., and Werner, H.J. (2016) Local complete active space second-order perturbation theory using pair natural orbitals (PNO-CASPT2). *J. Chem. Phys.*, **145**, 124115.

177 Fedorov, A., Batiste, L., Couzijn, E.P.A., and Chen, P. (2010) Experimental and theoretical study of a gold(I) aminonitrene complex in the gas phase. *ChemPhysChem*, **11**, 1002–1005.

178 Figgen, D., Rauhut, G., Dolg, M., and Stoll, H. (2005) Energy-consistent pseudopotentials for group 11 and 12 atoms: adjustment to multi-configuration Dirac–Hartree–Fock data. *Chem. Phys.*, **311**, 227–244.

179 Peterson, K. and Puzzarini, C. (2005) Systematically convergent basis sets for transition metals. II. Pseudopotential-based correlation consistent basis sets for the group 11 (Cu, Ag, Au) and 12 (Zn, Cd, Hg) elements. *Theor. Chem. Acc.*, **114**, 283–296.

180 Weigend, F., Köhn, A., and Hättig, C. (2002) Efficient use of the correlation consistent basis sets in resolution of the identity MP2 calculations. *J. Chem. Phys.*, **116**, 3175–3183.

181 Weigend, F. (2002) A fully direct RI-HF algorithm: Implementation, optimised auxiliary basis sets, demonstration of accuracy and efficiency. *Phys. Chem. Chem. Phys.*, **4**, 4285–4291.

182 Werner, H.J., Knowles, P.J., Knizia, G., Manby, F.R., and Schütz, M. (2011) Molpro: A general-purpose quantum chemistry program package. *WIREs Comput. Mol. Sci.*, **2**, 242–253.

183 Werner, H.J., Knowles, P.J., Knizia, G., Manby, F.R., Schütz, M., and and others (2016) Molpro, development version 2015.2, a package of ab initio programs. See http://www.molpro.net.

184 Hoyvik, I.M. and Jorgensen, P. (2016) Characterization and generation of local occupied and virtual Hartree–Fock orbitals. *Chem. Rev.*, **116**, 3306–3327.

185 Pipek, J. and Mezey, P.G. (1989) A fast intrinsic localization procedure applicable for ab initio and semiempirical linear combination of atomic orbital wave functions. *J. Chem. Phys.*, **90**, 4916–4926.

186 Edmiston, C. and Ruedenberg, K. (1963) Localized atomic and molecular orbitals. *Rev. Mod. Phys.*, **35**, 457–465.

187 Edmiston, C. and Ruedenberg, K. (1965) Localized atomic and molecular orbitals. II. *J. Chem. Phys.*, **43**, S97–S116.

188 Knizia, G. (2013) Intrinsic atomic orbitals: An unbiased bridge between quantum theory and chemical concepts. *J. Chem. Theory Comput.*, **9**, 4834–4843.

189 Janowski, T. (2014) Near equivalence of intrinsic atomic orbitals and quasiatomic orbitals. *J. Chem. Theory Comput.*, **10**, 3085–3091.

190 Lu, W.C., Wang, C.Z., Schmidt, M.W., Bytautas, L., Ho, K.M., and Ruedenberg, K. (2004) Molecule intrinsic minimal basis sets. I. Exact resolution of ab initio optimized molecular orbitals in terms of deformed atomic minimal-basis orbitals. *J. Chen. Phys.*, **120**, 2629–2637.

191 West, A.C., Schmidt, M.W., Gordon, M.S., and Ruedenberg, K. (2013) A comprehensive analysis of molecule-intrinsic quasi-atomic, bonding, and correlating orbitals. I. Hartree-Fock wave functions. *J. Chem. Phys.*, **139**, 234107.

JWST817-c01 JWST817-Gordon May 18, 2017 12:57 Printer Name: Trim: 244mm × 170mm

192 Lehtola, S. and Jónsson, H. (2013) Unitary optimization of localized molecular orbitals. *J. Chem. Theory Comput.*, **9**, 5365–5372.

193 Reed, A.E., Weinstock, R.B., and Weinhold, F. (1985) Natural population analysis. *J. Chem. Phys.*, **83**, 735–746.

194 Reed, A.E. and Weinhold, F. (1985) Natural localized molecular orbitals. *J. Chem. Phys.*, **83**, 1736–1740.

195 Reed, A.E. and Weinhold, F. (1983) Natural bond orbital analysis of near-Hartree-Fock water dimer. *J. Chem. Phys.*, **78**, 4066–4073.

196 Foster, J.P. and Weinhold, F. (1980) Natural hybrid orbitals. *J. Am. Chem. Soc.*, **102**, 7211–7218.

197 Pulay, P., Saebø, S., and Meyer, W. (1984) An efficient reformulation of the closed-shell self-consistent electron pair theory. *J. Chem. Phys.*, **81**, 1901–1905.

198 Scuseria, G.E., Janssen, C.L., and Schaefer III, H.F. (1988) An efficient reformulation of the closed-shell coupled cluster single and double excitation (CCSD) equations. *J. Chem. Phys*, **89**, 7382–7387.

199 Hampel, C., Peterson, K.A., and Werner, H.J. (2011) A comparison of the efficiency and accuracy of the quadratic configuration interaction (QCISD), coupled cluster (CCSD), and Brueckner coupled cluster (BCCD) methods. *J. Chem. Phys.*, **135**, 144116.

200 Boughton, J.W. and Pulay, P. (1993) Comparison of the Boys and Pipek-Mezey localizations in the local correlation approach and automatic virtual basis selection. *J. Comput. Chem.*, **14**, 736–740.

201 Kats, D. (2016) Speeding up local correlation methods: System-inherent domains. *J. Chem. Phys.*, **145**, 014103.

202 Stone, A. (1975) *Theoretical Models of Chemical Bonding, Part 4* (ed. Z.B. Maksić), Springer, Heidelberg, 102.

203 Werner, H.J. (2016) Communication: Multipole approximations of distant pair energies in local correlation methods with pair natural orbitals. *J. Chem. Phys.*, **145**, 201101.

204 Schütz, M., Masur, O., and Usvyat, D. (2014) Efficient and accurate treatment of weak pairs in local CCSD (T) calculations. II. Beyond the ring approximation. *J. Chem. Phys.*, **140**, 244107.

205 Schwilk, M., Ma, Q., Köppl, C., and Werner, H.J. (2017) A parallel PNO-LCCSD method. *To be published*.

206 Köppl, C. and Werner, H.J. (2015) Parallel and low-order scaling implementation of Hartree-Fock exchange using local density fitting. *J. Chem. Theory Comput.*, **12**, 3122–3134.

207 Kato, T. (1957) On the eigenfunctions of many-particle systems in quantum mechanics. *Comm. Pure Appl. Math.*, **10**, 151–177.

208 Pack, R.T. and Byers Brown, W. (1966) Cusp conditions for molecular wavefunctions. *J. Chem. Phys.*, **45**, 556–559.

209 Hylleraas, E.A. (1929) Neue Berechnung der Energie des Heliums im Grundzustande, sowie des tiefsten Terms von Ortho-Helium. *Z. Phys.*, **54**, 347–366.

210 Werner, H.J., Adler, T.B., Knizia, G., and Manby, F.R. (2010) Efficient explicitly correlated coupled-cluster approximations, in *Recent Progress in Coupled Cluster Methods* (eds. P. Čársky, J. Paldus, and J. Pittner), Springer, Heidelberg, pp. 573–619.

JWST817-c01 JWST817-Gordon May 18, 2017 12:57 Printer Name: Trim: 244mm × 170mm

211 Werner, H.J., Knizia, G., Adler, T.B., and Marchetti, O. (2010) Benchmark studies for explicitly correlated perturbation- and coupled cluster theories. *Z. Phys. Chem.*, **224**, 493–511.

212 Saebø, S., Tong, W., and Pulay, P. (1993) Efficient elimination of basis set superposition errors by the local correlation method: Accurate ab initio studies of the water dimer. *J. Chem. Phys.*, **98**, 2170–2175.

213 Dunlap, B.I., Connolly, J.W.D., and Sabin, J.R. (1979) On some approximations in applications of $X\alpha$ theory. *J. Chem. Phys.*, **71** (8), 3396–3402.

214 Dunlap, B.I. (2000) Robust and variational fitting. *Phys. Chem. Chem. Phys.*, **2**, 2113–2116.

215 Nieplocha, J., Palmer, B., Tipparaju, V., Krishnan, M., Trease, H., and Aprà, E. (2006) Advances, applications and performance of the global arrays shared memory programming toolkit. *International Journal of High Performance Computing Applications*, **20**, 203–231.

216 Karypis, G. and Kumar, V. (1998) A fast and high quality multilevel scheme for partitioning irregular graphs. *SIAM J. Sci. Comput.*, **20**, 359–392.

217 Grimme, S. (2003) Improved second-order Møller-Plesset perturbation theory by separate scaling of parallel- and antiparallel-spin pair correlation energies. *J. Chem. Phys.*, **118**, 9095–9102.

218 Rauhut, G., Azhary, A.E., Eckert, F., Schumann, U., and Werner, H.J. (1999) Impact of local approximations on MP2 vibrational frequencies. *Spectrochim. Acta*, **A 55**, 647–658.

219 Rauhut, G. and Werner, H.J. (2003) The vibrational spectra of furoxan and dichlorofuroxan: a comparative theoretical study using density functional theory and Local Electron Correlation Methods. *Phys. Chem. Chem. Phys.*, **5**, 2001–2008.

220 Claeyssens, F., Harvey, J.N., Manby, F.R., Mata, R.A., Mulholland, A.J., Ranaghan, K.E., Schütz, M., Thiel, S., Thiel, W., and Werner, H.J. (2006) High-Accuracy Computation of Reaction Barriers in Enzymes. *Angew. Chem. Int. Ed.*, **45**, 6856–6859.

221 Dieterich, J.M., Werner, H.J., Mata, R.A., Metz, S., and Thiel, W. (2010) Reductive half-eeaction of aldehyde oxidoreductase toward acetaldehyde: Ab initio and free energy QM/MM calculations. *J. Chem. Phys.*, **132**, 035101.

222 Rommel, J.B., Liu, Y., Werner, H.J., and Kästner, J. (2012) Role of Tunneling in the Enzyme Glutamate Mutase. *J. Phys. Chem. B*, **116**, 13682–13689.

223 ElAzhary, A., Rauhut, G., Pulay, P., and Werner, H.J. (1998) Analytical energy gradients for local second-order Møller-Plesset perturbation theory. *J. Chem. Phys.*, **108**, 5185–5193.

224 Rauhut, G. and Werner, H.J. (2001) Analytical energy gradients for local coupled-cluster methods. *Phys. Chem. Chem. Phys.*, **3**, 4853–4862.

225 Shamasundar, K.R., Knizia, G., and Werner, H.J. (2011) A new internally contracted multi-reference configuration interaction method. *J. Chem. Phys.*, **135**, 054101.